Analysis and Application of Optimization Techniques to Power System Security and Electricity Markets

by

José Rafael Avalos Muñoz

A thesis
presented to the University of Waterloo
in fulfillment of the
thesis requirement for the degree of
Doctor of Philosophy
in
Electrical and Computer Engineering

Waterloo, Ontario, Canada, 2008

I hereby declare that I am the sole author of this thesis. This is a true copy of the thesis, including any required final revisions, as accepted by my examiners.

I understand that my thesis may be made electronically available to the public.

Abstract

Determining the maximum power system loadability, as well as preventing the system from being operated close to the stability limits is very important in power systems planning and operation. The application of optimization techniques to power systems security and electricity markets is a rather relevant research area in power engineering. The study of optimization models to determine critical operating conditions of a power system to obtain secure power dispatches in an electricity market has gained particular attention. This thesis studies and develops optimization models and techniques to detect or avoid voltage instability points in a power system in the context of a competitive electricity market.

A thorough analysis of an optimization model to determine the maximum power loadability points is first presented, demonstrating that a solution of this model corresponds to either Saddle-node Bifurcation (SNB) or Limit-induced Bifurcation (LIB) points of a power flow model. The analysis consists of showing that the transversality conditions that characterize these bifurcations can be derived from the optimality conditions at the solution of the optimization model. The study also includes a numerical comparison between the optimization and a continuation power flow method to show that these techniques converge to the same maximum loading point. It is shown that the optimization method is a very versatile technique to determine the maximum loading point, since it can be readily implemented and solved. Furthermore, this model is very flexible, as it can be reformulated to optimize different system parameters so that the loading margin is maximized.

The Optimal Power Flow (OPF) problem with voltage stability (VS) constraints is a highly nonlinear optimization problem which demands robust and efficient solution techniques. Furthermore, the proper formulation of the VS constraints plays a significant role not only from the practical point of view, but also from the market/system perspective. Thus, a novel and practical OPF-based auction model is proposed that includes a VS constraint based on the singular value decomposition (SVD) of the power flow Jacobian. The newly developed model is tested using

realistic systems of up to 1211 buses to demonstrate its practical application. The results show that the proposed model better represents power system security in the OPF and yields better market signals. Furthermore, the corresponding solution technique outperforms previous approaches for the same problem. Other solution techniques for this OPF problem are also investigated. One makes use of a cutting planes (CP) technique to handle the VS constraint using a primal-dual Interior-point Method (IPM) scheme. Another tries to reformulate the OPF and VS constraint as a semidefinite programming (SDP) problem, since SDP has proven to work well for certain power system optimization problems; however, it is demonstrated that this technique cannot be used to solve this particular optimization problem.

Acknowledgments

I would like to express my sincere gratitude to Prof. Claudio A. Cañizares for his guidance, patience, and support throughout my Ph.D studies. His contribution to my life is simply priceless, thank you for everything Professor. I also offer an special acknowledgment to Prof. Miguel F. Anjos for all his suggestions and motivation. Their professionalism and dedication is a source of inspiration. It was a great honor to work with them.

An important recognition to my examining committee members: Prof. Kankar Bhattacharya, and Prof. Anthony Vannelli from the Electrical and Computer Engineering Department, and specially to Prof. Paul Calamai from the Systems Design Engineering Department for his important comments.

Special thanks to my officemates for their friendship and unique environment in the EMSOL lab: Hemant Barot, Amirhossein Hajimiragha, Hassan Ghasemi, Hamid Zareipour, Sameh Kodsi, Ismael El-Samahy, Hosein Haghighat, Mohammad Chehreghani, and Chaomin Luo. It was such a nice pleasure to learn many things from their cultures and values; they added another spice to my life. The continuous motivation from my friends in México and Waterloo who always cheered me up and made me smile is also appreciated. I also offer a sincere acknowledgment to Fr. Bob Liddy for all his blessings.

A bouquet of roses to Prof. Sukesh Ghosh and lovely Mrs. Nandita Ghosh for their kindness and support, and for teaching me important lessons about life. I discovered a treasure in your words and heart. Mysterious events happen in life, and I do believe that our encounter is one of them.

I wish I could put all the stars in the Universe in a vault to express with each one of them my love for my wonderful parents and family. Thank you for the best gift of my life and for making my dream come true. Nothing would have been possible without your support and love.

I am grateful for the scholarship granted by CONACyT México.

Dedication

This thesis is dedicated to all my family, and to the other part of my life who is yet to come...

Contents

List of Figures

List of Tables

List of Terms

Acronyms:

AMPL	:	A Modeling Language for Mathematical Programming
ATC	:	Available Transfer Capability
AVR	:	Automatic Voltage Regulator
CP	:	Cutting Planes
CPF	:	Continuation Power Flow
DM	:	Direct Method
EMS	:	Energy Management System
GRG	:	Generalized Reduced Gradient
HB	:	Hopf Bifurcation
IPM	:	Interior-point Method
KKT	:	Karush Kuhn Tucker
LIB	:	Limit-induced Bifurcation
LIDB	:	Limit-induced Dynamic Bifurcation
LISB	:	Limit-induced Static Bifurcation
LMP	:	Locational Marginal Price
LP	:	Linear Programming
MCP-OPF	:	Mixed Complementarity Constrained Optimal Power Flow
MSV	:	Minimum Singular Value
NLP	:	No Linear Programming
OPF	:	Optimal Power Flow
OS	:	Optimality Solution
SA	:	Security Assessment
SC-OPF	:	Security-constrained Optimal Power Flow
SDP	:	Semidefinite Programming
SIB	:	Singularity-induced Bifurcation
SLL	:	Switching Loadability Limit
SNB	:	Saddle-node Bifurcation

SSI	:	System Security Index
SVD	:	Singular Value Decomposition
SW	:	Social Welfare
UWPFLOW	:	University of Waterloo Power Flow
VS	:	Voltage Stability
VSC-OPF	:	Voltage-Stability-constrained OPF

Chapter 1

Introduction

1.1 Research Motivation

Among the different challenges faced by market and system operators, maintaining system security has become one of the main concerns in the wake of privatization and deregulation around the world. The new structure of the power industry has pushed power systems to be operated even closer to their limits, due to market pressures or physical limitations in the transmission network. Thus, system operators are demanding tools that allow them to make fast and effective decisions, in order to prevent the power system from being operated close to its stability limits, and at the same time generate adequate pricing signals for the market participants.

This challenge has motivated researchers to come up with Optimal Power Flow (OPF) models that better represent power system security in electricity markets. Particular interest has been given to the incorporation of voltage stability (VS) constraints in the OPF [1], since this phenomena is believed to be directly associated with many major blackouts experienced around the world during the past decade [2–4]. Consequently, different OPF models with an emphasis on system security have been proposed, such as Security-constrained OPFs (SC-OPFs) and VS-constrained OPFs (VSC-OPFs). However, further research to improve these models and the

corresponding solution techniques is needed, since the large computational burden of these models in the solution of real systems is still a problem. Thus, this thesis elaborates on the development of an enhanced VSC-OPF model, and a robust and efficient solution technique that can be used in realistic systems.

Determining the maximum power system loadability is very important in order to design preventive actions that help keep the system secure even in the worse contingency scenario (N-1 security criterion). The OPF-based Direct Method (OPF-DM) is a very flexible and efficient optimization technique that has been used to carry out this task [5, 6]. However, the theoretical background that supports the use of this model has not been fully addressed in the literature. Therefore, a full theoretical and numerical analysis, is presented in this thesis to formally prove the equivalency of OPF-DM and Continuation Power Flow (CPF) techniques to determine the maximum power system loadability.

The SC-OPF, VSC-OPF, and OPF-DM models have been developed using different optimization techniques, such as multiobjective optimization [1], successive linear programming [7], and Interior-point Method (IPM) [8]. These techniques have become a powerful tool in power engineering to, for example, minimize costs in an electricity market or to determine/prevent insecure operating conditions of a power system. Semidefinite Optimization (SDP) is a very active research area in mathematical optimization, and it has been applied to hydrothermal coordination and power dispatch problems [9,10]. However, the particular characteristics of SDP, which could be useful in solving VSC-OPFs have not yet been studied. Therefore, this subject is investigated here to determine whether SDP can be applied to the solution of the VSC-OPF problem.

1.2 Literature Review

One of the main objectives of any system or grid operator is to operate the electrical power system at the lowest cost, while guaranteeing system security. In order

to achieve this objective, the incorporation of advanced large-system analysis, optimization techniques and control technology in an Energy Management System (EMS) is required. The EMS is a large and complex hardware-software system used by the grid or system operator to perform on-line monitoring, assessment, and optimizing functions for the network, to prevent or correct operational problems while considering its most economic operation [11].

Security Assessment (SA) and optimization techniques are becoming a unified mathematical problem in modern power system operations [11, 12]. On the one hand, new models to appropriately and efficiently represent power system security are required. On the other hand, rapid optimization techniques to deal with very large and highly nonlinear models are also needed. Thus, researchers have been studying optimization methods to determine optimal control parameters guaranteeing certain security margins, particularly to avoid voltage collapse.

1.2.1 Voltage Stability

VS has become rather important in modern power systems, due to the fact that systems are being operated close to their security limits, as demonstrated by many recent major blackouts which can be directly associated with VS problems [13]. Furthermore, the implementation and application of open market principles have exacerbated this problem, since security margins are being reduced to respond to market pressures [14–16]. Consequently, the prediction, identification and avoidance of voltage instability points play a significant role in power systems planning and operation. Nonlinear phenomena, particularly Saddle-node Bifurcations (SNBs) and Limit-induced Bifurcations (LIBs), have been shown to be directly associated with VS problems in power systems [13]. Other types of bifurcations in power systems, such as Hopf Bifurcations (HB), associated with oscillatory instabilities [17], and Singularity-induced Bifurcations (SIB), associated with differential-algebraic models [13, 18, 19], have not been shown in practice to be directly related to VS problems [13], therefore, these bifurcations are not addressed in this thesis.

CPF and OPF-DM are two different techniques that are used to compute VS margins, i.e., the distance to an SNB or a particular LIB from the current loading point. The most widely used method is the CPF [20], which is a technique that consists of increasing the loading level until a voltage, current, or VS limit is detected in a power flow model. CPF is based on a predictor-corrector scheme to find the complete equilibrium profile or bifurcation manifold (PV curve) of a set of power flow equations, with respect to a given scalar variable. This scalar parameter is typically referred to as the bifurcation parameter or loading factor, as it is used to model changes in system demand [20, 21]. In [22], it is shown that this method can be viewed as a Generalized Reduced Gradient (GRG) approach for solving a maximum loadability optimization problem.

The OPF-DM is an optimization-based method that consists of maximizing the loading factor, while satisfying the power flow equations, bus-voltage, generators' reactive power limits, and other operating limits of interest (e.g., transmission-line thermal limits) [23, 24]. A variety of OPF models based on the OPF-DM have been proposed; for example, the authors in [1, 25, 26] propose a multiobjective OPF for maximizing both the social welfare and the loading factor. This type of optimization problem can be solved by means of IPMs, which have been shown to be computationally efficient for power system studies [27].

An important difference between the CPF and the most popular implementations of the OPF-DM is that, in the CPF, the voltage is kept constant at generation buses while their reactive power output is within limits (PV bus model). In the "standard" OPF-DM, generator voltages and reactive powers are allowed to change within limits, so that "optimal" operating conditions are obtained. These different approaches may lead to different solutions; an interesting discussion about this issue can be found in [15]. An OPF-DM model that is shown empirically to produce similar results to the CPF approach is presented and discussed in [6], where PV buses are modeled using complementarity constraints. The latter are shown here to be particularly important in demonstrating the equivalency of CPF and OPF-DM approaches. The use of complementarity constraints for representing generators'

limits is also discussed in [5], where an interesting analysis of the loadability surface of a power system is presented. This thesis presents a detailed theoretical analysis of the OPF-DM, demonstrating its "equivalency" with CPF approaches.

1.2.2 OPF-based Auction Models

OPFs have become one of the most widely used market tools in the electricity industry, particularly in planning, real-time operation, and electricity market auctions. New challenges have arisen with the introduction of competitive market principles in electricity markets that have pushed power systems to be operated closer to their stability limits in order to respond to market pressures. One of these challenges is the proper representation of power system security in traditional OPF-based auction models to guarantee reliable operations at reasonable electricity prices. Furthermore, with the lack of investment in and development of new transmission lines, and the increase in power transactions in a competitive electricity market, these challenges have become more relevant for market and system operators.

The objective of the present research is to develop OPF-based auction models that are computationally robust and can properly represent system security, so that these can be used in a market/system operating environment [12, 28, 29]. Thus, different approaches to represent system security limits in the OPF-based auction models have been proposed in the literature [30–34], so that the optimal solution guarantees a secure power dispatch. These OPFs have evolved from "classical" optimization models with simple lower and upper bounds in some of the operating constraints (e.g., bus voltage and reactive power limits [35]), to more sophisticated models such as the VSC-OPFs, which incorporate highly nonlinear constraints derived from traditional VS analysis (e.g., [34]).

The OPF models which look for optimal control settings in the pre-contingency state to prevent violations in the post-contingency state are commonly referred to as SC-OPFs [36]. An example of a SC-OPF model can be found in [35], where the

authors propose an OPF iterative technique that searches for secure voltage levels, which meet the bus voltage and reactive power limits after any single outage. The authors in [37, 38] put emphasis on secure generation schedules to prevent transmission lines from overloading. The authors in [39] propose the use of line outage distribution factors to formulate contingency constraints in the SC-OPF. An interesting approach of a linear SC-OPF, which includes bus voltage magnitudes and reactive power, is proposed in [40]; the model is formulated using graph theory. The main disadvantage of these models is that the operating constraints are calculated off-line; therefore, these constraints may impose a more restrictive operative region that does not necessarily reflect actual security levels, yielding improper market signals [1, 41]. Furthermore, the condition of voltage collapse is not well represented in any of these models.

The aforementioned disadvantages led to the development of VSC-OPFs, which include constraints that better represent VS limits (e.g., [1]). These models have been shown to yield more "relaxed" auction models, providing higher transaction levels and better electricity prices while guaranteeing proper system security levels. Thus, based on the idea of maximizing the distance to voltage collapse using optimization techniques, the authors in [14, 31, 42] propose a second set of power flow equations and associated security limits to represent a "critical" operating point associated with a voltage collapse condition. In this case, the objective is an optimal dispatch that is secure for both the current and critical operating conditions. Multiobjective optimization techniques to deal with both market and system security scenarios in the OPF have been proposed in [33]. In this context, the authors in [1, 26, 43] propose VSC-OPF models based on multiobjective optimization to optimize active and reactive power dispatch while maximizing voltage security. A second set of power flow equations to represent a critical operating condition is used in these papers. The problem with this approach is choosing proper values for the weighting factors in the multiobjective function; furthermore, the number of constraints practically doubles, making it computationally impractical. Consequently, other approaches have been proposed to reduce the number of constraints and to

make them more practical. One method consist of the use of VS indices (VSI) to represent proximity to voltage collapse in the OPF. Most of the proposed indices are based upon small perturbations in the load, loading margins, or the monitoring of some variables whose deviations at the collapse point can be predicted, such as the Available Transfer Capability (ATC), tangent vector indices, or reactive power indices [23, 30, 44–52].

The use of the minimum singular value (MSV) of the power flow Jacobian has been also proposed as a VSI for VS assessment [44, 45], since this index tends to become zero at the voltage collapse point. Thus, the authors in [34, 53] incorporate this index into the OPF as a VS constraint to guarantee a minimum distance to voltage collapse. Approximate derivatives are required during the solution process of this VSC-OPF, however, which may lead to convergence problems. The main disadvantage of available VSC-OPF models is that they present significant computational problems, which render them impractical. This thesis focuses on this particular issue by proposing novel solution techniques, so that VSC-OPFs can be better applied in practice.

1.3 Objectives

The following are the main objectives of this thesis, concentrating on the application of optimization techniques to VS analysis, and on the development of practical methods to solve VSC-OPFs:

1. Demonstrate that a solution of the OPF-DM correspond to either an SNB or LIB point of a power flow model.
2. Propose practical solution methods to solve a MSV-based VSC-OPF, so that it can be applied to more "realistic" systems.
3. Implement and test the proposed VSC-OPF solution technique using "standard" mathematical optimization tools.

4. Study the possible application of SDP to solve the VSC-OPF.

1.4 Thesis Outline

This thesis is organized into six chapters and one appendix as follows:

Chapter 2 presents a review of the main concepts of VS analysis and optimization techniques of interest in this thesis. It describes the models used in nonlinear theory for the characterization of VS in bifurcation analysis. Then, a brief introduction to power systems security assessment is presented, followed by a discussion of the most recently proposed VSC-OPF-based auction models. This chapter also summarizes the primal-dual IPM, and the basis of SDP.

Chapter 3 presents a comprehensive theoretical study of the OPF-DM. This work consist of reordering the the Karush-Kuhn-Tucker (KKT) conditions for optimality at the solution of the OPF-DM, so that the transversality conditions for SNB and LIB in bifurcation theory can be derived. The analytical results are further illustrated with numerical examples that show this optimization method yields equivalent maximum loading points as the CPF.

Chapter 4 describes the development of a solution technique for the MSV-based VSC-OPF, which is based on the SVD of the power flow Jacobian, plus an iterative solution process. The proposed model and solution technique is tested using two realistic test systems and compared with both a previously proposed method and a SC-OPF.

Chapter 5 presents an optimization method based on the primal-dual IPM and cutting planes (CP) to solve the MSV-based VSC-OPF. The proposed solution technique is first described, and then several simulations are carried out to study its performance. This is followed by numerical examples and a comparison with the proposed technique in Chapter 4. Finally, it presents an analysis of the possible application of SDP to the solution of the same VSC-OPF model.

Chapter 6 summarizes the conclusions and main contributions of this thesis, as well as discusses possible future work.

Finally, Appendix A presents a brief description of the test systems, and provides the data of the test systems.

Chapter 2

Background Review

2.1 Introduction

This chapter presents a review of the concepts, models, and tools related to the research work presented in this thesis. It first discusses the modeling and analysis of VS, using bifurcation theory, and also the tools used for VS assessment, as well as the use of these concepts and tools for power system security analysis. The most recent SC-OPFs and VSC-OPFs models are also discussed here, highlighting advantages and disadvantages of each one. The primal-dual IPM algorithm, and SDP are summarized in this chapter as well.

2.2 Voltage Stability Analysis

Voltage stability is associated with the capability of a power system to maintain steady acceptable voltages at all buses, not only under normal operating conditions, but also after being subjected to a disturbance [54]. It is a well established fact that voltage collapse in power systems is associated with system demand increasing beyond certain limits, as well as with the lack of reactive power support in the

system caused by limitations in the generation or transmission of reactive power. System contingencies such as generator or unexpected line outages exacerbate, if not trigger, the VS problems [13, 55]. Usually, VS analysis consists of determining the system conditions at which the equilibrium points of a dynamic model of the power system merge and disappear; these points have been associated with certain bifurcations of the corresponding system models [13].

Voltage stability is an important problem in modern power systems due to the catastrophic consequences of this phenomena. Thus, determining the largest possible margin to the point of voltage collapse is becoming an essential part of new electricity markets. These markets are also seeking ways to reduce operating costs; as a matter of fact the application of open market principles has resulted in stability margins being reduced to respond to market pressures [14, 15]. In an open electricity market, voltage security requirements are typically associated with transmission congestion and its associated high prices [16].

2.2.1 Effects of Increasing Demand

A slow increase in the system demand, such as that due to normal daily load variations, can have negative effects on VS. If any small increase in loading demand occurs, the reactive power demand will be greater than supply, and the voltage will decrease. As the voltage decreases, the difference between reactive power supply and demand increases, and the voltage falls even more until it eventually falls to a very small value. This phenomenon is generally known as voltage collapse. The two terms of voltage collapse are total voltage collapse and partial voltage collapse. The former means that the collapse in permanent; the latter is used when the voltage is below some technical acceptable limit and does not correspond to system instability but an emergency state [56].

It is well-known that an excess of reactive power results in voltage increase, while a deficit of reactive power results in a voltage decrease. Thus, consider the equilibrium point s shown in Figure 2.1. If one assumes that there is small negative

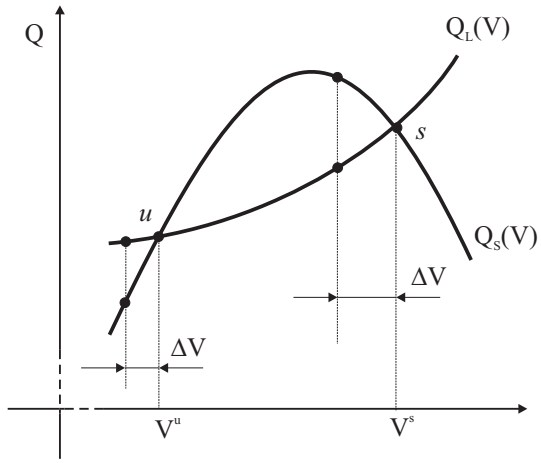

Figure 2.1: $Q_S(V)$ and $Q_L(V)$ characteristics and equilibrium points

voltage disturbance ΔV, the reactive power supply $Q_S(V)$ would be greater than the reactive power demand $Q_L(V)$. This excess of reactive power tends to increase the voltage until it returns to point s. If the disturbance produces an increase in voltage, the resulting deficit in reactive power will force the voltage to decrease and return to point s. Thus, one can conclude that the equilibrium point s is stable. If one now considers the equilibrium point u under the same small negative disturbance, the reduction in voltage will produce a deficit of reactive power with $Q_S(V) < Q_L(V)$, which will produce a further decrease in voltage. As a result of both the voltage and reactive power being reduced, the voltage will not recover; therefore, the equilibrium point u is unstable [56]. Notice that if the $Q_L(V)$ characteristic is lifted upward, the equilibrium points u and s tend to move toward each other until they eventually merge and disappear, which is a phenomenon explained using bifurcation theory as explained below.

2.2.2 System Models

Power systems are typically modeled with nonlinear differential-algebraic equations (DAE), which are a class of nonlinear systems, as follows:

$$\begin{bmatrix} \dot{x} \\ 0 \end{bmatrix} = \begin{bmatrix} f(x, y, \lambda, p) \\ g(x, y, \lambda, p) \end{bmatrix} = F(z, \lambda, p) \tag{2.1}$$

where $x \in \mathbb{R}^{n_x}$ is a vector of state variables that represents the dynamic states of generators, loads, and system controllers; $y \in \mathbb{R}^{n_y}$ is a vector of algebraic variables that typically results from neglecting fast dynamics, such as load bus voltages magnitudes and angles; $z = (x, y) \in \mathbb{R}^{n_z}$; $\lambda \in \mathbb{R}^{+}$ stands for a slow varying "uncontrollable" parameter, typically used to represent load changes that move the system from one equilibrium point to another; and $p \in \mathbb{R}^{n_p}$ represents "controllable" parameters associated with control settings, such as Automatic Voltage Regulator (AVR) set points. The function $f : \mathbb{R}^{n_x} \times \mathbb{R}^{n_y} \times \mathbb{R}^{+} \times \mathbb{R}^{n_p} \mapsto \mathbb{R}^{n_x}$ is a nonlinear vector field directly associated with the state variables x, and representing the system differential equations, such as those associated with the generator mechanical dynamics; and $g : \mathbb{R}^{n_x} \times \mathbb{R}^{n_y} \times \mathbb{R}^{+} \times \mathbb{R}^{n_p} \mapsto \mathbb{R}^{n_y}$ represents the system nonlinear algebraic constraints, such as the power flow equations, and algebraic constraints associated with the synchronous machine model.

If the Jacobian $\nabla_y^T g(\cdot)$ of the algebraic constraints is invertible, i.e., nonsingular along a "solution path" of (2.1), the behavior of the system is mainly defined by the following Ordinary Differential Equation (ODE) model

$$\dot{x} = f(x, y^{-1}(x, \lambda, p), \lambda, p)$$

where $y^{-1}(x, \lambda, p)$ results from applying the Implicit Function Theorem to the algebraic constraints along the system trajectories of interest [22, 57]. The interested reader is referred to [58] for a detailed discussion when $\nabla_y^T g(\cdot)$ is not guaranteed to be invertible. This problem is associated with SIBs, which go beyond the scope of this thesis, since this phenomenon is not directly related to VS problems in practice [13].

Equilibrium points $z_o = (x_o, y_o)$ of (2.1) are defined by the solutions of the nonlinear equations:

$$F(z_o, \lambda_o, p_o) = \begin{bmatrix} f(x_o, y_o, \lambda_o, p_o) \\ g(x_o, y_o, \lambda_o, p_o) \end{bmatrix} = 0$$

It is important to highlight the fact that the system equilibria are in practice obtained from a subset of equations:

$$G(\hat{z}_o, \lambda_o, \hat{p}_o) = G|_o = 0 \quad \subset \quad F(z_o, \lambda_o, p_o) = F|_o = 0 \tag{2.2}$$

where $G|_o = 0$ stands for the power flow equations; $G \subset g$; $\hat{z}_o \in \mathbb{R}^{n_{\hat{z}}} \subset z$ is the set of voltage and angles at all buses as well as the reactive power of the generator (PV) buses; and $\hat{p}_o \in \mathbb{R}^{n_{\hat{p}}} \subseteq p$ usually represents the voltage levels and "base" active power injections at PV buses, "base" active and reactive power injections at load buses, transformer fixed-tap settings and other controller settings.

Power flow models have been used in practice for VS assessment, since these models form the basis for defining the actual system operating conditions [13]. However, one should be aware that the solutions of the power flow equations do not necessarily correspond to system equilibria, since a solution of $G|_o = 0$ does not imply that $F|_o = 0$; however, in practice, this issue tends to be ignored.

2.2.3 Bifurcation Analysis

Bifurcation theory yields concepts and tools to classify, study, and give qualitative and quantitative information about the behavior of a nonlinear system close to bifurcation or "critical" equilibrium points as system parameters change [59]. The parameters are assumed to change "slowly", so that the system can be assumed to "move" from equilibrium point to equilibrium point by these changes (quasi-static assumption). Hence, bifurcation analysis is usually associated with the study of equilibria of the nonlinear system model [13].

In power systems, SNBs and some types of LIBs are basically characterized by the local merging and disappearance of power flow solutions as certain system parameters, particularly system demand, slowly change; this phenomena has been associated with VS problems [13]. These kinds of bifurcations are also referred to in the technical literature as fold or turning points.

Saddle-node Bifurcations

These types of codimension-1 (single parameter), generic bifurcations occur when two equilibrium points, one stable and one unstable in practice, merge and disappear as the parameter λ slowly changes, as illustrated in the PV curves of Figures 2.2 and 2.3. In these figures, V_{G_i} and Q_{G_i} stand for a generator i's terminal voltage magnitude and reactive power, respectively. Mathematically, the SNB point for the power flow model (2.2) is a solution point $(\hat{z}_c, \lambda_c, \hat{p}_o)$ where the Jacobian $\nabla_{\hat{z}}^T G|_c$ has a simple zero eigenvalue, with nonzero eigenvectors [60, 61]. The following *transversality conditions* can be used to characterize and detect SNBs [22]:

$$\nabla_{\hat{z}}^T G|_c \hat{v} = \nabla_{\hat{z}} G|_c \hat{w} = 0 \tag{2.3}$$

$$\nabla_\lambda G|_c \, \hat{w} \neq 0 \tag{2.4}$$

$$\hat{w}^T \left[\nabla_{\hat{z}}^{2^T} G|_c \hat{v} \right] \hat{v} \neq 0 \tag{2.5}$$

where $\hat{v}$ and $\hat{w} \in \mathbb{R}^{n_{\hat{z}}}$ are unique normalized right and left eigenvectors of the Jacobian $\nabla_{\hat{z}}^T G|_c$. The first condition implies that the Jacobian matrix is singular; the second and third conditions ensure that there are no equilibria near $(\hat{z}_c, \lambda_c, \hat{p}_o)$ for $\lambda > \lambda_c$ (or $\lambda < \lambda_c$, depending on the sign of (2.5)). Note that the subscript c is used throughout this thesis to denote a bifurcation point.

Limit-induced Bifurcations

These types of codimension-1 (single parameter), generic bifurcations in power systems were first studied in detail in [62], and can be typically encountered in these

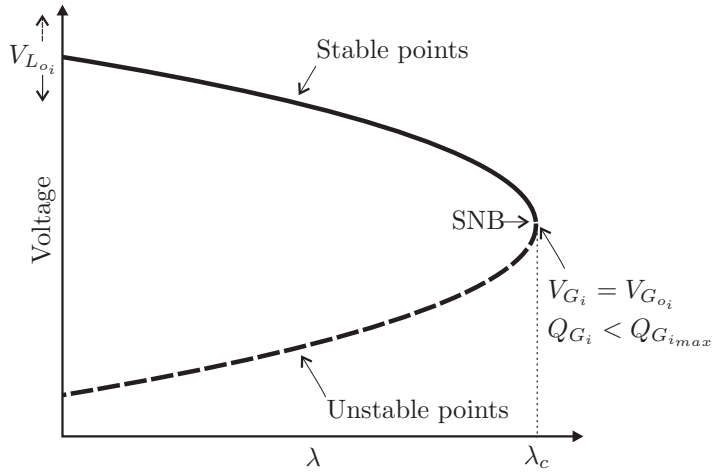

Figure 2.2: SNB without Q_G limits.

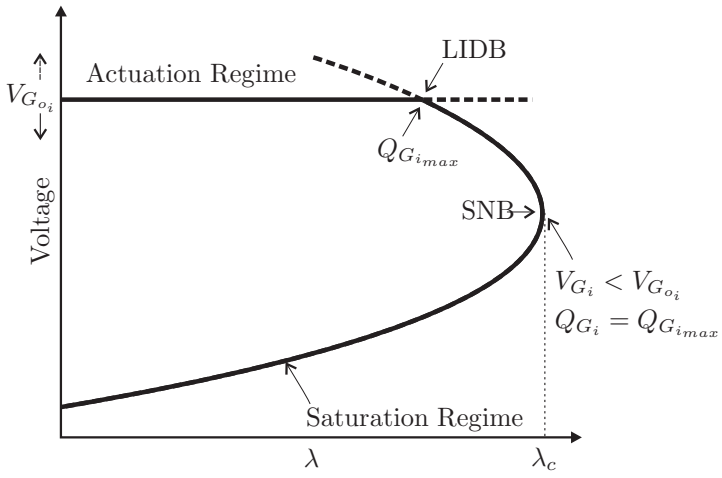

Figure 2.3: Stable limit point (LIDB) followed by a SNB.

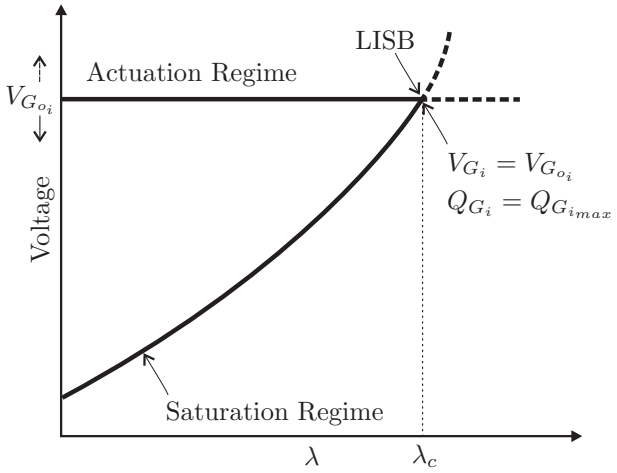

Figure 2.4: Unstable limit point (LISB).

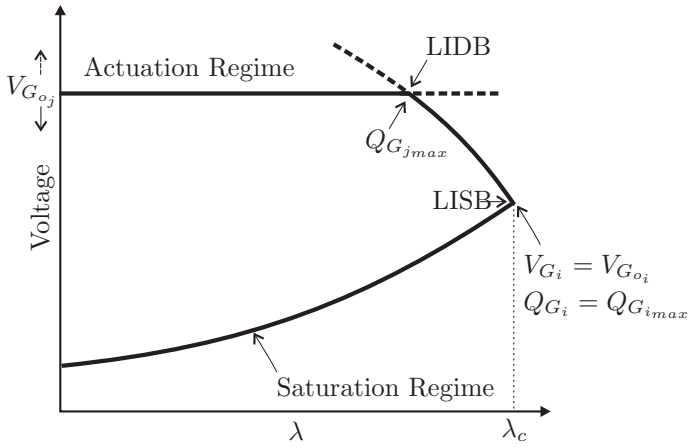

Figure 2.5: LISB preceded by a LIDB.

systems. Hence, as the load increases, reactive power demand generally increases and reactive power limits of generators or other voltage regulating devices are being reached. These bifurcations result in reduced VS margins, and in some cases the operating point "disappears" causing a voltage collapse [13], as illustrated in Figures 2.3-2.5. Mathematically, the LIBs associated with power flow models are solution points $(\hat{z}_c, \lambda_c, \hat{p}_o)$ where all the eigenvalues of the corresponding Jacobian $\nabla^T_{\hat{z}} G|_c$ have nonzero real parts, i.e., the power flow Jacobian is nonsingular [63]. The authors in [5] refer to this bifurcations as Switching Loadability Limit (SLL), to emphasize the absence of the singularity condition and their relation to reactive power limits being reached.

These bifurcations are divided into two types, namely, Limit-induced Dynamic Bifurcations (LIDB), and Limit-induced Static Bifurcations (LISB) [58]. In the case of LIDBs, the equilibrium points continue to exist after being reached as the bifurcation parameter λ changes, as illustrated in Figures 2.3 and 2.5. On the other hand, LISBs are somewhat similar to SNBs in the sense that these correspond to points at which two solutions merge and disappear as the bifurcation parameter λ changes, as depicted in Figure 2.4. Thus, LISBs also are associated with maximum loadability margins in power flow models.

In general, the limits that trigger LIBs can be categorized into three basic types of limits, namely, actuation limits, state limits and switching limits [63]. The actuation limits appear when certain variables, which are functions of some of the state variables, encounter a limit. These limits do not directly affect the state variables but the overall dynamics, and they can be modeled through the use of actuation functions. In power systems models, actuation limits typically depend on only one state variable at a time, and one of these inequalities becomes an equality upon encountering a limit. The state limits have a direct effect on the state variables and occur when a state reaches its limit. The result in the system dimension is that it drops by one, since the state variable becomes a constant in the model. These kinds of limits can be modeled by setting the state derivative equal to zero when the limits are reached. Finally, the switching limits are followed by pre-established

actions (e.g., relaying mechanisms or protective limiters in the physical system), which might result in a change in the whole system, and consequently in the states. These limits can be modeled, for instance, by introducing certain binary variables that represent the internal logic of a relay element.

For the power flow model, actuation limits can be directly associated with LIBs. Therefore, this thesis focuses on these types of limits to analyze LIBs, using the following representation that results from the proper ordering of the power flow equations (2.2), and with similar notation to the one proposed in [63]:

$$G(\hat{z}, \lambda, \hat{p}) = \begin{bmatrix} \hat{g}(\tilde{z}, \hat{r}, \lambda, \hat{p}) \\ \hat{r} - \hat{s}(\tilde{z}, \lambda, \hat{p}) \end{bmatrix} = 0 \tag{2.6}$$

where $\tilde{z} \in \mathbb{R}^{n_{\tilde{z}}}$, $\hat{r} \in \mathbb{R}^{n_{\hat{r}}}$, $\hat{z} = (\tilde{z}, \hat{r})$, and the actuation limits are modeled as:

$$\hat{r}_i = \begin{cases} \hat{r}_{i_{min}}, & \text{if } \hat{s}_i(\tilde{z}, \lambda, \hat{p}) < \hat{r}_{i_{min}} \\ \hat{s}_i(\tilde{z}, \lambda, \hat{p}), & \text{if } \hat{r}_{i_{min}} \leq \hat{s}_i(\tilde{z}, \lambda, \hat{p}) \leq \hat{r}_{i_{max}} \\ \hat{r}_{i_{max}}, & \text{if } \hat{s}_i(\tilde{z}, \lambda, \hat{p}) > \hat{r}_{i_{max}} \end{cases} \tag{2.7}$$

Since in power flow models, LIBs of interest are typically associated with generators reaching their maximum reactive power limits, at a LIB point $(\hat{z}_c, \lambda_c, \hat{p}_o) = (\tilde{z}_c, \hat{r}_c, \lambda_c, \hat{p}_o)$, the following two sets of equations apply:

$$G_a(\hat{z}_c, \lambda_c, \hat{p}_o) = \begin{bmatrix} \hat{g}(\tilde{z}_c, \hat{r}_c, \lambda_c, \hat{p}_o) \\ \hat{r}_{k_c} - \hat{s}_k(\tilde{z}_c, \lambda_c, \hat{p}_o) \quad \forall k \neq i \\ \hat{r}_{i_c} - \hat{s}_i(\tilde{z}_c, \lambda_c, \hat{p}_o) \end{bmatrix} = 0 \tag{2.8}$$

$$G_b(\hat{z}_c, \lambda_c, \hat{p}_o) = \begin{bmatrix} \hat{g}(\tilde{z}_c, \hat{r}_c, \lambda_c, \hat{p}_o) \\ \hat{r}_{k_c} - \hat{s}_k(\tilde{z}_c, \lambda_c, \hat{p}_o) \quad \forall k \neq i \\ \hat{r}_{i_c} - \hat{r}_{i_{max}} \end{bmatrix} = 0 \tag{2.9}$$

where (2.8) corresponds to the system equations "before" a limit is reached, and (2.9) represents the system "after" a limit is reached as λ increases. These system conditions can be referred to as the system in actuation regime and in saturation

regime, respectively, as depicted in Figures 2.3-2.5. Notice that a "critical" solution or bifurcation point must satisfy both sets of equations, and that the difference between (2.8) and (2.9) is only the equation corresponding to actuation limit i, since a LIB occurs when a single generator i reaches its maximum reactive power limit.

The transversality conditions for LIBs may then be defined as follows [63]:

1. $G_a|_c = G_b|_c = 0$
2. Jacobians $J_a^i = \nabla_{\hat{z}}^T G_a|_c$ and $J_b^i = \nabla_{\hat{z}}^T G_b|_c$ have nonzero real parts, i.e.,
$$\det(J_a^i) \neq 0 \quad \text{and} \quad \det(J_b^i) \neq 0 \tag{2.10}$$
3. The index:
$$\alpha = \frac{\det J_a^i}{\det J_b^i} \neq 0 \tag{2.11}$$
defines the type of LIB; thus, $\alpha > 0$ for a LISB, and $\alpha < 0$ for a LIDB.

Chapter 3 concentrates on demonstrating that the transversality conditions (2.3)-(2.5) for an SNB point, and (2.10)-(2.11) for a LIB point, can be derived from the optimality conditions of the OPF-DM described in Section 2.4.2.

2.3 Power System Security

Power system security can be defined as the ability of the system to survive any credible contingency without serious consequences [16, 64]. NERC defines reliability as the degree to which the performance of electrical system could result in power being delivered to consumers within accepted standards and desired amounts. NERC's definition of reliability encompasses two concepts: adequacy and security. *Adequacy* is the ability of a power system to properly supply consumers' electrical power and energy requirements at all times. *Security* is defined as the ability of a power system to withstand sudden disturbances [65].

System security is composed of three major functions that are carried out in a control center:

1. *System Monitoring:* Provides the operators of the power system with up-to-date information on the conditions on the power system.

2. *Contingency Analysis:* The results of this analysis allow systems to be operated defensively.

3. *SC-OPF:* A contingency analysis is combined with an OPF, so that no contingencies result in limit violations. A SC-OPF model is discussed in detail in Section 2.5.2.

Transmission-line failures cause changes in the flows and voltages on transmission equipment remaining connected to the system. Therefore, the analysis of transmission failures requires methods to predict these flows and voltages so as to be sure they are within their respective limits. One way to gain speed in the solution of a contingency analysis procedure is to use an approximate model of the power system. For many systems, the use of DC load flow models provides adequate capability. In such systems, the voltage magnitudes may not be of great concern, and hence the DC load flow provides sufficient accuracy with respect to the megawatt flows. For other systems, when voltage is a concern, a full AC load flow analysis is required [36].

2.3.1 Security Assessment

Security Assessment is the process by which the power system static security level is determined, by means of detecting limit violations in its pre-contingency or post-contingency operating states [11, 64]. The first function in this process is violation detection in the actual operating state (e.g., monitoring actual flows or voltage limits). The second is contingency analysis, which identifies potential emergency

operating states, through iterative simulations on the power system in the context of what would happen if certain outages occur [11,64]. The second function implies several difficulties in practice; for instance, how to handle the power system, determine which contingency scenarios are more likely to happen, and speed up the process, since the solution of many contingency cases requires a significant computational effort. In the same manner, the determination of the VS margin consists of finding how much the system can be stressed in a particular load direction from its current operating state and yet remain secure [16].

Two alternative definitions of SA exist, namely, direct and indirect. In direct SA, the objective is to estimate the probability of the power system changing from the normal state to the emergency state. In indirect SA, one defines the system "security" variables that must be maintained within limits to provide adequate reserve margins [64].

2.3.2 Available Transfer Capability

The ATC is defined as "a measure of the transfer capability remaining in the physical transmission network for further commercial activity over and above already committed uses". Mathematically, ATC is defined as [66]:

$$\text{ATC} = \text{TTC - TRM - ETC}$$

where:

- *Total Transfer Capability* (TTC): Is the maximum loading level of the system considering an N-1 contingency criterion. The TTC is defined as:

$$\text{TTC} = \min\{P_{I_{\text{lim}}}^{\text{max}}, P_{V_{\text{lim}}}^{\text{max}}, P_{S_{\text{lim}}}^{\text{max}}\} \tag{2.12}$$

  where I_{lim}, V_{lim} and S_{lim} represent the thermal, voltage magnitude, and stability limits, respectively [67].

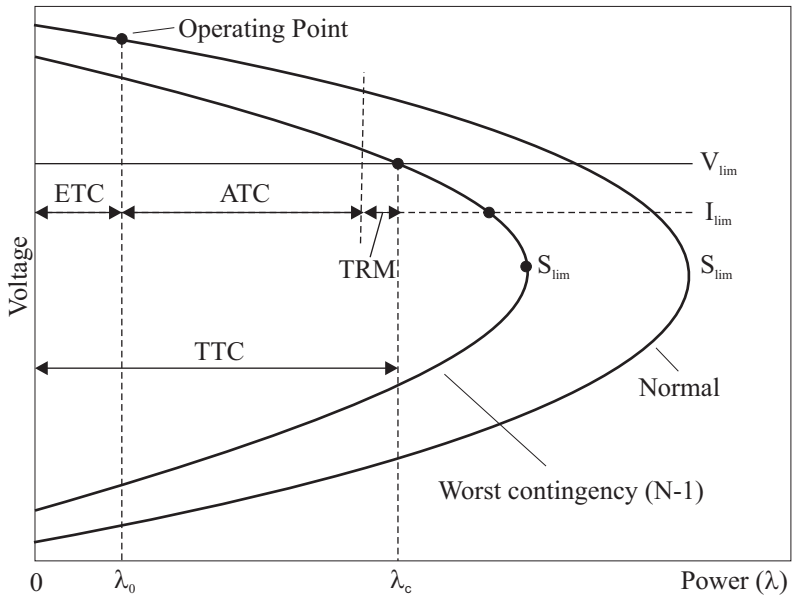

Figure 2.6: ATC evaluation with dominant voltage limits.

- *Transmission Reliability Margin* (TRM): This measure considers uncertainty to account for other contingencies; it is usually assumed to be a fixed value (e.g., WECC's 5% of TTC). The authors in [68], propose a formula that calculates the TRM based on a probabilistic approach for various uncertainties.

- *Existing Transmission Commitments* (ETC): Basically, represents the current loading level.

- *Capacity Benefit Margin* (CBM): is a reserve made by load-serving entities to guarantee access to generation from different interconnected systems to meet their generation reliability requirements [69]. This could be considered to be included in the ETC.

2.3.3 Loading Margin

The *maximum loading margin* can be defined as the distance between a given operating point and a maximum loading condition reached in a particular pattern of

load increase. This margin is the most basic and widely accepted index of voltage collapse [13]. Mathematically, the loading margin for a typical power flow model is defined as follows:

$$\lambda = \lambda_c - \lambda_o$$

where λ_c is the maximum loading of the system at a given limit, either the bus voltage limit (V_{lim}), thermal limit (I_{lim}), or VS limit (S_{lim}), which corresponds to an SNB or LIB point in the PV curve of a power flow model [67], and λ_o stands for the base or current operating point. The parameter λ typically represents variations in load and generation schedules as follows:

$$P_G = P_{G_o} + (\lambda + K_G)P_S \quad (2.13)$$

$$P_L = P_{L_o} + \lambda P_D \quad (2.14)$$

$$Q_L = Q_{L_o} + \lambda K_L P_D \quad (2.15)$$

where P_{G_o}, P_{L_o} and Q_{L_o} stand for the "base" generation and load levels, thus defining an "initial" operating point; K_G is a variable used to represent a distributed slack bus; and K_L is a parameter used to represent a load with a constant power factor. P_S and P_D are used here to define the generation and load "directions", respectively, needed to compute loading margins and PV curves. All loads are typically assumed to have constant power factors.

Figure 2.6 depicts the computation of ATC based on the loading margin in terms of PV curve typically used in VS studies [13]. In this analysis, system stability is assumed to be represented by VS margins, which is an adequate approximation, since blackouts are typically associated with VS problems. The "external" PV curve corresponds to the system under normal operating conditions and assuming certain dispatch, whereas the "internal" PV curve is the system under the worst single contingency for the assumed system conditions. Observe that the voltage limits in this example are assumed to define the lowest loading level corresponding to the TTC. The current operating point defines the ETC (and CBM), any point before the ATC is considered a "safe" operating point, and the TRM is a small

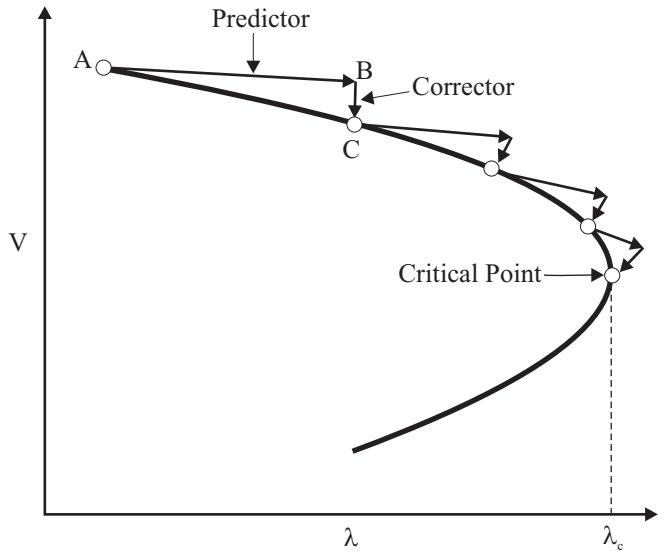

Figure 2.7: Predictor-corrector scheme in the CPF.

margin away from any operating point at risk of collapse. Hence, based on the use of PV curves, the ATC terms can be defined as [70]:

$$\begin{aligned} \text{TTC} &= \sum P_{L_o} + \lambda_c \sum P_D \\ \text{ETC} &= \sum P_{L_o} \\ \text{TRM} &= 0.05 \text{ TTC} \end{aligned}$$

The most widely used techniques to find the maximum loading factor λ_c are the CPF and the OPF-DM, which are described in Section 2.4.

2.4 Voltage Stability Analysis Tools

2.4.1 Continuation Power Flow (CPF)

The algorithm of the CPF method simply considers a set of power flow equations reformulated to include a load parameter λ, basically using the generation and load

directions shown in (2.13)-(2.15). The power flow model in this technique is solved for automatic changes in λ using a predictor-corrector scheme that remains well-conditioned at and around the critical point, i.e., the maximum loadability point λ_c.

Figure 2.7 illustrates the iterative process of a typical CPF technique. The algorithm starts from a known solution A which corresponds to a power flow solution at the current loading point. Then, it uses a tangent predictor to estimate a solution B corresponding to an increased value of the load parameter, and it finally uses a "corrector" to find the exact solution C using a classical Newton-Raphson technique [20]. This method allows one to trace the voltage profile of a power flow model, also known as an equilibrium profile or bifurcation manifold. Hence, it allows for the calculation of security indices such as the ATC.

The advantage of this method is that additional information regarding the behavior of some system variables can be obtained during the solution process. This information, then, can be used as indices to predict proximity to a voltage collapse. However, although this algorithm is very robust, it is computationally expensive, especially for large systems with multiple limits [71].

UWPFLOW is a CPF research tool that allows one to trace PV curves and calculate λ_c values [72]. This tool is used in this thesis to obtain all the PV curves and VSI.

2.4.2 OPF-based Direct Method (OPF-DM)

Optimization methods can be used to compute maximum loadability points of power flow models, which are directly associated with SNBs and LISBs of the corresponding model equations, as initially proposed in [23]. Thus, based on the SNB and LIB definitions presented in Section 2.2.3, the bifurcation point directly corresponds to the solution of the following optimization model, as formally demon-

strated in Section 3.2:

$$\max_{\tilde{z},\hat{r},\lambda} \quad \lambda \tag{2.16a}$$

$$\text{s.t.} \quad \hat{g}(\tilde{z},\hat{r},\lambda,\hat{p}_o) = 0 \tag{2.16b}$$

$$\hat{h}(\tilde{z},\hat{r},\lambda,\hat{p}_o) = 0 \tag{2.16c}$$

$$\hat{r}_{min} \leq \hat{r} \leq \hat{r}_{max} \tag{2.16d}$$

where the nonlinear function $\hat{h}$ is used to represent the actuation limit equations introduced in (2.6), since in these optimization models the actuation limits are typically not represented explicitly, as illustrated below. The issue of how constraints (2.16c) are actually represented in this model, and the effect of this modeling on the solution of the optimization problem (2.16) is discussed in detail below. Note that (2.16d) basically corresponds to (2.7).

OPF-DM in Standard Form

For a typical power flow model, let $\tilde{z} = (\delta, V_L, K_G)$, $\hat{r} = (Q_G, V_G)$, and $\hat{p} = (P_S, P_D)$. In this case, δ stands for all the bus voltage phasor angles but one (slack bus); V_L and V_G correspond to the load and generator bus voltage phasor magnitudes, respectively, and Q_G represents the generator reactive power output. The variables P_S and P_D define the change in power generation and demand, as shown in (2.13)-(2.15).

Based on the aforementioned variable definition and if the actuation functions (2.16c) are omitted, the model can be restated as:

$$\max_{\substack{\delta,V_L,K_G \\ Q_G,V_G,\lambda}} \quad \lambda \tag{2.17a}$$

$$\text{s.t.} \quad \widehat{G}(\delta, V_L, K_G, Q_G, V_G, \lambda, P_S, P_D) = 0 \tag{2.17b}$$

$$Q_{G_{i_{min}}} \leq Q_{G_i} \leq Q_{G_{i_{max}}} \quad \forall i \in \mathcal{G} \tag{2.17c}$$

$$V_{G_{i_{min}}} \leq V_{G_i} \leq V_{G_{i_{max}}} \quad \forall i \in \mathcal{G} \tag{2.17d}$$

where $\widehat{G}$ stand for the classical active and reactive power balanced equations for each generator and load bus (two for every system bus), as defined in (2.6), i.e.,

$$P_{G_i} - P_{L_i} - \widehat{G}_p(\delta, V_L, V_G, G_{ij}, B_{ij}) = 0 \quad \forall i \in \mathcal{B} \tag{2.18}$$

$$Q_{G_i} - Q_{L_i} - \widehat{G}_q(\delta, V_L, V_G, G_{ij}, B_{ij}) = 0 \quad \forall i \in \mathcal{B} \tag{2.19}$$

P_{G_i}, P_{L_i}, and Q_{L_i} are defined in (2.13)-(2.15); G_{ij} and B_{ij} are the real and imaginary part of the bus admittance matrix, respectively; $\mathcal{G}$ is the set of indices of generating units; and $\mathcal{B}$ is the set of indices of network buses. Observe that $\widehat{G} \subset G$ in (2.2), since G contains some additional equations representing limits as per (2.6). It is also important to highlight the fact that in this optimization model no other limits such as load bus voltage magnitude limits, generator active power limits, or power transfer limits, which are typical operating limits considered in such OPF models, are represented here. The reason for this is that these are "hard" limits and not actuation limits, i.e., limits that basically define "undesirable" operating conditions which may be associated with system protections rather than system controls, and hence do not lead to LIBs. These limits would only clutter the theoretical analyzes presented in Chapter 3, without adding much to the discussions.

It has been shown that if no limits become active, the sufficient KKT optimality conditions evaluated at the solution point of (2.17) are equivalent to the transversality conditions (2.3) and (2.4) for SNBs [22]. However, it has not yet been formally shown that the third transversality condition (2.5) will also be met, which is an issue addressed in Chapter 3. It can also be argued that this model may provide a maximum loading point different from that obtained using the CPF technique if reactive power limits become active [6]. This is due to the fact that the objective of the optimization model (2.17) is to "optimize" the generator voltage and reactive power levels so that the loading factor is maximized. Hence, there is no guarantee that the voltage at generation buses would be maintained at a constant level while the reactive power output at such buses is within its limits. This is the typical representation of the generator voltage regulation controls in the power flow models used in CPF techniques.

If limits are considered, and the parameters P_S and P_D are free to change, the problem is transformed into an optimal active and reactive dispatch problem for the maximization of the loading margin. Indeed, other optimization problems can be derived from this concept, such as the maximization of the social welfare while ensuring a loading margin, as discussed in Section 2.5.2.

OPF-DM with Complementarity Constraints

An optimization model that has been empirically shown to yield the same SNB or LISB points as a CPF technique has been proposed in [6]. The authors in this paper propose an optimization model that is based upon the idea that many problems encountered in engineering, physics, or economics, which behave according to different rules under different circumstances, can be modeled using complementarity constraints because these constraints can be used to model a change in system behavior. Thus, the change from a PV to a PQ bus, when a generation reactive power limit is reached can be modeled using these type of constraints in the OPF problem as follows [73]:

$$\begin{aligned} 0 \leq (Q_{G_k} - Q_{G_{k_{min}}}) \perp V_{a_k} \geq 0 \\ \Rightarrow \ (Q_{G_k} - Q_{G_{k_{min}}}) V_{a_k} = 0 \end{aligned}$$

$$\begin{aligned} 0 \leq (Q_{G_{k_{max}}} - Q_{G_k}) \perp V_{b_k} \geq 0 \\ \Rightarrow \ (Q_{G_k} - Q_{G_{k_{max}}}) V_{b_k} = 0 \end{aligned}$$

where V_a and V_b are auxiliary, nonnegative variables that allow increasing or decreasing the generator voltage set point, depending on the state of Q_G. Thus:

$$\begin{aligned} \text{if } Q_{G_k} = Q_{G_{k_{min}}} \Rightarrow V_{a_k} \geq 0 \text{ and } V_{b_k} = 0 \\ \text{if } Q_{G_{k_{min}}} < Q_{G_k} < Q_{G_{k_{max}}} \Rightarrow V_{a_k} = V_{b_k} = 0 \\ \text{if } Q_{G_k} = Q_{G_{k_{max}}} \Rightarrow V_{a_k} = 0 \text{ and } V_{b_k} \geq 0 \end{aligned}$$

This yields the following Mixed Complementarity Problem (MCP) [6]:

$$\max_{\substack{\delta,V_L,K_G \\ Q_G,V_G,\lambda}} \quad \lambda \tag{2.20a}$$

$$\text{s.t.} \quad \widehat{G}(\delta, V_L, K_G, Q_G, V_G, \lambda, P_S, P_D) = 0 \tag{2.20b}$$

$$(Q_{G_k} - Q_{G_{k_{min}}})V_{a_k} = 0 \quad \forall k \in \mathcal{G} \tag{2.20c}$$

$$(Q_{G_k} - Q_{G_{k_{max}}})V_{b_k} = 0 \quad \forall k \in \mathcal{G} \tag{2.20d}$$

$$V_{G_k} = V_{G_{k_o}} + V_{a_k} - V_{b_k} \quad \forall k \in \mathcal{G} \tag{2.20e}$$

$$Q_{G_{k_{min}}} \leq Q_{G_k} \leq Q_{G_{k_{max}}} \quad \forall k \in \mathcal{G} \tag{2.20f}$$

$$V_{a_k}, V_{b_k} \geq 0 \quad \forall k \in \mathcal{G} \tag{2.20g}$$

where V_{G_o} is the generator voltage regulator set point, i.e., the generator terminal voltage level if Q_G, is within limits; and the constraints (2.20c)-(2.20e), associated with the auxiliary variables V_a and V_b, are used to model the actuation limits associated with the generator voltage regulators. Hence, in this model, $\tilde{z} = (\delta, V_L, K_G, V_G)$, $\hat{r} = (Q_G, V_a, V_b)$, $\hat{p} = (P_S, P_D, V_{G_o})$, and $\hat{g}$ and $\hat{h}$ are contained within constraints (2.20b)-(2.20e). The actual representation of these two vector functions is discussed in detail in Section 3.2.

2.5 Optimal Power Flow Models with Security Constraints

An independent system operator has to deal with the market participants by receiving their bids and offers, so that it can accommodate the necessary transactions to balance supply and demand while maintaining power system security. Typically, the system operator accomplishes these objectives through a cost minimization process based on an OPF. This section briefly discusses the most recent OPF models that include security constraints.

The first model represents system security by imposing limits on the transmission system power flows. The second makes use of a multiobjective optimization

technique and a second set of power flow equations to represent system security, whereas the third model uses the MSV of a power flow Jacobian to represent VS.

2.5.1 Security-Constrained OPF (SC-OPF)

The following optimization model, typically referred to as an SC-OPF, corresponds to a single-period auction model; the objective function in this case is social welfare, to ensure that generators maximize their income from power production, while loads minimize the prices paid for their power demand:

$$\max_{\substack{\delta,V_L,Q_G \\ V_G,P_S,P_D}} \quad \sum_{j\in\mathcal{D}} C_{D_j}P_{D_j} - \sum_{i\in\mathcal{G}} C_{S_i}P_{S_i} \tag{2.21a}$$

$$\text{s.t} \quad \widehat{G}(\delta, V_L, Q_G, V_G, P_S, P_D) = 0 \tag{2.21b}$$

$$P_{S_{i_{min}}} \leq P_{S_i} \leq P_{S_{i_{max}}} \quad \forall i \in \mathcal{G} \tag{2.21c}$$

$$P_{D_{j_{min}}} \leq P_{D_j} \leq P_{D_{j_{max}}} \quad \forall j \in \mathcal{D} \tag{2.21d}$$

$$Q_{G_{i_{min}}} \leq Q_{G_i} \leq Q_{G_{i_{max}}} \quad \forall i \in \mathcal{G} \tag{2.21e}$$

$$V_{i_{min}} \leq V_i \leq V_{i_{max}} \quad \forall i \in \mathcal{B} \tag{2.21f}$$

$$I_{ij}(\delta, V) \leq I_{ij_{max}} \quad \forall (i,j) \in \mathcal{T}, i \neq j \tag{2.21g}$$

$$P_{ij}(\delta, V) \leq P_{ij_{max}} \quad \forall (i,j) \in \mathcal{T}, i \neq j \tag{2.21h}$$

Here C_S and C_D are the cost functions; $P_{S_{min}}$ and $P_{S_{max}}$ represent the minimum and maximum power output limits of the generators' bid power; $P_{D_{min}}$ and $P_{D_{max}}$ represent the minimum and maximum power limits of demand bid blocks; and $I_{ij}(\delta, V)$ represents the current in the transmission element between buses i and j. The function $P_{ij}(\delta, V)$ is used to represent transmission system security limits, which are determined off-line by means of stability and contingency studies, in order to represent security limits in the auction model. Finally, $\mathcal{D}$ is the set of indices of loads, and $\mathcal{T}$ is the set of indices of transmission lines and transformers.

It is important to highlight that the stability limits $P_{ij_{max}}$ used in this model are computed off-line using possible dispatch scenarios that do not necessarily represent

the actual system conditions [1, 43]. Thus, VSC-OPF models have been proposed to better represent system security by means of including additional constraints, such as the MSV of the power flow Jacobian, as described in the following section.

2.5.2 Voltage-Stability-Constrained OPF (VSC-OPF)

Multiobjective VSC-OPF

A technique for representing system security in the operation of decentralized electricity markets, with special emphasis on VS, is proposed in [1]. In this case, the proposed optimization model is:

$$\max_{\substack{P_S,P_D,\lambda_c,Q_{G_c}\\ Q_G,V,V_c,\delta,\delta_c,k_{G_c}}} \quad w_1\left(\sum_{j\in\mathcal{D}} C_{D_j}P_{D_j} - \sum_{i\in\mathcal{G}} C_{S_i}P_{S_i}\right) + w_2\lambda_c \tag{2.22a}$$

$$\text{s.t.} \quad \widehat{G}(\delta, V, K_G, Q_G, P_S, P_D) = 0 \tag{2.22b}$$

$$\widehat{G}_c(\delta_c, V_c, K_G, Q_{G_c}, \lambda_c, P_S, P_D) = 0 \tag{2.22c}$$

$$\lambda_{c_{min}} \leq \lambda_c \leq \lambda_{c_{max}} \tag{2.22d}$$

$$P_{S_{i_{min}}} \leq P_{S_i} \leq P_{S_{i_{max}}} \quad \forall i \in \mathcal{G} \tag{2.22e}$$

$$P_{D_{j_{min}}} \leq P_{D_j} \leq P_{D_{j_{max}}} \quad \forall j \in \mathcal{D} \tag{2.22f}$$

$$Q_{G_{i_{min}}} \leq Q_{G_i} \leq Q_{G_{i_{max}}} \quad \forall i \in \mathcal{G} \tag{2.22g}$$

$$Q_{G_{i_{min}}} \leq Q_{Gc_i} \leq Q_{G_{i_{max}}} \quad \forall i \in \mathcal{G} \tag{2.22h}$$

$$V_{i_{min}} \leq V_i \leq V_{i_{max}} \quad \forall i \in \mathcal{B} \tag{2.22i}$$

$$V_{i_{min}} \leq V_{c_i} \leq V_{i_{max}} \quad \forall i \in \mathcal{B} \tag{2.22j}$$

$$P_{ij}(\delta, V) \leq P_{ij_{max}} \quad \forall (i,j) \in \mathcal{T} \quad i \neq j \tag{2.22k}$$

$$P_{ij}(\delta_c, V_c) \leq P_{ij_{max}} \quad \forall (i,j) \in \mathcal{T} \quad i \neq j \tag{2.22l}$$

This model accounts for the system security by including a second set of power flow equations, reactive power and voltage limits at the critical condition associated with the maximum loading point λ_c, hence the subscript c. The maximum or critical loading point could be either associated with a thermal or bus voltage limit, or a VS

limit corresponding to a system singularity SNB or LISB. The loading margin λ_c is free to change between certain limits which ensures a minimum level of security, while the upper limit defines a maximum required level of security.

The multiobjective function (2.22a) is composed of two terms weighted by two factors $w_1 > 0$ and $w_2 > 0$. The first term represents the social welfare, whereas the second term ensures that the distance between the market solution and the critical point is maximized [1]. The disadvantage of this formulation is that the solution will depend on the value of the weighting factors, leading to "improper" market signals. Notice that w_1 must be greater than zero, otherwise there would be no representation of the social welfare, and if w_2 is zero, λ_c does not necessarily represent a maximum loading condition. To link the social welfare and the maximum loading condition, the author in [74] defines $w_1 = (1 - w)$ and $w_2 = w$ for $0 < w < 1$.

In this model, the generator and load powers at the current and maximum loading condition are defined as follows:

$$\begin{array}{rclcrcl} P_G & = & P_{G_o} + P_S & & P_{G_c} & = & (1 + \lambda_c + K_G)P_G \\ P_L & = & P_{L_o} + P_D & & P_{L_c} & = & (1 + \lambda_c)P_L \end{array} \tag{2.23}$$

where K_G in this case is used to distribute the system losses associated with the power flow equations that represent the critical conditions, in proportion to the value of P_S obtained in the solution process.

A similar VSC-OPF model that considerers an N-1 contingency criterion is proposed in [74]. The model is essentially the same as the one shown in (2.22); the main difference is that contingencies are included by taking out selected lines when formulating the power flow equations at the critical point (2.22c). By doing this, it is ensured that the current solution of the VSC-OPF problem is also feasible for the worst single contingency. Similar OPF approaches are proposed in [14, 31, 41, 42].

The disadvantages of this model are as follows: the number of constraints increases considerably; the difficulty of choosing adequate values for the weighting

factors; and the presence of the loading margin in the objective function. This final disadvantage leads to not having pure market signals.

A mixed CPF-OPF technique based on sensitivities obtained from the OPF Lagrangian multipliers is proposed in [32]. The sensitivities are used to approximate the power directions for the CPF method in order to calculate the loading parameter based upon an N-1 contingency criterion. This technique has important advantages over previous work proposed by the authors in [1], since the multi-objective optimization is no longer used because of the drawback of dealing with weighting factors, and not providing pure market solutions. However, the computational effort is still a problem.

MSV-based VSC-OPF

A model to improve the representation of VS margins in the OPF has been proposed in [34, 53]. The resulting VSC-OPF market clearing and power dispatch optimization model is defined as follows:

$$\max_{\substack{\delta,V_L,Q_G \\ V_G,P_S,P_D}} \quad \sum_{j\in\mathcal{D}} C_{D_j}P_{D_j} - \sum_{i\in\mathcal{G}} C_{S_i}P_{S_i} \tag{2.24a}$$

$$\text{s.t} \quad \widehat{G}(\delta, V_L, Q_G, V_G, P_S, P_D) = 0 \tag{2.24b}$$

$$\sigma_{min}\{J\} \geq \sigma_c \tag{2.24c}$$

$$P_{S_{i_{min}}} \leq P_{S_i} \leq P_{S_{i_{max}}} \quad \forall i \in \mathcal{G} \tag{2.24d}$$

$$P_{D_{j_{min}}} \leq P_{D_j} \leq P_{D_{jmax}} \quad \forall j \in \mathcal{D} \tag{2.24e}$$

$$Q_{G_{i_{min}}} \leq Q_{G_i} \leq Q_{G_{i_{max}}} \quad \forall i \in \mathcal{G} \tag{2.24f}$$

$$V_{i_{min}} \leq V_i \leq V_{i_{max}} \quad \forall i \in \mathcal{B} \tag{2.24g}$$

$$I_{ij}(\delta, V) \leq I_{ij_{max}} \quad \forall (i,j) \in \mathcal{T}, i \neq j \tag{2.24h}$$

where J is the power flow Jacobian of the system at a power flow solution point, and σ_{min} is the MSV of J. This model is basically the same as the SC-OPF, except for the transmission system limits on P_{ij}, which are implicitly represented in the VS

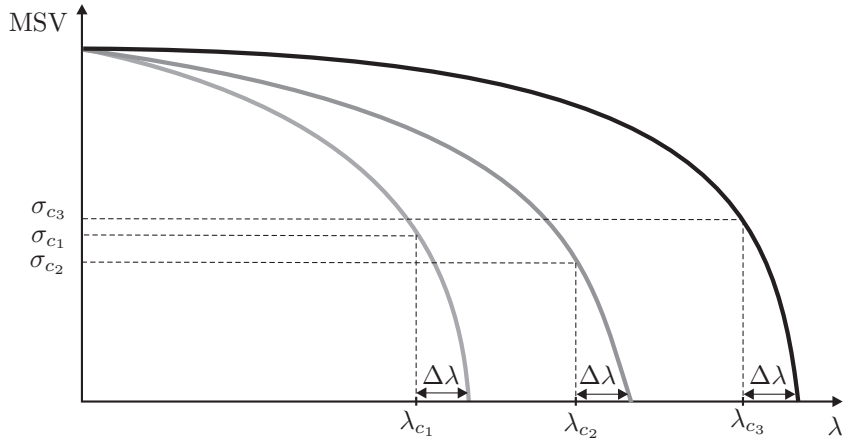

Figure 2.8: σ_c versus λ_c changes for different power dispatches.

constraint (2.24c). This constraint is a performance index used to determine how close the system is to a voltage collapse point associated with a singularity of the power flow Jacobian (SNB point), and is commonly used in VS studies [13]. Therefore, σ_c (obtained from off-line voltage studies) is used to guarantee a minimum distance from a voltage collapse point, considering, at least, an N-1 contingency criterion. The constraint (2.24f) is used to represent LIBs, which are also responsible for voltage collapse problems as previously discussed. Hence, (2.24c), (2.24f), (2.24g) and (2.24h), are used to directly represent security limits in the auction model (2.24).

The advantage of this model is that it accounts for the two most important types of bifurcations responsible for voltage collapse problems in practice, as well as other security limits such as thermal limits. Another important advantage is that the σ_c value used in the VS constraint (2.24c) exhibits a low dependency on the power dispatch, unlike the associated λ_c value used in model (2.22), as illustrated in Figure 2.8, where $\Delta\lambda$ represents a security margin. However, the main disadvantage of this model is that it is mathematically and numerically difficult to implement and solve, as the constraint (2.24c) is an implicit function. Hence, the derivatives needed to solve this OPF problem can be only approximated using

interval formulas that may lead to convergence problems [34], since the MSV can behave in a rather nonlinear way [13]. As a result, this constraint becomes a "soft" constraint, and it may not guarantee an accurate solution in some cases, as demonstrated in Section 4.3. Furthermore, current mathematical programming languages and large-scale solvers available for nonlinear optimization cannot be used for its implementation and solution, since these are not able to handle this type of implicit function constraint.

The aforementioned drawbacks are what motivates the development of the practical solution method for this particular VSC-OPF model. The proposed solution method, which is described and analyzed in detail in Chapter 4, concentrates on the practical reformulation of constraint (2.24c).

2.5.3 Locational Marginal Prices (LMP)

The theory of spot pricing states that the spot market price must reflect the interaction of supply and demand. Thus, the price in a competitive market is set by the highest cost supplier when there is enough supply, and by the marginal (lowest value) demand [75]. In this context, a central operator receives voluntary bids from market participants, assuming that the submitted bids reflects true *marginal costs*[1] of production and *marginal benefits*[2] of consumption. The operator then finds an optimal operating state by means of a cost minimization process, which is based on an OPF. The solution must satisfy all the transmission constraints, balance of power, and minimum cost, and must provide the Locational Marginal Prices (LMPs), which are basically the Lagrange multipliers of the OPF, as shown below. The LMPs differ by location because energy is cheaper to produce in some locations, and the transmission line capacity is limited. For this reason, locational pricing of energy is also called *congestion pricing* [77, 78].

[1]The change in total cost that results from a unit increase in output. It is calculated as the increase in total cost divided by the increase in output [76].

[2]The extra benefit received from a small increase in the consumption of a good or service. It is calculated as the increase in total benefit divided by the increase in consumption [76].

Consider the following standard OPF model:

$$\min_{\substack{\delta,V_L,Q_G\\V_G,P_S,P_D}} \quad \sum_{i\in\mathcal{G}} C_{S_i}P_{S_i} - \sum_{j\in\mathcal{D}} C_{D_j}P_{D_j} \tag{2.25a}$$

$$\text{s.t} \quad \widehat{G}(\delta, V_L, Q_G, V_G, P_S, P_D) = 0 \tag{2.25b}$$

$$0 \le P_{S_i} \le P_{S_{i_{max}}} \quad \forall i \in \mathcal{G} \tag{2.25c}$$

$$0 \le P_{D_j} \le P_{D_{j_{max}}} \quad \forall j \in \mathcal{D} \tag{2.25d}$$

$$Q_{G_{i_{min}}} \le Q_{G_i} \le Q_{G_{i_{max}}} \quad \forall i \in \mathcal{G} \tag{2.25e}$$

$$V_{i_{min}} \le V_i \le V_{i_{max}} \quad \forall i \in \mathcal{B} \tag{2.25f}$$

$$P_{ij}(\delta, V) \le P_{ij_{max}} \quad \forall (i,j) \in \mathcal{T}, i \ne j \tag{2.25g}$$

which can be restated as the following Lagrangian function using a logarithmic barrier IPM approach:

$$\begin{aligned}
\min \mathcal{L} \;=\; & \textstyle\sum_{i\in\mathcal{G}} C_{S_i}P_{S_i} - \sum_{j\in\mathcal{D}} C_{D_j}P_{D_j} \\
& -\mu_G^T \widehat{G}(\delta, V_L, K_G, Q_G, V_G, P_S, P_D) \\
& -\mu_{P_{S_{max}}}^T (P_{S_{max}} - P_S - s_{P_{S_{max}}}) \\
& -\mu_{P_{D_{max}}}^T (P_{D_{max}} - P_D - s_{P_{D_{max}}}) \\
& -\mu_{Q_{G_{max}}}^T (Q_{G_{max}} - Q_G - s_{Q_{G_{max}}}) \\
& -\mu_{Q_{G_{min}}}^T (Q_G - Q_{G_{min}} - s_{Q_{G_{min}}}) \\
& -\mu_{V_{max}}^T (V_{max} - V - s_{V_{max}}) \\
& -\mu_{V_{min}}^T (V - V_{min} - s_{V_{min}}) \\
& -\mu_{P_{ijmax}} (P_{ij_{max}} - P_{ij_{max}} - s_{P_{ijmax}}) \\
& -\mu_s (\textstyle\sum_i \ln s_i)
\end{aligned} \tag{2.26}$$

where $[\mu_{\widehat{G}}^T\, \mu_{P_{S_{max}}}^T\, \mu_{P_{D_{max}}}^T\, \mu_{Q_{G_{max}}}^T\, \mu_{Q_{G_{min}}}^T\, \mu_{V_{max}}^T\, \mu_{V_{min}}^T\, \mu_{P_{ijmax}}^T\, \mu_s^T] > 0$ is a vector of Lagrange multipliers, and $[s_{P_{S_{max}}}^T\, s_{P_{D_{max}}}^T\, s_{Q_{G_{max}}}^T\, s_{Q_{G_{min}}}^T\, s_{V_{max}}^T\, s_{V_{min}}^T\, s_{P_{ijmax}}^T] \ge 0$ is a vector of slack variables. Thus, the marginal cost for supply and demand can be defined as [41]:

$$\frac{\partial \mathcal{L}}{\partial P_{S_i}} = \quad C_{S_i} - \mu_{\widehat{G}_{S_i}} + \mu_{P_{S_{i_{max}}}} \tag{2.27}$$

$$\frac{\partial \mathcal{L}}{\partial P_{D_i}} = \quad -C_{D_i} + \mu_{\widehat{G}_{D_i}} + \mu_{P_{D_{i_{max}}}} \tag{2.28}$$

as $\frac{\partial \widehat{G}_i}{\partial P_{S_i}} = 1$ and $\frac{\partial \widehat{G}_i}{\partial P_{D_i}} = -1$, and where $\mu_{\widehat{G}} = [\mu^T_{\widehat{G}_S}\, \mu^T_{\widehat{G}_D}\, \mu^T_{\widehat{G}_Q}]$. Thus, from (2.27) and (2.28), the LMP or shadow price for each market participant is given by the corresponding Lagrange multiplier [79]:

$$LMP_i = \begin{cases} \mu_{\widehat{G}_{S_i}} \\ \mu_{\widehat{G}_{D_i}} \end{cases} \tag{2.29}$$

Furthermore, conditions (2.27) and (2.28) set the suppliers' and consumers' operation conditions, so that their marginal cost and marginal benefit match the corresponding market price [77].

It is well-known that as the loading level increases, the stability margin decreases, and some control actions have to be taken; however, this might result in increased operating cost. Hence, the associated cost of such actions can be considered as the operational cost of improving system security [26] [42].

2.6 Optimization Methods

2.6.1 Primal-Dual Interior-Point Method (IPM)

Optimality Conditions

In general, the OPF problem is a non-linear programming (NLP) problem that is used to determine the "optimal" control parameter settings to minimize a desired objective function, subject to certain system constraints [42]. An OPF can be generally represented as follows:

$$\min_{\chi} \quad \bar{F}(\chi) \tag{2.30a}$$

$$\text{s.t.} \quad \bar{G}(\chi) = 0 \tag{2.30b}$$

$$\underline{H} \leq H(\chi) \leq \overline{H} \tag{2.30c}$$

$$\underline{\chi} \leq \chi \leq \overline{\chi} \tag{2.30d}$$

where $\bar{F}(\chi) : \mathbb{R}^{n_\chi} \to \mathbb{R}$ is the objective function, e.g, the social welfare in (2.21a) or the loading factor λ; $\bar{G}(\chi) : \mathbb{R}^{n_\chi} \to \mathbb{R}^m$ generally represents the power flow equations (G); and $H(\chi) : \mathbb{R}^{n_\chi} \to \mathbb{R}^p$ can represent transmission line limits, voltage or reactive power, with lower and upper limits represented by $\underline{H}$ and $\overline{H}$, respectively. The vector of system variables $\chi \in \mathbb{R}^{n_\chi}$ typically includes voltage magnitudes and angles, active and reactive power levels, or control variables; their lower and upper limits are represented by $\underline{\chi}$ and $\overline{\chi}$, respectively.

Thus, assume that $\bar{F}(\chi)$, $\bar{G}(\chi)$ and $H(\chi)$ are twice continuously differentiable. The first step to state the optimality conditions is to transform the inequality constraints into equality constraints by adding slack variables. The slack variables are handled implicitly by incorporating them into the objective function using a logarithmic barrier term, imposing strict positivity on the slack variables as follows:

$$\begin{aligned}
\min \quad & \bar{F}(\chi) - \bar{\mu}^k \sum_{i=1}^{p} (\ln \iota_i + \ln \kappa_i) && \text{(2.31a)}\\
\text{s.t} \quad & \bar{G}(\chi) = 0 && \text{(2.31b)}\\
& -\iota - \kappa + \overline{H} - \underline{H} = 0 && \text{(2.31c)}\\
& -H(\chi) - \kappa + \overline{H} = 0 && \text{(2.31d)}\\
& \iota > 0, \kappa > 0 && \text{(2.31e)}
\end{aligned}$$

where $\iota \in \mathbb{R}^p$ and $\kappa \in \mathbb{R}^p$ are slack variables. The Lagrangian function $\mathcal{L}_{\bar{\mu}}(\phi)$ is then stated as follows:

$$\begin{aligned}
\mathcal{L}_{\bar{\mu}}(\phi) = \bar{F}(\chi) - \bar{\mu}^k \sum_{i=1}^{P} (\ln \iota_i + \ln \kappa_i) \\
- \rho^T \bar{G}(\chi) - \beta^T \left(-\iota - \kappa + \overline{H} - \underline{H}\right) - \gamma^T \left(-H(\chi) - \kappa + \overline{H}\right)
\end{aligned} \tag{2.32}$$

where $\phi = [\iota^T \kappa^T \beta^T \gamma^T \chi^T \rho^T]$; $\rho \in \mathbb{R}^m$, $\beta \in \mathbb{R}^p$ and $\gamma \in \mathbb{R}^p$ are the Lagrange multipliers, also called dual variables. A local minimum of (2.32) satisfies the

following KKT optimality conditions:

$$\nabla_\phi \mathcal{L}_{\bar{\mu}}(\phi) = \begin{bmatrix} \nabla_\iota \mathcal{L}_{\bar{\mu}}(\phi) \\ \nabla_\kappa \mathcal{L}_{\bar{\mu}}(\phi) \\ \nabla_\beta \mathcal{L}_{\bar{\mu}}(\phi) \\ \nabla_\gamma \mathcal{L}_{\bar{\mu}}(\phi) \\ \nabla_\chi \mathcal{L}_{\bar{\mu}}(\phi) \\ \nabla_\rho \mathcal{L}_{\bar{\mu}}(\phi) \end{bmatrix} = \begin{bmatrix} \Theta\beta - \bar{\mu}^k e \\ \Lambda\varpi - \bar{\mu}^k e \\ \iota + \kappa - \overline{H} + \underline{H} \\ H(\chi) + \kappa - \overline{H} \\ \nabla_\chi \bar{F}(\chi) - J_{\bar{G}}(\chi)^T \rho + J_H(\chi)^T \gamma \\ -\bar{G}(\chi) \end{bmatrix} = 0 \qquad (2.33)$$

where $\Theta = \text{diag}(\iota_1, \iota_2, ..., \iota_p)$; $\Lambda = diag(\kappa_1, \kappa_2, ..., \kappa_p)$; $e = [1\,1\,...\,1]^T$; $\varpi = \gamma + \beta$; $\nabla_\chi \bar{F} : \mathbb{R}^{n_\chi} \to \mathbb{R}^{n_\chi}$ is the gradient of $\bar{F}(\chi)$; $J_{\bar{G}} : \mathbb{R}^{n_\chi} \to \mathbb{R}^{m \times n_\chi}$ is the Jacobian of $\bar{G}(\chi)$; and $J_H : \mathbb{R}^{n_\chi} \to \mathbb{R}^{p \times n_\chi}$ is the Jacobian of $H(\chi)$.

The third, fourth and sixth terms in (2.33) along with $(\iota, \kappa) \geq 0$ ensure *primal feasibility*. The fifth term along with $(\beta, \varpi) \geq 0$ ensures *dual feasibility*, and the first and second terms are the *$\bar{\mu}$-complementarity conditions*.

Primal-dual Interior-Point Method Algorithm

The primal-dual IPM algorithm, is based on Newton's method to solve nonlinear equations. Figure 2.9 shows the algorithm's flow chart, and the steps are described below.

Computing Newton Directions

The solution of the KKT optimality conditions with Newton's method leads to the following indefinite system of equations parameterized by $\bar{\mu}^k$, which are used to compute the Newton direction at every iteration:

$$\begin{bmatrix} J_o & -J_{\bar{G}}^T \\ -J_{\bar{G}} & 0 \end{bmatrix} \begin{bmatrix} \Delta\chi \\ \Delta\rho \end{bmatrix} = \begin{bmatrix} \varphi_x \\ \varphi_\rho \end{bmatrix} \qquad (2.34)$$

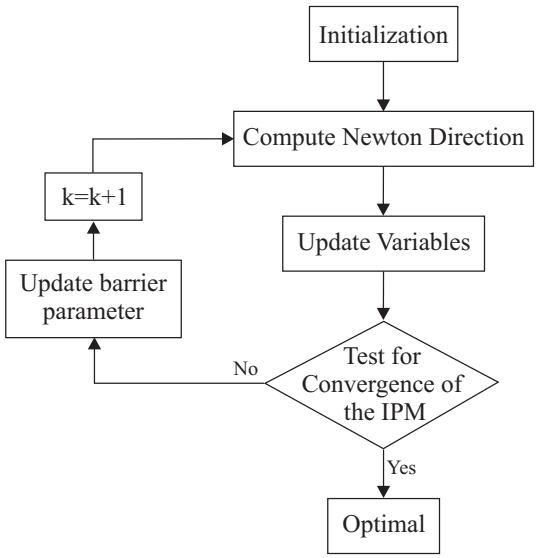

Figure 2.9: Primal-dual IPM

$$\begin{aligned} \Delta\kappa &= -J_H(\chi)\Delta\chi \\ \Delta\iota &= -\Delta\kappa \\ \Delta\beta &= -\bar{\mu}^k\Theta^{-2}\Delta\iota \\ \Delta\gamma &= -\bar{\mu}^k\Lambda^{-2}\Delta\kappa - \Delta\beta \end{aligned} \tag{2.35}$$

where

$$J_o = \nabla^2_\chi L_{\bar{\mu}}(\phi) + \bar{\mu}^k J_H(\chi)^T(\Theta^{-2} + \Lambda^{-2})J_H(\chi) \tag{2.36}$$

$$\nabla^2_\chi L_{\bar{\mu}}(\phi) = \nabla^2_\chi \bar{F}(\chi) - \sum_{j=1}^{m} \rho_j \nabla^2_\chi \bar{G}_j(\chi) + \sum_{j=1}^{p} \gamma_j \nabla^2_\chi H_j(\chi) \tag{2.37}$$

Detailed information about the reduced system shown in (2.34)-(2.35) and other issues regarding the algorithm can be found in [27, 80, 81].

Updating variables

Once the Newton direction has been computed, the next step is to update the primal and dual variables. Separate step lengths for primal and dual variables are

calculated as follows:

$$\alpha_P^k = \min\left\{1, \gamma \min_i \left\{ \frac{-\iota_i^k}{\Delta\iota_i} \middle| \Delta\iota_i < 0, \frac{-\kappa_i^k}{\Delta\kappa_i} \middle| \Delta\kappa_i < 0 \right\}\right\} \tag{2.38}$$

$$\alpha_D^k = \min\left\{1, \gamma \min_i \left\{ \frac{-\beta_i^k}{\Delta\beta_i} \middle| \Delta\beta_i < 0, \frac{-\varpi_i^k}{\Delta\varpi_i} \middle| \Delta\varpi_i < 0 \right\}\right\} \tag{2.39}$$

where the scalars $\alpha_P^k \in (0, 1]$ and $\alpha_D^k \in (0, 1]$ are the step length parameters; and the scalar $\gamma \in (0, 1]$ is a safety factor to ensure that the next point will satisfy the strict positivity conditions (a typical value is $\gamma = 0.99995$). Thus, the variables are updated as follows:

$$\begin{array}{rclcrcl} \chi^{k+1} &=& \chi^k &+& \alpha_P^k \Delta\chi & \rho^{k+1} &=& \rho^k &+& \alpha_D^k \Delta\rho \\ \iota^{k+1} &=& \iota^k &+& \alpha_P^k \Delta\iota & \beta^{k+1} &=& \beta^k &+& \alpha_D^k \Delta\beta \\ \kappa^{k+1} &=& \kappa^k &+& \alpha_P^k \Delta\kappa & \gamma^{k+1} &=& \gamma^k &+& \alpha_D^k \Delta\gamma \end{array} \tag{2.40}$$

Testing for Convergence and Reducing the Barrier Parameter

The last step in the IPM algorithm is to test for convergence and reduce the barrier parameter. The criterion to stop the iterative process is based on the primal (ξ_1) and dual (ξ_2) feasibilities, as well as complementarity conditions (ξ_3), to satisfy certain tolerances. Thus, the residual of the complementarity conditions, called the complementarity gap, is computed at the point ϕ^k from:

$$\zeta^k = (\iota^k)^T \beta^k + (\kappa^k)^T \nu^k \tag{2.41}$$

$$\bar{\mu}^{k+1} = \sigma_{\text{dir}}^k \frac{\zeta^k}{2p} \tag{2.42}$$

where the parameter $\sigma_{\text{dir}}^k \in (0, 1]$ is called the centering parameter. If $\sigma_{\text{dir}}^k = 1$, it defines a centering direction, and if $\sigma_{\text{dir}}^k = 0$, it gives a pure Newton step, known as the affine-scaling direction. In practice, to decide whether to improve centrality or reduce $\bar{\mu}^k$, σ_{dir}^k is computed using to the following heuristic:

$$\begin{array}{rcl} \sigma_{\text{dir}}^0 &=& 0.2 \\ \sigma_{\text{dir}}^k &=& \max\{0.99\sigma_{\text{dir}}^{k-1}, 0.1\} \end{array} \tag{2.43}$$

The algorithm is stopped when one of the two sets of the following conditions are met:

$$\begin{array}{rcl} \xi_1^k & \leq & \epsilon_1 \\ \xi_2^k & \leq & \epsilon_1 \\ \xi_3^k & \leq & \epsilon_2 \\ \xi_2^k & \leq & \epsilon_2 \end{array} \quad \text{or} \quad \begin{array}{rcl} \bar{\mu}^k & \leq & \epsilon_{\bar{\mu}} \\ ||\Delta\chi||_\infty & \leq & \epsilon_2 \\ ||\bar{G}(\chi^k)||_\infty & \leq & \epsilon_1 \\ \xi_4^k & \leq & \epsilon_2 \end{array} \tag{2.44}$$

where

$$\xi_1 = \max\left\{ \max\left\{\underline{H} - H(\chi)\right\}, \max\left\{H(\chi) - \overline{H}\right\}, ||\bar{G}(\chi)||_\infty \right\} \tag{2.45}$$

$$\xi_2 = \frac{||\Delta_\chi \bar{F}(\chi) - J_{\bar{G}}(\chi)^T\rho + J_H(\chi)^T\gamma||_\infty}{1 + ||\chi||_2 + ||\rho||_2 + ||\gamma||_2} \tag{2.46}$$

$$\xi_3 = \frac{\zeta}{1 + ||\chi||_2} \tag{2.47}$$

$$\xi_4 = \frac{\bar{F}(\chi^k) - \bar{F}(\chi^{k-1})}{1 + |\bar{F}(\chi^k)|} \tag{2.48}$$

Typical tolerances are $\epsilon_1 = 10^{-4}$, $\epsilon_2 = 10^{-2}\epsilon_1$, and $\epsilon_{\bar{\mu}} = 10^{-12}$.

Choosing an Initial Point

An important characteristic of the primal-dual IPM is that a strictly feasible point is not mandatory, hence the usual denomination *infeasible primal-dual interior-point method*. Nonetheless, $(\iota, \kappa) > 0$ and $(\beta, \varpi) > 0$ have to be satisfied at every point, so the IPM starts from a point ϕ^0 such that $(\iota^0, \kappa^0) > 0$ and $(\beta^0, \varpi^0) > 0$. Besides the strict positivity conditions, a good starting point should also satisfy two other conditions. First, the point should be well-centered, and second, the point should not be "too unfeasible"; that is, the duality gap should not be too large [81].

In practice, IPMs perform better if some initialization heuristic is used. For the OPF the following estimations are suggested in [27, 81]:

- Estimate χ as a flat start using the middle point between the upper and lower limits for the bounded variables.

- The primal slack variables are initialized as follows:

$$\begin{aligned} \iota^0 &= \min\{\max\{\gamma H^\Delta, H(\chi^0) - \underline{H}\}, (1-\gamma)H^\Delta\} \\ \kappa^0 &= H^\Delta - \iota^0 \end{aligned}$$

  where $H^\Delta := \underline{H} - \overline{H}$, and $\gamma := 0.25$.

- The initial dual variables β^0 and γ^0 are defined as:

$$\begin{aligned} \beta^0 &= \bar{\mu}^0(\Theta^0)^{-1}e, \\ \gamma^0 &= \bar{\mu}^0(\Lambda^0)^{-1}e - \beta^0 \end{aligned}$$

2.6.2 Semidefinite Programming (SDP)

In SDP one minimizes a linear function of a symmetric matrix X, subject to linear constraints on the entries in X, under the restriction that X must be positive semidefinite. Such a constraint is nonlinear and nonsmooth, but convex, so SDP problems are convex optimization problems. This is significant because, for convex optimization problems, any local minimum is a global minimum. SDP unifies several standard problems (e.g., linear programming) and finds many applications in engineering and combinatorial optimization [82–84]. A SDP problem is an optimization problem of the following form:

$$\begin{aligned} \min \quad & C \cdot X && \text{(2.49a)} \\ \text{s.t} \quad & A_i \cdot X = b_i, \quad i = 1, ..., m && \text{(2.49b)} \\ & X \succeq 0 && \text{(2.49c)} \end{aligned}$$

where $X \in S^n$ is the matrix variable, and S^n is the set of symmetric $n \times n$ matrices, and $C \in S^n$ is the matrix of coefficients of the objective function. $X \succeq 0$ denotes that X is positive semidefinite (PSD), and:

$$C \cdot X = \text{trace}(CX)$$

is the standard inner product in S^n. A matrix $A \in S^n$ is said to be positive semidefinite (PSD) if:

$$\tilde{v}^T A \tilde{v} = \sum_{i=1}^{n} \sum_{j=1}^{n} A_{ij} \tilde{v}_i \tilde{v}_j \geq 0 \quad \forall \tilde{v} \in \mathbb{R}^n$$

It may be helpful to think of $X \succeq 0$ as stating that each of the n eigenvalues of X must be non-negative. This concept fosters the application of SDP to the MSV-based VSC-OPF problem, since the power flow Jacobian tends to be either singular or close to singularity at a voltage collapse point.

2.7 Summary

This chapter introduces power system security concepts and the basis of VS. Bifurcation theory definitions used to characterize the VS phenomena in power systems are presented, as well as the techniques used to determine SNB and LIB points of a power flow model. This chapter also discusses the OPF-DM, and the most recently proposed VSC-OPFs market clearing and power dispatch models. Finally, the primal-dual IPM for NLP, and a brief introduction to SDP is presented.

The concepts presented in this chapter are used throughout this thesis to study and propose optimization-based techniques to better represent VS in OPF-based auction models in competitive electricity markets.

Chapter 3

Analysis of the OPF-DM

3.1 Introduction

This chapter presents a detailed theoretical analysis of the application of OPF-DM to the study of SNBs and LIBs in power systems. Previous works have formally shown that optimization methods can be used to compute SNBs in power system models, and that these methods are basically equivalent to more "classical" computational approaches [22]. Also, some issues associated with the application of OPF-DMs to the computation of LIBs are discussed in [85], and the structure of the loadability surface is studied in [5] using similar optimization methods. In [86], fold bifurcations are also studied using an optimization model. However, up to now, to the author's knowledge, the links between solutions of OPF-DMs and SNBs and LIBs have not yet been dealt with in the technical literature as formally and systematically as is done here. Hence, this chapter concentrates on demonstrating that solution points obtained from a given OPF-DM model correspond to either SNB or LIB points; this is accomplished by showing that the optimality conditions of these solution points yield the transversality conditions of the corresponding bifurcation points. A simple but realistic test system example is used to numerically illustrate the theoretical discussions presented here.

3.2 Theoretical Analysis of the OPF-DM

In this section, it is formally shown that a solution to the OPF-DM model (2.20) corresponds to either an SNB or a LISB, by demonstrating that the transversality conditions of the corresponding bifurcations are met, based on the necessary and sufficient optimality conditions of the optimal solution. Only LIBs associated with maximum reactive power limits are analyzed here, since VS problems in practice are typically associated with generators reaching these limits as demand in the system increases. Therefore, in this thesis, actual SNBs and LIBs (2.1) are assumed to correspond to similar "bifurcation" points of the power flow equations. This is the case in certain power system models [61,87]; thus, this chapter concentrates on the analysis of SNBs and LIBs of (2.2).

The following assumptions are made for the statement of the theorems and corollary presented next [88]:

- Regularity and strict complementarity conditions must be met at the optimal point, i.e., there must not be degeneracy of the optimization problem at the solution point.
- The constraints should be C^2 and convex in a neighborhood of the optimal solution.

These assumptions are referred to throughout the rest of the chapter as optimality solution (OS) assumptions for convenience. It is important to highlight the fact that there is no guarantee that all possible solutions of (2.20) would meet these OS assumptions. If these conditions are not met, then the solution could not be classified as an SNB or LIB point with certainty, as per the theorems proved below. However, from numerical results reported in various papers (e.g., [6, 23]), where these types of optimization problems are solved for a variety of small and large electrical power systems, these solutions are shown to meet these assumptions [86]. This is due to the fact that in nonlinear system theory, codimension-1 (single parameter) bifurcations SNBs and LIBs are considered generic [59], i.e., they are expected in power

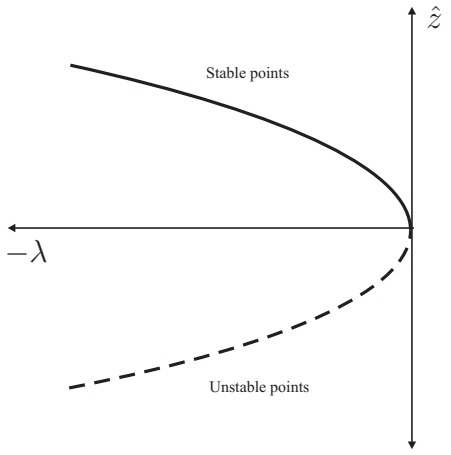

Figure 3.1: Solution points for the system (3.1).

systems under typical operating conditions and modeling assumptions [47,89]. Furthermore, it can be reasonably argued that the characteristics of the power flow model in which (2.20) is based, should in general meet these OS assumptions. For illustration purposes, consider the following examples:

Example 3.1: In general, an SNB can be described by the following equation [59]:

$$\widehat{G}(\hat{z}, \lambda) = \hat{z}^2 + \lambda \tag{3.1}$$

The solution points of this equation describe a parabola which just exists for $\lambda \leq 0$, as depicted in Figure 3.1. For $\lambda < 0$, two solution points may be found, one stable and one unstable, as defined by $\hat{z} = \pm\sqrt{-\lambda}$. For $\lambda = \lambda_c = 0$, only one solution $\hat{z}_c = 0$ exists, which corresponds to the SNB point. Thus, the gradient at the bifurcation point is

$$\nabla_{\hat{z}}\widehat{G}|_c = 2\hat{z}_c = 0 \tag{3.2}$$

and the Hessian is

$$\nabla^2_{\hat{z}}\widehat{G}|_c = 2 > 0 \quad \text{(positive definite)} \tag{3.3}$$

Hence, λ_c is a strict local maximum satisfying the OS assumptions.

However, there are other examples were the positiveness of the Hessian is not met, thus:

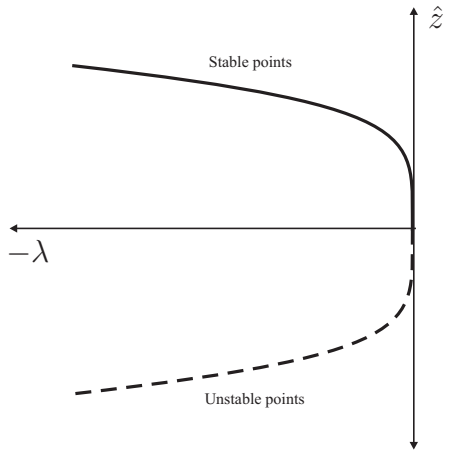

Figure 3.2: Solution points for the system (3.4).

Example 3.2: Consider the following equation:

$$\widehat{G}(\hat{z}, \lambda) = \hat{z}^4 + \lambda \tag{3.4}$$

The solution points of this equation, given by $\hat{z} = \pm\sqrt[4]{-\lambda}$, also trace a "parabolic" function for $\lambda \leq 0$, as depicted in Figure 3.2. Thus, the gradient at the bifurcation point $(\hat{z}_c, \lambda_c) = (0, 0)$ is

$$\nabla_{\hat{z}} \widehat{G}|_c = 4\hat{z}_c^3 = 0 \tag{3.5}$$

and the Hessian is

$$\nabla_{\hat{z}}^2 \widehat{G}|_c = 12\hat{z}_c^2 = 0 \tag{3.6}$$

Therefore, the Hessian is not positive definite at the bifurcation point.

It is now argued that the first example is more representative of the OPF-DM context. This is because the only constraints that are not linear (or equivalent to linear at optimality) are the power flow equations:

$$P_i + jQ_i = (e_{r_i} + jf_{r_i}) \sum_{k=1}^{n_b} [(G_{ik} + jB_{ik})(e_{r_k} + jf_{r_k})]^* \tag{3.7}$$

where

$$P_i = P_{G_{o_i}} + (\lambda + K_G)P_{S_i} - P_{L_{o_i}} - \lambda P_{D_i} \tag{3.8}$$

$$Q_i = Q_{G_i} - Q_{G_{o_i}} - \lambda K_L P_{D_i} \tag{3.9}$$

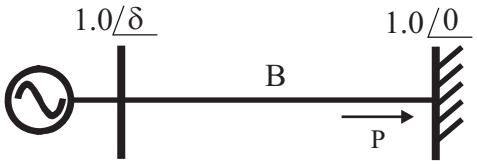

Figure 3.3: Generator-Infinite Bus system

are the power injections at bus i, as per (2.13)-(2.15); $Y_{ik} = G_{ik} + jB_{ik}$; n_b is the number of buses; and $\hat{V_k} = e_{r_k} + jf_{r_k}$ are the complex bus voltages in rectangular coordinates. Hence, the power flow equations $(\Delta P, \Delta Q)$ can be written as follows:

$$P_{G_{o_i}} + (\lambda + K_G)P_{S_i} - P_{L_{o_i}} - \lambda P_{D_i} = \sum_{j=1}^{n_b} \left[e_{r_i}(e_{r_j}G_{ij} - f_{r_j}B_{ij}) + f_{r_i}(f_{r_j}G_{ij} + e_{r_j}B_{ij}) \right] \quad (3.10)$$

$$Q_{G_i} - Q_{G_{o_i}} - \lambda K_L P_{D_i} = \sum_{j=1}^{n_b} \left[f_{r_i}(e_{r_j}G_{ij} - f_{r_j}B_{ij}) - f_{r_i}(f_{r_j}G_{ij} + e_{r_j}B_{ij}) \right] \quad (3.11)$$

Observe that this model has basically the same structure as (3.1): a quadratic form on e_r, f_r and a linear term in λ. This special structure, plus the empirical evidence (e.g., [90]), make reasonable to assume that the OPF-DM satisfy the OS assumptions. It is further noted that the sufficient KKT conditions imply that $\exists \mu_1, \mu_2$ such that

$$\mu_1 \nabla^2_{\hat{z}} \Delta P|_c + \mu_2 \nabla^2_{\hat{z}} \Delta Q|_c \succ 0 \quad (3.12)$$

The following two examples further illustrate the properties of the power flow model used in the OPF-DM. Notice that these examples basically show that (3.12) is positive definite:

Example 3.3: Consider the generator-infinite bus shown in Figure (3.3). The active power flow equation in this case is defined as:

$$P = BV \sin \delta \quad (3.13)$$

since $e_r = V\cos\delta$ and $f_r = V\sin\delta$, it follows that:

$$P = BV\sin\delta \quad \Leftrightarrow \quad \lambda = Bf_r \tag{3.14}$$

The maximum loading point optimization problem here can be formulated as follows:

$$\begin{aligned} \min_{e_r, f_r, \lambda} \quad & -\lambda && \text{(3.15a)} \\ \text{s.t.} \quad & Bf_r - \lambda = 0 && \text{(3.15b)} \\ & e_r^2 + f_r^2 - 1 = 0 && \text{(3.15c)} \end{aligned}$$

where (3.15c) is a constraint on the voltage magnitude at the generation bus. The Lagrangian function can then be stated as:

$$\mathcal{L}(e_r, f_r, \lambda, \mu_1, \mu_2) = -\lambda + \mu_1(Bf_r - \lambda) + \mu_2(e_r^2 + f_r^2 - 1) \tag{3.16}$$

and the first-order KKT conditions are:

$$\begin{aligned} \nabla_{e_r}\mathcal{L}|_c &= 2e_{r_c}\mu_{2_c} = 0 && \text{(3.17)} \\ \nabla_{f_r}\mathcal{L}|_c &= B\mu_{1_c} + 2f_{r_c}\mu_{2_c} = 0 && \text{(3.18)} \\ \nabla_{\lambda}\mathcal{L}|_c &= -\mu_{1_c} - 1 = 0 && \text{(3.19)} \\ \nabla_{\mu_1}\mathcal{L}|_c &= Bf_{r_c} - \lambda_c = 0 && \text{(3.20)} \\ \nabla_{\mu_2}\mathcal{L}|_c &= e_{r_c}^2 + f_{r_c}^2 - 1 = 0 && \text{(3.21)} \end{aligned}$$

Thus, the optimal solution is:

$$\begin{bmatrix} e_{r_c} \\ f_{r_c} \\ \lambda_c \\ \mu_{1_c} \\ \mu_{2_c} \end{bmatrix} = \begin{bmatrix} 0 \\ 1 \\ B \\ -1 \\ \frac{B}{2} \end{bmatrix} \tag{3.22}$$

On the other hand, the Hessian of the Lagrangian function can be written as follows:

$$\nabla^2_{(e_r, f_r, \lambda)}\mathcal{L} = \begin{bmatrix} 2\mu_2 & 0 & 0 \\ 0 & 2\mu_2 & 0 \\ 0 & 0 & 0 \end{bmatrix} \tag{3.23}$$

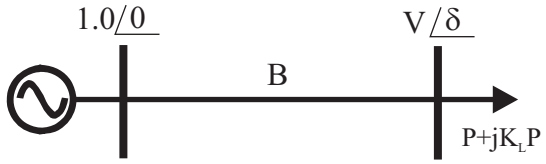

Figure 3.4: Generator-Infinite Bus system

which evaluated at the optimal point yields:

$$\nabla^2_{(e_r,f_r,\lambda)}\mathcal{L}|_c = \begin{bmatrix} B & 0 & 0 \\ 0 & B & 0 \\ 0 & 0 & 0 \end{bmatrix} \tag{3.24}$$

Hence,

$$\mu_{1_c}\nabla^2_{(e_r,f_r)}(Bf_r - \lambda)|_c + \mu_{2_c}\nabla^2_{(e_r,f_r)}(e_r^2 + f_r^2 - 1)|_c \succ 0 \tag{3.25}$$

i.e.,

$$-1\begin{bmatrix} 0 & 0 \\ 0 & 0 \end{bmatrix} + \frac{B}{2}\begin{bmatrix} 2 & 0 \\ 0 & 2 \end{bmatrix} = \begin{bmatrix} B & 0 \\ 0 & B \end{bmatrix} \succ 0 \tag{3.26}$$

Example 3.4: Consider the generator-load bus shown in Figure 3.4. The active and reactive power flow equations are defined in this case as:

$$P = -BV\sin\delta \quad \Leftrightarrow \quad -f_rB - \lambda = 0 \tag{3.27}$$

$$K_LP = -BV^2 + BV\cos\delta \quad \Leftrightarrow \quad -B(e_r^2 + f_r^2) + Be_r - K_L\lambda = 0 \tag{3.28}$$

The maximum loading point can then be calculated as follows:

$$\min_{e_r,f_r,\lambda} \quad -\lambda \tag{3.29a}$$

$$\text{s.t.} \quad -Bf_r - \lambda = 0 \tag{3.29b}$$

$$-B(e_r^2 + f_r^2) + Be_r - K_L\lambda = 0 \tag{3.29c}$$

and the Lagrangian can be stated as:

$$\mathcal{L}(e_r, f_r, \lambda, \mu_1, \mu_2) = -\lambda + \mu_1(-Bf_r - \lambda) + \mu_2[-B(e_r^2 + f_r^2) + Be_r - K_L\lambda] \tag{3.30}$$

Therefore, the first order KKT conditions are:

$$\nabla_{e_r}\mathcal{L}|_c = B(1-2e_{r_c})\mu_{2_c} = 0 \tag{3.31}$$

$$\nabla_{f_r}\mathcal{L}|_c = -B(\mu_{1_c}+2f_{r_c}\mu_{2_c}) = 0 \tag{3.32}$$

$$\nabla_{\lambda}\mathcal{L}|_c = -\mu_{1_c}-K_L\mu_{2_c}-1 = 0 \tag{3.33}$$

$$\nabla_{\mu_1}\mathcal{L}|_c = -Bf_{r_c}-\lambda_c = 0 \tag{3.34}$$

$$\nabla_{\mu_2}\mathcal{L}|_c = -B(e_{r_c}^2+f_{r_c}^2-e_{r_c})-K_L\lambda_c = 0 \tag{3.35}$$

which yields the optimal solution:

$$\begin{bmatrix} e_{r_c} \\ f_{r_c} \\ \lambda_c \\ \mu_{1_c} \\ \mu_{2_c} \end{bmatrix} = \begin{bmatrix} \frac{1}{2} \\ \frac{K_L-\sqrt{K_L^2+1}}{2} \\ -B\frac{K_L-\sqrt{K_L^2+1}}{2} \\ \frac{K_L-\sqrt{K_L^2+1}}{\sqrt{K_L^2+1}} \\ -\frac{1}{\sqrt{K_L^2+1}} \end{bmatrix} \tag{3.36}$$

Hence, the Hessian of the Lagrangian (3.30) is:

$$\nabla^2_{(e_r,f_r,\lambda)}\mathcal{L} = \begin{bmatrix} -2B\mu_2 & 0 & 0 \\ 0 & -2B\mu_2 & 0 \\ 0 & 0 & 0 \end{bmatrix} \tag{3.37}$$

which evaluated at the optimal reduces to:

$$\nabla^2_{(e_r,f_r,\lambda)}\mathcal{L}|_c = \begin{bmatrix} \frac{2B}{\sqrt{K_L^2+1}} & 0 & 0 \\ 0 & \frac{2B}{\sqrt{K_L^2+1}} & 0 \\ 0 & 0 & 0 \end{bmatrix} \tag{3.38}$$

And

$$\mu_{1_c}\nabla^2_{(e_r,f_r)}(-Bf_r-\lambda)|_c + \mu_{2_c}\nabla^2_{(e_r,f_r)}[-B(e_r^2+f_r^2)+Be_r-K_L\lambda]|_c \succ 0 \tag{3.39}$$

i.e.,

$$\frac{K_L-\sqrt{K_L^2+1}}{\sqrt{K_L^2+1}}\begin{bmatrix}0 & 0\\ 0 & 0\end{bmatrix} - \frac{1}{\sqrt{K_L^2+1}}\begin{bmatrix}-2B & 0\\ 0 & -2B\end{bmatrix} = \begin{bmatrix}\frac{2B}{\sqrt{K_L^2+1}} & 0\\ 0 & \frac{2B}{\sqrt{K_L^2+1}}\end{bmatrix} \succ 0 \tag{3.40}$$

Other types of bifurcations for systems with codimension 2 and higher are studied in [90], which may have similar forms as (3.4), however, these types of bifurcations are out of the scope of this thesis.

The theorem below shows that an optimal solution of (2.20), at which a given generator is at its reactive power limit while its terminal voltage is at its regulator set point, corresponds to a LISB and cannot be a LIDB. This is something one can intuitively deduce from Figure 2.5, if the OS assumptions are met.

Theorem 3.1. *Let $(\hat{z}_c, \lambda_c)$, $\hat{z}_c = (\tilde{z}_c, \hat{r}_c)$, be a local optimum of* (2.20) *that meets the aforementioned OS assumptions for $\hat{p} = \hat{p}_o$, where a given generator i satisfies:*

$$\left.\begin{array}{c} Q_{G_{i_c}} = Q_{G_{i_{max}}} \\ V_{G_{i_c}} = V_{G_{i_o}} \end{array}\right\} \;\Rightarrow\; V_{a_i} = V_{b_i} = 0 \tag{3.41}$$

while some other generators $j \neq i \in \mathcal{G}_j \subset \mathcal{G}$ satisfy:

$$\left.\begin{array}{c} Q_{G_{j_c}} = Q_{G_{j_{max}}} \\ V_{G_{j_c}} < V_{G_{j_o}} \end{array}\right\} \;\Rightarrow\; \left\{\begin{array}{l} V_{a_j} = 0 \\ V_{b_j} > 0 \end{array}\right. \tag{3.42}$$

and the rest of the generators $\bar{\jmath} \neq j \neq i \in \mathcal{G}_{\bar{\jmath}} \subset \mathcal{G}$ are not at their reactive power limits, i.e.,

$$\left.\begin{array}{c} Q_{G_{\bar{\jmath}_{min}}} < Q_{G_{\bar{\jmath}_c}} < Q_{G_{\bar{\jmath}_{max}}} \\ V_{G_{\bar{\jmath}_c}} = V_{G_{\bar{\jmath}_o}} \end{array}\right\} \;\Rightarrow\; V_{a_{\bar{\jmath}}} = V_{b_{\bar{\jmath}}} = 0 \tag{3.43}$$

(Assumptions (3.42) *generalizes the case where a LISB occurs after a LIDB in λ space, as depicted in Figure 2.5.) Then, $(\hat{z}_c, \lambda_c, \hat{p}_o)$ is a LISB of the power flow model defined by equations* (2.20b)-(2.20e)*.*

Proof. Let $Q_G = (Q_{\overline{G}}, Q_{G_i})$, i.e., the generator reactive power variables are ordered so that generator i is the last variable; similarly for V_G, V_a and V_b. Hence, the

Lagrangian function of (2.20) may then be expressed as:

$$\begin{aligned}\mathcal{L} &= \lambda - \hat{\mu}_1^T \widehat{G}_S(\hat{z}_c, \lambda_c, \hat{p}_o) - \hat{\mu}_2^T \widehat{G}_{Q_{\overline{G}}}(\hat{z}_c, \lambda_c, \hat{p}_o) \\ &\quad -\hat{\mu}_3 \widehat{G}_{Q_{G_i}}(\hat{z}_c, \lambda_c, \hat{p}_o) - \hat{\mu}_4^T (Q_{\overline{G}} - Q_{\overline{G}_{min}}) V_{\bar{a}} \\ &\quad -\hat{\mu}_5^T (Q_{\overline{G}} - Q_{\overline{G}_{max}}) V_{\bar{b}} - \hat{\mu}_6 (Q_{G_i} - Q_{G_{i_{min}}}) V_{a_i} \\ &\quad -\hat{\mu}_7 (Q_{G_i} - Q_{G_{i_{max}}}) V_{b_i} - \hat{\mu}_8^T \left(Q_{\overline{G}_{min}} - Q_{\overline{G}}\right) \\ &\quad -\hat{\mu}_9^T \left(Q_{\overline{G}} - Q_{\overline{G}_{max}}\right) - \hat{\mu}_{10} \left(Q_{G_{i_{min}}} - Q_{G_i}\right) \\ &\quad -\hat{\mu}_{11} \left(Q_{G_i} - Q_{G_{i_{max}}}\right) - \hat{\mu}_{12}^T \left(V_{\overline{G}} - V_{\overline{G}_o} - V_{\bar{a}} + V_{\bar{b}}\right) \\ &\quad -\hat{\mu}_{13} \left(V_{G_i} - V_{G_{i_o}} - V_{a_i} + V_{b_i}\right) - \hat{\mu}_{14}^T (-V_{\bar{a}}) \\ &\quad -\hat{\mu}_{15}^T (-V_{\bar{b}}) - \hat{\mu}_{16} (-V_{a_i}) - \hat{\mu}_{17} (-V_{b_i})\end{aligned}$$

where the functions $\widehat{G}_S$, $\widehat{G}_{Q_{\overline{G}}}$ and $\widehat{G}_{Q_{G_i}}$ are appropriately defined subsets of $\widehat{G}$; and the $\hat{\mu}$'s correspond to the Lagrange multipliers of (2.20).

The KKT optimality conditions state that the gradient of the Lagrangian function must be equal to zero at the optimum [88]. Thus:

$$\nabla_\delta \mathcal{L}|_c = -\nabla_\delta \widehat{G}_S|_c \hat{\mu}_{1_c} - \nabla_\delta \widehat{G}_{Q_{\overline{G}}}|_c \hat{\mu}_{2_c} - \nabla_\delta \widehat{G}_{Q_{G_i}}|_c \hat{\mu}_{3_c} = 0 \tag{3.44}$$

$$\nabla_{V_L} \mathcal{L}|_c = -\nabla_{V_L} \widehat{G}_S|_c \hat{\mu}_{1_c} - \nabla_{V_L} \widehat{G}_{Q_{\overline{G}}}|_c \hat{\mu}_{2_c} - \nabla_{V_L} \widehat{G}_{Q_{G_i}}|_c \hat{\mu}_{3_c} = 0 \tag{3.45}$$

$$\nabla_{K_G} \mathcal{L}|_c = -\nabla_{K_G} \widehat{G}_S|_c \hat{\mu}_{1_c} = 0 \tag{3.46}$$

$$\nabla_{Q_{\overline{G}}} \mathcal{L}|_c = -\hat{\mu}_{2_c} - M_{\bar{a}_c} \hat{\mu}_{4_c} - M_{\bar{b}_c} \hat{\mu}_{5_c} + \hat{\mu}_{8_c} - \hat{\mu}_{9_c} = 0 \tag{3.47}$$

$$\nabla_{Q_{G_i}} \mathcal{L}|_c = -\hat{\mu}_{3_c} - V_{a_{i_c}} \hat{\mu}_{6_c} - V_{b_{i_c}} \hat{\mu}_{7_c} + \hat{\mu}_{10_c} - \hat{\mu}_{11_c} = 0 \tag{3.48}$$

$$\nabla_{V_{\overline{G}}} \mathcal{L}|_c = -\nabla_{V_{\overline{G}}} \widehat{G}_S|_c \hat{\mu}_{1_c} - \nabla_{V_{\overline{G}}} \widehat{G}_{Q_{\overline{G}}}|_c \hat{\mu}_{2_c} - \nabla_{V_{\overline{G}}} \widehat{G}_{Q_{G_i}}|_c \hat{\mu}_{3_c} - \hat{\mu}_{12_c} = 0 \tag{3.49}$$

$$\begin{aligned}\nabla_{V_{G_i}} \mathcal{L}|_c &= -\nabla_{V_{G_i}} \widehat{G}_S|_c \hat{\mu}_{1_c} - \nabla_{V_{G_i}} \widehat{G}_{Q_{\overline{G}}}|_c \hat{\mu}_{2_c} \\ &\quad -\nabla_{V_{G_i}} \widehat{G}_{Q_{G_i}}|_c \hat{\mu}_{3_c} - \hat{\mu}_{13_c} = 0\end{aligned} \tag{3.50}$$

$$\nabla_\lambda \mathcal{L}|_c = -\nabla_\lambda \widehat{G}_S|_c \hat{\mu}_{1_c} - \nabla_\lambda \widehat{G}_{Q_{\overline{G}}}|_c \hat{\mu}_{2_c} - \nabla_\lambda \widehat{G}_{Q_{G_i}}|_c \hat{\mu}_{3_c} + 1 = 0 \tag{3.51}$$

$$\nabla_{V_{\bar{a}}} \mathcal{L}|_c = -M_{Q_{\overline{G}_{min_c}}} \hat{\mu}_{4_c} + \hat{\mu}_{12_c} + \hat{\mu}_{14_c} = 0 \tag{3.52}$$

$$\nabla_{V_{\bar{b}}} \mathcal{L}|_c = -M_{Q_{\overline{G}_{max_c}}} \hat{\mu}_{5_c} - \hat{\mu}_{12_c} + \hat{\mu}_{15_c} = 0 \tag{3.53}$$

$$\nabla_{V_{a_i}} \mathcal{L}|_c = -(Q_{G_{i_c}} - Q_{G_{i_{min}}}) \hat{\mu}_{6_c} + \hat{\mu}_{13_c} + \hat{\mu}_{16_c} = 0 \tag{3.54}$$

$$\nabla_{V_{b_i}} \mathcal{L}|_c = -(Q_{G_{i_c}} - Q_{G_{i_{max}}}) \hat{\mu}_{7_c} - \hat{\mu}_{13_c} + \hat{\mu}_{17_c} = 0 \tag{3.55}$$

where $M_{\bar{a}_c} = \text{diag}(V_{\bar{a}_c})$, $M_{\bar{b}_c} = \text{diag}(V_{\bar{b}_c})$, $M_{Q_{\overline{G}_{min_c}}} = \text{diag}(Q_{\overline{G}_c} - Q_{\overline{G}_{min}})$, and $M_{Q_{\overline{G}_{max_c}}} = \text{diag}(Q_{\overline{G}_c} - Q_{\overline{G}_{max}})$ are diagonal matrices. Also, the equality constraints must be equal to zero and the inequality constraints are less than or equal to zero at the optimum, i.e., this point must be feasible.

The complementarity slackness condition provides an indication of whether an inequality constraint is active or not. Hence, based on the regularity and strict complementarity OS assumptions, which imply that $\mu_c = (\mu_{1_c}, \ldots, \mu_{17_c}) \neq 0$ is unique, and that $\mu_{l_c} > 0 \; \forall l \in \{\text{Active Constraint Set}\}$ [88], it follows from (3.41)-(3.43) that:

$$\hat{\mu}_{8_{k_c}}(Q_{G_{k_{min}}} - Q_{G_{k_c}}) = 0 \;\Rightarrow\; \hat{\mu}_{8_{k_c}} = 0 \; \forall k \in \bar{\mathcal{G}} \tag{3.56}$$

$$\hat{\mu}_{9_{\bar{j}_c}}(Q_{G_{\bar{j}_c}} - Q_{G_{\bar{j}max}}) = 0 \;\Rightarrow\; \hat{\mu}_{9_{\bar{j}_c}} = 0 \; \forall \bar{j} \in \mathcal{G}_{\bar{j}} \tag{3.57}$$

$$\hat{\mu}_{9_{j_c}}(Q_{G_{j_c}} - Q_{G_{jmax}}) = 0 \;\Rightarrow\; \hat{\mu}_{9_{j_c}} > 0 \; \forall j \in \mathcal{G}_j \tag{3.58}$$

$$\hat{\mu}_{10_c}(Q_{G_{i_{min}}} - Q_{G_{i_c}}) = 0 \;\Rightarrow\; \hat{\mu}_{10_c} = 0 \tag{3.59}$$

$$\hat{\mu}_{11_c}(Q_{G_{i_c}} - Q_{G_{imax}}) = 0 \;\Rightarrow\; \hat{\mu}_{11_c} > 0 \tag{3.60}$$

$$\hat{\mu}_{14_{k_c}}(-V_{a_{k_c}}) = 0 \;\Rightarrow\; \hat{\mu}_{14_{k_c}} > 0 \; \forall k \in \bar{\mathcal{G}} \tag{3.61}$$

$$\hat{\mu}_{15_{\bar{j}_c}}(-V_{b_{\bar{j}_c}}) = 0 \;\Rightarrow\; \hat{\mu}_{15_{\bar{j}_c}} > 0 \; \forall \bar{j} \in \mathcal{G}_{\bar{j}} \tag{3.62}$$

$$\hat{\mu}_{15_{j_c}}(-V_{b_{j_c}}) = 0 \;\Rightarrow\; \hat{\mu}_{15_{j_c}} = 0 \; \forall j \in \mathcal{G}_j \tag{3.63}$$

$$\hat{\mu}_{16_c}(-V_{a_{i_c}}) = 0 \;\Rightarrow\; \hat{\mu}_{16_c} > 0 \tag{3.64}$$

$$\hat{\mu}_{17_c}(-V_{b_{i_c}}) = 0 \;\Rightarrow\; \hat{\mu}_{17_c} > 0 \tag{3.65}$$

where $\bar{\mathcal{G}} = \mathcal{G}_{\bar{j}} \cup \mathcal{G}_j$.

Now, based on (3.41)-(3.43), the following actuation regime and saturation regime equations, evaluated at the solution point $(\hat{z}_c, \lambda_c, \hat{p}_o)$, are the minimum subsets of constraints (2.20b)-(2.20g) that uniquely define $\hat{z}_c$ for a given $(\lambda_c, \hat{p}_o)$, since the number of equations and unknowns is the same, i.e., $N = 2n_b + n_{\mathcal{G}}$, where n_b is the number of system buses and $n_{\mathcal{G}}$ is the number of generators:

$$G_a|_c = \begin{bmatrix} \widehat{G}(\delta_c, V_{L_c}, K_{G_c}, Q_{G_c}, V_{G_c}, \lambda_c, P_{S_o}, P_{D_o}) \\ V_{G_{\bar{j}_c}} - V_{G_{\bar{j}_o}} \quad \forall \bar{j} \in \mathcal{G}_{\bar{j}} \\ Q_{G_{j_c}} - Q_{G_{j_{max}}} \quad \forall j \in \mathcal{G}_j \\ V_{G_{i_c}} - V_{G_{i_o}} \end{bmatrix} = 0 \tag{3.66}$$

$$G_b|_c = \begin{bmatrix} \widehat{G}(\delta_c, V_{L_c}, K_{G_c}, Q_{G_c}, V_{G_c}, \lambda_c, P_{S_o}, P_{D_o}) \\ V_{G_{\bar{j}_c}} - V_{G_{\bar{j}_o}} \quad \forall \bar{j} \in \mathcal{G}_{\bar{j}} \\ Q_{G_{j_c}} - Q_{G_{j_{max}}} \quad \forall j \in \mathcal{G}_j \\ Q_{G_{i_c}} - Q_{G_{i_{max}}} \end{bmatrix} = 0 \tag{3.67}$$

Notice that these equations have a similar form as (2.8) and (2.9) respectively, where $\tilde{z}_c = (\delta_c, V_{L_c}, K_{G_c}, V_{G_c})$, $\hat{r}_c = Q_{G_c}$, $\hat{p}_o = (P_{S_o}, P_{D_o}, V_{G_o})$, $\hat{g}|_c = \widehat{G}|_c$, and

$$\hat{r}_c - s|_c \equiv \begin{bmatrix} V_{G_{\bar{j}_c}} - V_{G_{\bar{j}_o}} \quad \forall \bar{j} \in \mathcal{G}_{\bar{j}} \\ Q_{G_{j_c}} - Q_{G_{j_{max}}} \quad \forall j \in \mathcal{G}_j \\ V_{G_{i_c}} - V_{G_{i_o}} \end{bmatrix} \tag{3.68}$$

Observe that in this case, some of the actuation limit functions are implicit instead of explicit functions of the corresponding variables $\hat{r}$. Hence, for the optimal solution to be a LISB, one must first prove that the Jacobians J_a^i and J_b^i associated with (3.66) and (3.67) are nonsingular.

Let first prove that J_b^i is not singular. Hence, from (3.44)-(3.55) and with the proper ordering of variables and equations in (3.67), and assuming that $V_{\overline{G}} = (V_{G_{\bar{j}}} \, \forall \bar{j} \in \mathcal{G}_{\bar{j}}, V_{G_j} \, \forall j \in \mathcal{G}_j)$, and similarly for $Q_{\overline{G}}$, it can be shown that:

$$J_b^{i^T} \hat{x}_b = \hat{b}_b \tag{3.69}$$

where

$$J_b^{i^T} = \left[\begin{array}{ccccc|c} \nabla_\delta \widehat{G}_S|_c & \nabla_\delta \widehat{G}_{Q_{\overline{G}}}|_c & \nabla_\delta \widehat{G}_{Q_{G_i}}|_c & 0 & 0 & 0 \\ \nabla_{V_L} \widehat{G}_S|_c & \nabla_{V_L} \widehat{G}_{Q_{\overline{G}}}|_c & \nabla_{V_L} \widehat{G}_{Q_{G_i}}|_c & 0 & 0 & 0 \\ \nabla_{K_G} \widehat{G}_S|_c & 0 & 0 & 0 & 0 & 0 \\ \nabla_{V_{\overline{G}}} \widehat{G}_S|_c & \nabla_{V_{\overline{G}}} \widehat{G}_{Q_{\overline{G}}}|_c & \nabla_{V_{\overline{G}}} \widehat{G}_{Q_{G_i}}|_c & U & 0 & 0 \\ 0 & I_{n_{\bar{\mathcal{G}}}} & 0 & 0 & W & 0 \\ 0 & 0 & 1 & 0 & 0 & 1 \\ \hline \nabla_{V_{G_i}} \widehat{G}_S|_c & \nabla_{V_{G_i}} \widehat{G}_{Q_{\overline{G}}}|_c & \nabla_{V_{G_i}} \widehat{G}_{Q_{G_i}}|_c & 0 & 0 & 0 \end{array}\right]$$

$$= \left[\begin{array}{c|c} A^T & e \\ \hline c^T & 0 \end{array}\right]$$

$$\hat{x}_b = \left[\begin{array}{c} \hat{\mu}_{1_c} \\ \hat{\mu}_{2_c} \\ \hat{\mu}_{3_c} \\ \hat{\mu}_{12_{\mathcal{G}_{\bar{j}c}}} \\ \hline \hat{\mu}_{9_{\mathcal{G}_{j_c}}} \\ \hat{\mu}_{11_c} \end{array}\right]$$

$$\hat{b}_b = \left[\begin{array}{c} 0 \\ 0 \\ 0 \\ -W\hat{\mu}_{12_{\mathcal{G}_{j_c}}} \\ -M_{\bar{a}_c}\hat{\mu}_{4_c} - M_{\bar{b}_c}\hat{\mu}_{5_c} + \hat{\mu}_{8_c} - U\hat{\mu}_{9_{\mathcal{G}_{\bar{j}_c}}} \\ -V_{a_{i_c}}\hat{\mu}_{6_c} - V_{b_{i_c}}\hat{\mu}_{7_c} + \hat{\mu}_{10_c} \\ \hline \hat{\mu}_{13_c} \end{array}\right]$$

and $\hat{\mu}_9 = (\hat{\mu}_{9_{\mathcal{G}_{\bar{j}}}}, \hat{\mu}_{9_{\mathcal{G}_j}})$, $\hat{\mu}_{12} = (\hat{\mu}_{12_{\mathcal{G}_{\bar{j}}}}, \hat{\mu}_{12_{\mathcal{G}_j}})$,

$$U = \left[\begin{array}{c} I_{n_{\mathcal{G}_{\bar{j}}}} \\ 0 \end{array}\right], \quad W = \left[\begin{array}{c} 0 \\ I_{n_{\mathcal{G}_j}} \end{array}\right]$$

where I_n is an $n \times n$ identity matrix. From (3.48), (3.59) and (3.60):

$$\hat{\mu}_{3_c} = -\hat{\mu}_{11_c} \neq 0 \tag{3.70}$$

From (3.58)

$$\hat{\mu}_{9_{\mathcal{G}_{j_c}}} \neq 0 \tag{3.71}$$

And from (3.55) and (3.65)

$$\hat{\mu}_{13_c} = \hat{\mu}_{17_c} \neq 0 \tag{3.72}$$

Hence, from (3.70)-(3.72), it follows that:

$$\hat{x}_b \neq 0 \quad \text{and} \quad \hat{b}_b \neq 0$$

and are both unique. Therefore, one can conclude from (3.69) that J_b^i is nonsingular, i.e.,

$$\det(J_b^i) \neq 0 \tag{3.73}$$

Similarly, it can be readily shown that:

$$J_a^{i^T} \hat{x}_a = \hat{b}_a \tag{3.74}$$

where

$$J_a^{i^T} = \left[\begin{array}{c|c} A^T & 0 \\ \hline c^T & 1 \end{array}\right] \tag{3.75}$$

$$\hat{x}_a = \left[\begin{array}{c} \hat{\mu}_{1_c} \\ \hat{\mu}_{2_c} \\ \hat{\mu}_{3_c} \\ \hat{\mu}_{12_{\mathcal{G}_{\bar{j}c}}} \\ \hline \hat{\mu}_{9_{\mathcal{G}_{j_c}}} \\ \hat{\mu}_{13_c} \end{array}\right]$$

$$\hat{b}_a = \left[\begin{array}{c} 0 \\ 0 \\ 0 \\ -W\hat{\mu}_{12_{\mathcal{G}_{j_c}}} \\ -M_{\bar{a}_c}\hat{\mu}_{4_c} - M_{\bar{b}_c}\hat{\mu}_{5_c} + \hat{\mu}_{8_c} - U\hat{\mu}_{9_{\mathcal{G}_{\bar{j}_c}}} \\ \hline -V_{a_{i_c}}\hat{\mu}_{6_c} - V_{b_{i_c}}\hat{\mu}_{7_c} + \hat{\mu}_{10_c} - \hat{\mu}_{11_c} \\ 0 \end{array}\right]$$

Therefore, from (3.70)-(3.72), it follows that:

$$\hat{x}_a \neq 0 \quad \text{and} \quad \hat{b}_a \neq 0$$

and are both unique, yielding a nonsingular J_a^i, from (3.74) i.e.,

$$\det(J_a^i) \neq 0 \tag{3.76}$$

Thus, from (3.73) and (3.76), it is clear that the solution point $(\hat{z}_c, \lambda_c, \hat{p}_o)$ meets transversality conditions (2.10).

The second transversality condition (2.11) simply states that the ratio of the determinants of J_a^i and J_b^i must be positive for $(\hat{z}_c, \lambda_c, \hat{p}_o)$ to be a LISB. Thus, from (3.70) and (3.75), and based on Schur's Complements [91], it follows that:

$$\begin{aligned} \det(J_a^i) &= \det(A) \\ \det(J_b^i) &= -e^T A^{-1} c \det(A) \end{aligned}$$

Therefore:

$$\alpha = \frac{\det(J_a^i)}{\det(J_b^i)} = \frac{1}{-e^T A^{-1} c} \tag{3.77}$$

Now, from (3.66), it follows that:

$$\nabla_{\hat{z}}^T G_a|_c \, \mathrm{d}\hat{z} + \nabla_{V_{G_{i_o}}}^T G_a|_c \, \mathrm{d}V_{G_{i_o}} = 0$$

which from (3.75) can be rewritten as:

$$\left[\begin{array}{c|c} A & c \\ \hline 0 & 1 \end{array}\right] \left[\begin{array}{c} \mathrm{d}\bar{z} \\ \hline \mathrm{d}\bar{V}_{G_i} \end{array}\right] - \left[\begin{array}{c} 0 \\ \hline 1 \end{array}\right] \mathrm{d}V_{G_{i_o}} = 0$$

where $\hat{z} = (\bar{z}, V_{G_i})$. This yields:

$$\mathrm{d}\bar{z} = -A^{-1} c \, \mathrm{d}V_{G_i} \tag{3.78}$$

$$\mathrm{d}V_{G_i} = \mathrm{d}V_{G_{i_o}} \tag{3.79}$$

On the other hand, from (3.67) and (3.70), one knows that:

$$\left[\begin{array}{c|c} A & c \\ \hline e^T & 0 \end{array}\right] \left[\begin{array}{c} \mathrm{d}\bar{z} \\ \hline \mathrm{d}V_{G_i} \end{array}\right] - \left[\begin{array}{c} 0 \\ \hline 1 \end{array}\right] \mathrm{d}Q_{G_{i_{max}}} = 0$$

which yields (3.78) as well as:

$$\mathrm{d}Q_{G_i} = e^T \, \mathrm{d}\bar{z} = \mathrm{d}Q_{G_{i_{max}}} \tag{3.80}$$

Thus, from (3.78), (3.79) and (3.80), it follows that:

$$\left.\frac{\mathrm{d}Q_{G_{i_{max}}}}{\mathrm{d}V_{G_{i_o}}}\right|_c = -e^T A^{-1} c$$

which, from (3.77), leads to:

$$\alpha = \left.\frac{\mathrm{d}V_{G_{i_o}}}{\mathrm{d}Q_{G_{i_{max}}}}\right|_c \tag{3.81}$$

Now, from the optimization model (2.20), the sensitivities of the objective function with respect to $Q_{G_{i_{max}}}$ and $V_{G_{i_o}}$ evaluated at the optimal point can be stated as [92]:

$$\begin{aligned} \hat{\mu}_{11_c} &= \left.\frac{d\lambda}{dQ_{G_{i_{max}}}}\right|_c \\ \hat{\mu}_{13_c} &= \left.\frac{d\lambda}{dV_{G_{i_o}}}\right|_c \end{aligned}$$

Hence, from (3.60), (3.72), and (3.81), it follows that:

$$\alpha = \frac{\hat{\mu}_{11_c}}{\hat{\mu}_{13_c}} > 0 \tag{3.82}$$

which satisfies the second transversality condition (2.11). Therefore, the optimal solution $(\hat{z}_c, \lambda_c, \hat{p}_o)$ which meets the given OS assumptions is a LISB.

Finally, observe that at a LIDB, assumptions (3.41)-(3.43) are also met. However, (3.82) rules out the possibility of a LIDB being a solution of (2.20). □

This theorem basically proves that a given local optimum of (2.20) can be a LISB and not a LIDB, and that it can be preceded by some generators reaching reactive power limits, i.e., LIDBs. The following theorem shows that this local optimum can also be an SNB.

Theorem 3.2. *Let $(\hat{z}_c, \lambda_c)$ be local optimum of (2.20) that meets the abovementioned OS assumptions for $\hat{p} = \hat{p}_o$, where some generators $j \in \mathcal{G}_j \subset \mathcal{G}$ satisfy:*

$$\left.\begin{array}{c} Q_{G_{j_c}} = Q_{G_{j_{max}}} \\ V_{G_{j_c}} < V_{G_{j_o}} \end{array}\right\} \Rightarrow \left\{\begin{array}{l} V_{a_j} = 0 \\ V_{b_j} > 0 \end{array}\right. \tag{3.83}$$

while the rest of the generators $\bar{\jmath} \neq j \in \mathcal{G}_{\bar{\jmath}} \subset \mathcal{G}$, $\mathcal{G} = \mathcal{G}_{\bar{\jmath}} \cup \mathcal{G}_j$, are not at their reactive power limits, i.e.,

$$\left.\begin{array}{c} Q_{G_{\bar{\jmath}_{min}}} < Q_{G_{\bar{\jmath}_c}} < Q_{G_{\bar{\jmath}_{max}}} \\ V_{G_{\bar{\jmath}_c}} = V_{G_{\bar{\jmath}_o}} \end{array}\right\} \Rightarrow V_{a_{\bar{\jmath}}} = V_{b_{\bar{\jmath}}} = 0 \tag{3.84}$$

(Assumptions (3.83) and (3.84) generalize the case where an SNB occurs after a LIDB in λ space, as depicted in Figure 2.3.) Then, $(\hat{z}_c, \lambda_c, \hat{p}_o)$ is an SNB of the power flow model defined by equations (2.20b)-(2.20e).

Proof. Following a similar approach to the proof of Theorem 3.1, let $Q_G = (Q_{\overline{G}}, Q_{\widetilde{G}})$, where $Q_{\overline{G}} = (Q_{G_{\bar{\jmath}}} \ \forall \bar{\jmath} \in \mathcal{G}_{\bar{\jmath}}, Q_{G_j} \ \forall j \in \mathcal{G}_j)$, and similarly for V_G, V_a and V_b. Hence, the Lagrangian function of (2.20) may then be expressed as:

$$\begin{aligned} \mathcal{L} \ = \ & \lambda - \hat{\mu}_1^T \widehat{G}_S(\hat{z}_c, \lambda_c, \hat{p}_o) - \hat{\mu}_2^T \widehat{G}_{Q_{\overline{G}}}(\hat{z}_c, \lambda_c, \hat{p}_o) \\ & - \hat{\mu}_3 \widehat{G}_{Q_{\widetilde{G}}}(\hat{z}_c, \lambda_c, \hat{p}_o) - \hat{\mu}_4^T (Q_{\overline{G}} - Q_{\overline{G}_{min}}) V_{\tilde{a}} \\ & - \hat{\mu}_5^T (Q_{\overline{G}} - Q_{\overline{G}_{max}}) V_{\tilde{b}} - \hat{\mu}_6^T (Q_{\widetilde{G}} - Q_{\widetilde{G}_{min}}) V_{\tilde{a}} \\ & - \hat{\mu}_7^T (Q_{\widetilde{G}} - Q_{\widetilde{G}_{max}}) V_{\tilde{b}} - \hat{\mu}_8^T \left(Q_{\overline{G}_{min}} - Q_{\overline{G}}\right) \\ & - \hat{\mu}_9^T \left(Q_{\overline{G}} - Q_{\overline{G}_{max}}\right) - \hat{\mu}_{10}^T \left(Q_{\widetilde{G}_{min}} - Q_{\widetilde{G}}\right) \\ & - \hat{\mu}_{11}^T \left(Q_{\widetilde{G}} - Q_{\widetilde{G}_{max}}\right) - \hat{\mu}_{12}^T \left(V_{\overline{G}} - V_{\overline{G}_o} - V_{\tilde{a}} + V_{\tilde{b}}\right) \\ & - \hat{\mu}_{13} \left(V_{\widetilde{G}} - V_{\widetilde{G}_o} - V_{\tilde{a}} + V_{\tilde{b}}\right) - \hat{\mu}_{14}^T (-V_{\tilde{a}}) \\ & - \hat{\mu}_{15}^T (-V_{\tilde{b}}) - \hat{\mu}_{16}^T (-V_{\tilde{a}}) - \hat{\mu}_{17}^T (-V_{\tilde{b}}) \end{aligned}$$

From the KKT optimality conditions, it follows that:

$$\nabla_\delta \mathcal{L}|_c = -\nabla_\delta \widehat{G}_S|_c \hat{\mu}_{1_c} - \nabla_\delta \widehat{G}_{Q_{\overline{G}}}|_c \hat{\mu}_{2_c} - \nabla_\delta \widehat{G}_{Q_{\tilde{G}}}|_c \hat{\mu}_{3_c} = 0 \quad (3.85)$$

$$\nabla_{V_L} \mathcal{L}|_c = -\nabla_{V_L} \widehat{G}_S|_c \hat{\mu}_{1_c} - \nabla_{V_L} \widehat{G}_{Q_{\overline{G}}}|_c \hat{\mu}_{2_c} - \nabla_{V_L} \widehat{G}_{Q_{\tilde{G}}}|_c \hat{\mu}_{3_c} = 0 \quad (3.86)$$

$$\nabla_{K_G} \mathcal{L}|_c = -\nabla_{K_G} \widehat{G}_S|_c \hat{\mu}_{1_c} = 0 \quad (3.87)$$

$$\nabla_{Q_{\overline{G}}} \mathcal{L}|_c = -\hat{\mu}_{2_c} - M_{\bar{a}_c} \hat{\mu}_{4_c} - M_{\bar{b}_c} \hat{\mu}_{5_c} + \hat{\mu}_{8_c} - \hat{\mu}_{9_c} = 0 \quad (3.88)$$

$$\nabla_{Q_{\tilde{G}}} \mathcal{L}|_c = -\hat{\mu}_{3_c} - M_{\tilde{a}_c} \hat{\mu}_{6_c} - M_{\tilde{b}_c} \hat{\mu}_{7_c} + \hat{\mu}_{10_c} - \hat{\mu}_{11_c} = 0 \quad (3.89)$$

$$\nabla_{V_{\overline{G}}} \mathcal{L}|_c = -\nabla_{V_{\overline{G}}} \widehat{G}_S|_c \hat{\mu}_{1_c} - \nabla_{V_{\overline{G}}} \widehat{G}_{Q_{\overline{G}}}|_c \hat{\mu}_{2_c} - \nabla_{V_{\overline{G}}} \widehat{G}_{Q_{\tilde{G}}}|_c \hat{\mu}_{3_c} - \hat{\mu}_{12_c} = 0 \quad (3.90)$$

$$\nabla_{V_{\tilde{G}}} \mathcal{L}|_c = -\nabla_{V_{\tilde{G}}} \widehat{G}_S|_c \hat{\mu}_{1_c} - \nabla_{V_{\tilde{G}}} \widehat{G}_{Q_{\overline{G}}}|_c \hat{\mu}_{2_c} - \nabla_{V_{\tilde{G}}} \widehat{G}_{Q_{\tilde{G}}}|_c \hat{\mu}_{3_c} - \hat{\mu}_{13_c} = 0 \quad (3.91)$$

$$\nabla_\lambda \mathcal{L}|_c = -\nabla_\lambda \widehat{G}_S|_c \hat{\mu}_{1_c} - \nabla_\lambda \widehat{G}_{Q_{\overline{G}}}|_c \hat{\mu}_{2_c} - \nabla_\lambda \widehat{G}_{Q_{\tilde{G}}}|_c \hat{\mu}_{3_c} + 1 = 0 \quad (3.92)$$

$$\nabla_{V_{\bar{a}}} \mathcal{L}|_c = -M_{Q_{\overline{G}_{min_c}}} \hat{\mu}_{4_c} + \hat{\mu}_{12_c} + \hat{\mu}_{14_c} = 0 \quad (3.93)$$

$$\nabla_{V_{\bar{b}}} \mathcal{L}|_c = -M_{Q_{\overline{G}_{max_c}}} \hat{\mu}_{5_c} - \hat{\mu}_{12_c} + \hat{\mu}_{15_c} = 0 \quad (3.94)$$

$$\nabla_{V_{\tilde{a}}} \mathcal{L}|_c = -M_{Q_{\tilde{G}_{min_c}}} \hat{\mu}_{6_c} + \hat{\mu}_{13_c} + \hat{\mu}_{16_c} = 0 \quad (3.95)$$

$$\nabla_{V_{\tilde{b}}} \mathcal{L}|_c = -M_{Q_{\tilde{G}_{max_c}}} \hat{\mu}_{7_c} - \hat{\mu}_{13_c} + \hat{\mu}_{17_c} = 0 \quad (3.96)$$

where $M_{\bar{a}_c} = \text{diag}(V_{\bar{a}_c})$, and similarly for $M_{\bar{b}_c}$, $M_{\tilde{a}_c}$, $M_{\tilde{b}_c}$; and $M_{Q_{\overline{G}_{min_c}}} = \text{diag}(Q_{\overline{G}_c} - Q_{\overline{G}_{min}})$, and similarly for $M_{Q_{\overline{G}_{max_c}}}$, $M_{Q_{\tilde{G}_{min_c}}}$, and $M_{Q_{\tilde{G}_{max_c}}}$. Furthermore, all the equality constraints must be equal to zero, while the inequality constraints must be less than or equal to zero.

From the regularity and strict complementarity OS assumptions, which imply a unique $\mu_c = (\mu_{1_c}, \ldots, \mu_{17_c}) \neq 0$, with $\mu_{l_c} > 0 \ \forall l \in \{\text{Active Constraint Set}\}$, it follows from (3.83) and (3.84) that:

$$\hat{\mu}_{8_{\bar{j}_c}}(Q_{G_{\bar{j}_{min}}} - Q_{G_{\bar{j}_c}}) = 0 \ \Rightarrow \ \hat{\mu}_{8_{\bar{j}_c}} = 0 \ \forall \bar{j} \in \mathcal{G}_{\bar{j}} \quad (3.97)$$

$$\hat{\mu}_{9_{\bar{j}_c}}(Q_{G_{\bar{j}_c}} - Q_{G_{\bar{j}_{max}}}) = 0 \ \Rightarrow \ \hat{\mu}_{9_{\bar{j}_c}} = 0 \ \forall \bar{j} \in \mathcal{G}_{\bar{j}} \quad (3.98)$$

$$\hat{\mu}_{10_{j_c}}(Q_{G_{j_{min}}} - Q_{G_{j_c}}) = 0 \ \Rightarrow \ \hat{\mu}_{10_{j_c}} = 0 \ \forall j \in \mathcal{G}_j \quad (3.99)$$

$$\hat{\mu}_{11_{j_c}}(Q_{G_{j_c}} - Q_{G_{j_{max}}}) = 0 \ \Rightarrow \ \hat{\mu}_{11_{j_c}} > 0 \ \forall j \in \mathcal{G}_j \quad (3.100)$$

$$\hat{\mu}_{14_{\bar{j}_c}}(-V_{a_{\bar{j}_c}}) = 0 \ \Rightarrow \ \hat{\mu}_{14_{\bar{j}_c}} > 0 \ \forall \bar{j} \in \mathcal{G}_{\bar{j}} \quad (3.101)$$

$$\hat{\mu}_{15_{\bar{j}_c}}(-V_{b_{\bar{j}_c}}) = 0 \ \Rightarrow \ \hat{\mu}_{15_{\bar{j}_c}} > 0 \ \forall \bar{j} \in \mathcal{G}_{\bar{j}} \quad (3.102)$$

$$\hat{\mu}_{16_{j_c}}(-V_{a_{j_c}}) = 0 \ \Rightarrow \ \hat{\mu}_{16_{j_c}} > 0 \ \forall j \in \mathcal{G}_j \quad (3.103)$$

$$\hat{\mu}_{17_{j_c}}(-V_{b_{j_c}}) \;\; = 0 \;\Rightarrow \quad \hat{\mu}_{17_{j_c}} = 0 \; \forall j \in \mathcal{G}_j \tag{3.104}$$

Now, based on (3.83) and (3.84), the following equations, evaluated at the solution point $(\hat{z}_c, \lambda_c, \hat{p}_o)$, form the minimum subset of constraints (2.20b)-(2.20g) that uniquely define $\hat{z}_c$ for a given $(\lambda_c, \hat{p}_o)$, since the number of equations and unknowns are the same, i.e., N:

$$G|_c = \begin{bmatrix} \widehat{G}(\delta_c, V_{L_c}, K_{G_c}, Q_{G_c}, V_{G_c}, \lambda_c, P_{S_o}, P_{D_o}) \\ V_{\overline{G}_c} - V_{\overline{G}_o} \\ Q_{\tilde{G}_c} - Q_{\tilde{G}_{max}} \end{bmatrix} = 0 \tag{3.105}$$

Hence, for the optimal solution to be an SNB, one must first prove that the Jacobian $J = \nabla^T_{\hat{z}} G|_c$ is singular with unique nonzero eigenvectors, where $\hat{z} = (\delta, V_L, K_G, V_G, Q_G)$.

From (3.85)-(3.96) and with the proper ordering of variables and equations in (3.67), it can be shown that:

$$\nabla_{\hat{z}} G|_c \; \hat{w} = \hat{b} \tag{3.106}$$

where,

$$\nabla_{\hat{z}} G|_c = \begin{bmatrix} \nabla_\delta \widehat{G}_S|_c & \nabla_\delta \widehat{G}_{Q_{\overline{G}}}|_c & \nabla_\delta \widehat{G}_{Q_{\tilde{G}}}|_c & 0 & 0 \\ \nabla_{V_L} \widehat{G}_S|_c & \nabla_{V_L} \widehat{G}_{Q_{\overline{G}}}|_c & \nabla_{V_L} \widehat{G}_{Q_{\tilde{G}}}|_c & 0 & 0 \\ \nabla_{K_G} \widehat{G}_S|_c & 0 & 0 & 0 & 0 \\ \nabla_{V_{\overline{G}}} \widehat{G}_S|_c & \nabla_{V_{\overline{G}}} \widehat{G}_{Q_{\overline{G}}}|_c & \nabla_{V_{\overline{G}}} \widehat{G}_{Q_{\tilde{G}}}|_c & I_{n_{\mathcal{G}_{\bar{j}}}} & 0 \\ \nabla_{V_{\tilde{G}}} \widehat{G}_S|_c & \nabla_{V_{\tilde{G}}} \widehat{G}_{Q_{\overline{G}}}|_c & \nabla_{V_{\tilde{G}}} \widehat{G}_{Q_{\tilde{G}}}|_c & 0 & 0 \\ 0 & I_{n_{\mathcal{G}_{\bar{j}}}} & 0 & 0 & 0 \\ 0 & 0 & I_{n_{\mathcal{G}_j}} & 0 & I_{n_{\mathcal{G}_j}} \end{bmatrix} \tag{3.107}$$

$$\hat{w} = \begin{bmatrix} \hat{\mu}_{1_c} \\ \hat{\mu}_{2_c} \\ \hat{\mu}_{3_c} \\ \hat{\mu}_{12_c} \\ \hat{\mu}_{11_c} + M_{\bar{b}_c}\hat{\mu}_{7_c} \end{bmatrix} \tag{3.108}$$

$$\hat{b} = \begin{bmatrix} 0 \\ 0 \\ 0 \\ 0 \\ -\hat{\mu}_{13_c} \\ -M_{\bar{a}_c}\hat{\mu}_{4_c} - M_{\bar{b}_c}\hat{\mu}_{5_c} + \hat{\mu}_{8_c} - \hat{\mu}_{9_c} \\ -M_{\tilde{a}_c}\hat{\mu}_{6_c} + \hat{\mu}_{10_c} \end{bmatrix}$$

Now, from (3.96) and (3.104):

$$\hat{\mu}_{13_c} = \hat{\mu}_{17_c} = 0 \tag{3.109}$$

From (3.84), (3.97) and (3.98):

$$-M_{\bar{a}_c}\hat{\mu}_{4_c} - M_{\bar{b}_c}\hat{\mu}_{5_c} + \hat{\mu}_{8_c} - \hat{\mu}_{9_c} = 0 \tag{3.110}$$

From (3.83) and (3.99):

$$-M_{\tilde{a}_c}\hat{\mu}_{6_c} + \hat{\mu}_{10_c} = 0 \tag{3.111}$$

Hence, from (3.109)-(3.111), it follows that:

$$\nabla_{\hat{z}} G|_c \; \hat{w} = 0$$

Finally, from the regularity and strict complementarity OS assumptions, it follows that $\mu_{1_c} \neq 0$, $\mu_{2_c} \neq 0$, and $\mu_{3_c} \neq 0$, as $\hat{\mu}_c \neq 0$ and is unique. Hence, $\hat{w} \neq 0$ and is unique, from which it can be concluded that the optimum $(\hat{z}_c, \lambda_c, \hat{p}_o)$ meets the SNB transversality condition (2.3).

Now, from (3.92), (3.105) and (3.108), it follows that:

$$\nabla_\lambda \mathcal{L}|_c = -\nabla_\lambda G|_c \, \hat{w} + 1 = 0$$

$$\Rightarrow \; \nabla_\lambda G|_c \, \hat{w} \neq 0$$

which corresponds to the SNB transversality condition (2.4).

The third SNB transversality condition (2.5) is now verified. Thus, from assumptions (3.83) and (3.84) regarding the optimum $(\hat{z}_c, \lambda_c, \hat{p}_o)$, and from (3.105), as well as based on the previous analysis, the optimization model (2.20) can be restated as follows, since it would yield the same optimal solution:

$$\begin{aligned} \max \quad & \lambda \\ \text{s.t.} \quad & G(\hat{z}, \lambda, \hat{p}_o) = 0 \end{aligned}$$

The corresponding Lagrangian function may then be defined as:

$$\mathcal{L}(\hat{z}, \lambda, \hat{p}_o, \hat{\mu}) = \lambda - \hat{\mu}^T G(\hat{z}, \lambda, \hat{p}_o)$$

which, based on the KKT optimality conditions, leads to:

$$\nabla_{\hat{z}} \mathcal{L}|_c = -\nabla_{\hat{z}} G|_c \hat{\mu}_c = -\nabla_{\hat{z}} G|_c \hat{w} = 0 \tag{3.113}$$

$$\nabla_{\hat{\mu}} \mathcal{L}|_c = -G|_c = 0 \tag{3.114}$$

$$\nabla_\lambda \mathcal{L}|_c = -\nabla_\lambda G|_c \hat{w} + 1 = 0 \tag{3.115}$$

Based on the OS assumptions, which guarantee that the set of equations (3.113)-(3.115) have a unique solution, the full Hessian of the Lagrangian function, i.e., the Jacobian of these equations, must be nonsingular; thus:

$$\nabla^2_{(\hat{z},\hat{\mu},\lambda)} \mathcal{L}(\hat{z}_c, \lambda_c, \hat{p}_o, \hat{w}) \; \rho \neq 0 \quad \forall \rho \neq 0 \tag{3.116}$$

where

$$\nabla^2_{(\hat{z},\hat{\mu},\lambda)} \mathcal{L}|_c = -\begin{bmatrix} \nabla^2_{\hat{z}} G|_c \hat{w} & \nabla_{\hat{z}} G|_c & \nabla^2_{\lambda\hat{z}} G|_c \hat{w} \\ \nabla^T_{\hat{z}} G|_c & 0 & \nabla^T_\lambda G|_c \\ \hat{w}^T \nabla^{2^T}_{\hat{z}\lambda} G|_c & \nabla_\lambda G|_c & \nabla^2_\lambda G|_c \hat{w} \end{bmatrix} \tag{3.117}$$

Hence, for a chosen $\rho = (\hat{v}, 0, 0) \neq 0$, from (3.116) one has that:

$$\left[\nabla^2_{\hat{z}} G|_c \hat{w}\right] \hat{v} \neq 0 \tag{3.118}$$

since, in this case, $\nabla^{2^T}_{\hat{z}\lambda} G|_c = \nabla^2_{\lambda\hat{z}} G|_c = 0$. On the other hand, from the second-order KKT necessary optimality conditions [88]:

$$\hat{\rho}^T \; \nabla^2_{(\hat{z},\lambda)} \mathcal{L}|_c \; \hat{\rho} \leq 0 \quad \forall \hat{\rho} \in \mathcal{U}(\hat{z}_c, \lambda_c) \tag{3.119}$$

where

$$\mathcal{U}(\hat{z}_c, \lambda_c) = \left\{ \hat{\rho} \in \mathbb{R}^{n_{\hat{z}}+1} : \left[\nabla^T_{\hat{z}} G|_c \, \nabla^T_{\lambda} G|_c\right] \hat{\rho} = 0 \right\}$$

Hence, for $\hat{\rho} = (\hat{v}, 0)$ it follows from (3.117) and (3.119) that:

$$\hat{v}^T \left[\nabla^2_{\hat{z}} G|_c \hat{w}\right] \hat{v} \geq 0$$

Therefore, from (3.118), it can be concluded that:

$$\hat{v}^T \left[\nabla^2_{\hat{z}} G|_c \hat{w}\right] \hat{v} > 0$$

Finally, taking the transpose of this equation and considering the properties of tensor products:

$$\hat{w}^T \left[\nabla^{2^T}_{\hat{z}} G|_c \hat{v}\right] \hat{v} > 0$$

This corresponds to the third SNB transversality condition (2.5). □

It is important to highlight that this theorem proves that the solution is not simply a fold but an SNB, since the uniqueness of the zero eigenvectors is demonstrated here. Finally, the following corollary argues that an optimum of (2.20) can only be a LISB or an SNB.

Corollary 3.1. *Any solution point* $(\hat{z}_c, \lambda_c, \hat{p}_o)$ *of* (2.20) *that meets the aforementioned OS assumptions is either a LISB or an SNB.*

Proof. Observe that Theorem 3.1 proofs that a LIDB cannot be a solution of (2.20). Now, notice that all possible limit conditions of the inequality constraints of (2.20)

are considered in assumptions (3.41)-(3.43) and (3.83)-(3.84) of Theorems 3.1 and 3.2, respectively. Thus, the cases of none or all generators reaching their limits are simply particular cases of these assumptions. Hence, any feasible solution of (2.20), would either meet assumptions (3.41)-(3.43) or (3.83)-(3.84). Therefore, the solution point $(\hat{z}_c, \lambda_c, \hat{p}_o)$ can only be a LISB or a SNB. □

3.3 Numerical Examples

This section presents a numerical comparison between the OPF-DM and the CPF method to illustrate some of the theoretical issues discussed in the previous section. Thus, the maximum loading factor, voltage, and reactive power levels obtained from solving (2.20) are compared with those obtained using the standard CPF, for a variety of test cases for the 6-bus system shown in Figure A.1 [1]. In these cases, the generators' voltage set points and reactive power limits are assumed to be $V_{G_o} = 1.05$ p.u. and $Q_G = \pm 1.5$ p.u., respectively. The CIGRE-32 test system described in Appendix A is also used to compare both techniques.

3.3.1 Practical Implementation Issues

The OPF-DM with complementarity constraints can be implemented in AMPL, using the `complements` operator [93, 94], which allows complementarity conditions to be directly specified in the constraint declarations, and then solved using solvers specifically designed for complementarity problems such as KNITRO [95]. Alternatively, the complementarity constraints can be specified as nonsmooth constraints as in (2.20), solving the optimization problem with nonlinear programming solvers such as LOQO, KNITRO or IPOPT. This second approach is used here to obtain the numerical results discussed in this section. On the other hand, UWPFLOW [72], which is a popular and well-tested software tool with a robust implementation of a CPF technique, was used to obtain PV curves for illustrative and comparison

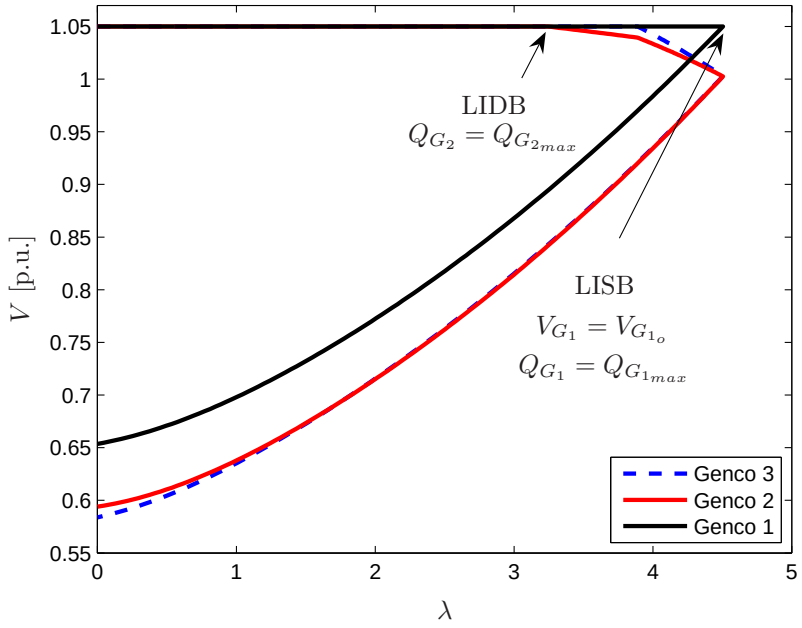

Figure 3.5: Generators' PV curve for the 6-bus system: The base case exhibits a LISB.

purposes. For both techniques, the generation and load variations were assumed to be defined by (2.13)-(2.15).

It is important to highlight the fact that the initial operating point is rather important, since it is used to define the generator voltage set points for the optimization problem as well as the starting point for the CPF; and it must be obtained by running an initial power flow simulation. The auxiliary variables used in the definition of the complementarity constraints must be initialized to zero.

3.3.2 Numerical Results

The PV curves in Figures 3.5-3.7 present three bifurcation profiles under different operating conditions: Figure 3.5 shows a LISB at $\lambda_c = 4.5049$ p.u., preceded by LIDBs, for the base system topology; Figure 3.6 shows an SNB at $\lambda_c = 1.9081$ p.u., preceded by LIDBs, when line 2-4 is removed from the system; and Figure 3.7 shows

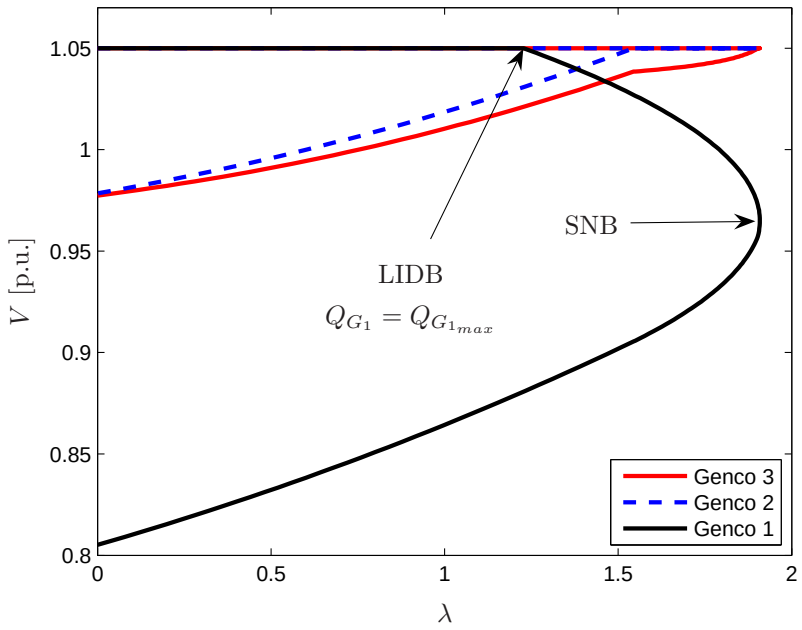

Figure 3.6: Generators' PV curve for the 6-bus system: A contingency scenario shows a LIDB followed by an SNB.

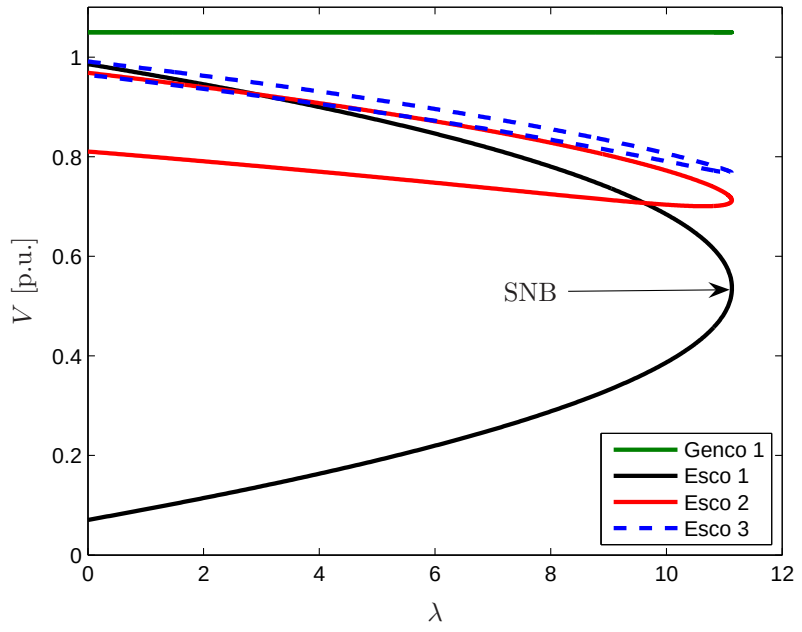

Figure 3.7: Generators' PV curve for the 6-bus system: SNB with no Q_G-limits.

Table 3.1: OPF-DM vs CPF for the 6-bus test system

	LISB		SNB (with Q_G-limits)		SNB (without Q_G-limits)	
	OPF-DM	CPF	OPF-DM	CPF	OPF-DM	CPF
V_{G_1}	1.0500	1.0500	0.9648	0.9657	1.0500	1.0500
V_{G_2}	1.0025	1.0026	1.0500	1.0500	1.0500	1.0500
V_{G_3}	1.0029	1.0029	1.0500	1.0500	1.0500	1.0500
V_{L_4}	0.8458	0.8458	0.6027	0.6048	0.5360	0.5360
V_{L_5}	0.8546	0.8545	0.8586	0.8591	0.7129	0.7125
V_{L_6}	0.8687	0.8686	0.9465	0.9466	0.7679	0.7677
Q_{G_1}	1.5	1.5	1.5	1.5	3.1588	3.1600
Q_{G_2}	1.5	1.5	0.9577	0.9511	6.2724	6.2734
Q_{G_3}	1.5	1.5	1.4712	1.4682	3.5828	3.5856
λ_c	4.4966	4.5049	1.9046	1.9081	11.1141	11.1330

All values in p.u.

another SNB at a $\lambda_c = 11.1330$ p.u. when Q_G-limits are ignored for the base system. Observe in these plots that the bifurcations in the first two cases are preceded by some LIDBs in λ space. Also, in the last case, the SNB occurs at a larger loading factor, with the voltages at generator buses remaining constant. Notice as well the sharp "edge" of the bifurcation manifold at the maximum loading point defined by a LISB, which is a characteristic of these type of bifurcations, and the "quadratic" shape of the manifolds around the SNBs which are also typical.

Table 3.1 presents a comparison of the solutions obtained using the optimization model (2.20) as well as the equivalent results obtained from the CPF, depicted in Figures 3.5-3.7. The results presented in the first and second columns correspond to the base case, and they show that GENCO 1 satisfies the LISB condition

$Q_{G1_c} = Q_{G1_{max}}$ and $V_{G1_c} = V_{G1_o}$ at λ_c, while GENCO 2 and GENCO 3 are at their reactive power limits with their voltages below the corresponding set points. That is, the system has undergone 2 LIDBs before reaching a LISB in λ space, as clearly illustrated in Figure 3.5. The results in the third and fourth columns, obtained by removing line 2-4, show GENCO 2 and GENCO 3 within their reactive power limits and at their corresponding voltage set points. Meanwhile, GENCO 1 has reached its maximum reactive power limit and its voltage is below its set point, indicating the occurrence of a LIDB before the SNB in λ space, as depicted in Figure 3.6. Finally, the results presented in the last two columns, which correspond to the base system without generator reactive power limits, show all generators at their voltage set points as well as large reactive power outputs. That is, there are no LIDBs before the SNB in λ space. This table shows that both techniques essentially give the same solution; the small differences can be basically attributed to numerical approximations, particularly in the case of the CPF. The execution time for the OPF-DM was in the range of 0.12s, which was faster than the CPF.

The sequence of generators reaching the maximum reactive power limit can be also obtained from the OPF-DM, by ranking the difference $\Delta V_{G_{ic}} = V_{G_{io}} - V_{G_{ic}}$ in descending order. Thus, the largest difference corresponds to the first generator's reaching its maximum reactive power limit, and so on. If the difference is negative, then the generator would have reached the minimum reactive power limit. For example, the ranked differences for the base case are: $\Delta V_{G_{2c}} = 0.0475$, $\Delta V_{G_{3c}} = 0.0471$ and $\Delta V_{G_{1c}} = 0$, which agrees with what is observed in Figure 3.5.

A test was carried out to study the effect of setting the upper voltage limits at generation buses at their corresponding set points for the model without complementarity constraints (2.17), with the objective that by defining $V_{G_{max}} = V_{G_o}$, the optimization solution process would "fix" the generator voltages at their initial maximum voltage levels. This would yield similar results as those obtained by solving (2.20), since voltages at generation buses, if not fixed, typically increase when increasing the load. It is interesting to notice that this approach generated the same results as those depicted in Table 3.1. However, this was not the case for

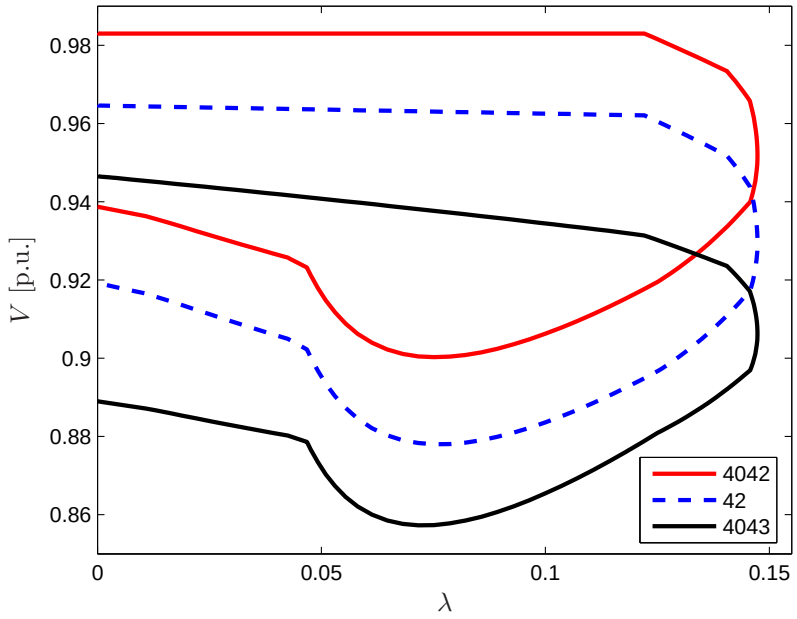

Figure 3.8: PV curve for the CIGRE-32 test system: The base case exhibits an SNB.

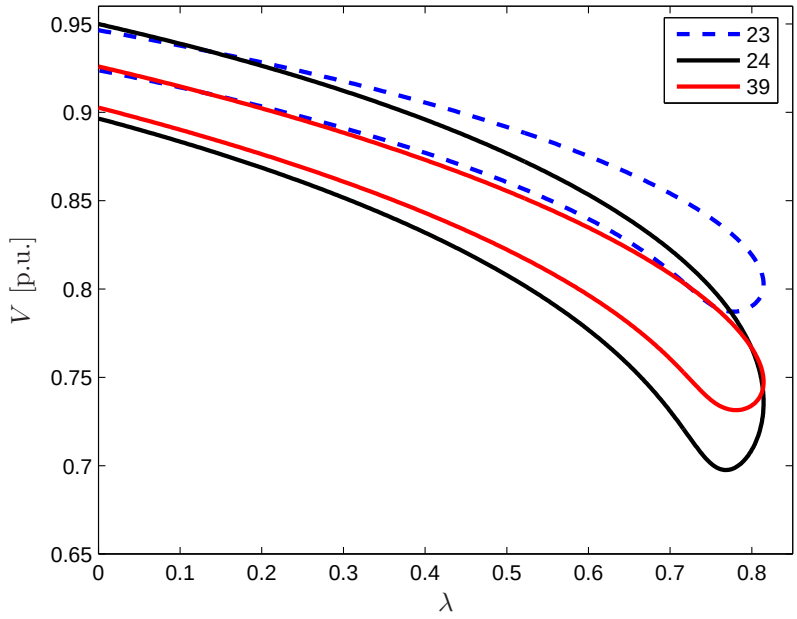

Figure 3.9: PV curve for the CIGRE-32 system: SNB with no Q_G-limits.

other test systems, since (2.17) does not necessarily guarantee that generators are going to be at their maximum voltage values (voltage set points in this case) if their reactive power limits have not been reached. For instance, Table 3.2 summarizes the results for the CIGRE-32 test system corresponding to the PV curves shown in Figure 3.8 and Figure 3.9, where an SNB at $\lambda = 0.1473$, and at $\lambda = 0.8144$ are shown for the base case and neglecting Q_G-limits, respectively. Observe in this table that the reactive power at some buses is significantly different from that obtained using CPF, if complementarity constraints are not used. Also notice that in some generators:

- $V_G = V_{G_o}$ when the reactive power is within limits, e.g., $Q_{G_{4047_{max}}} = 6.0$ p.u., and $V_{G_{o_{4044}}} = 0.9473$ p.u.
- $V_G < V_{G_o}$ if a Q_G-limit is reached, e.g., $Q_{G_{4042_{max}}} = 3.5$ p.u., and $V_{G_{o_{4042}}} = 0.9831$ p.u.
- both Q_G and V_G are set to the upper limit, e.g., $Q_{G_{4011_{max}}} = 5.0$ p.u., $Q_{G_{4012_{max}}} = 4.0$ p.u., $V_{G_{o_{4011}}} = 1.05$ p.u., and $V_{G_{o_{4012}}} = 1.04$ p.u.

Table 3.2: Comparison of the OPF-DM vs CPF for the CIGRE-32 system

	SNB (with Q_G-limits)			SNB (without Q_G-limits)		
	OPF-DM		CPF	OPF-DM		CPF
	(2.17)	(2.20)		(2.17)	(2.20)	
$V_{G_{4011}}$	1.0500	1.0500	1.0500	0.9341	1.0500	1.0500
$V_{G_{4012}}$	1.0400	1.0400	1.0400	0.2430	1.0400	1.0400
$V_{G_{4042}}$	0.9537	0.9521	0.9521	0.9831	0.9831	0.9830
$V_{G_{42}}$	0.9314	0.9298	0.9298	0.9457	0.9467	0.9465
$V_{G_{4043}}$	0.9075	0.9066	0.9065	0.8099	0.8030	0.8029
$V_{G_{43}}$	0.8820	0.8811	0.8810	0.7537	0.7477	0.7476
$V_{G_{4047}}$	0.9473	0.9473	0.9470	0.9473	0.9473	0.9470

Continued on next page

Table 3.2 – continued from previous page

	SNB (with Q_G-limits)			SNB (without Q_G-limits)		
	OPF-DM		CPF	OPF-DM		CPF
	(2.17)	(2.20)		(2.17)	(2.20)	
$V_{G_{4046}}$	0.9064	0.9059	0.9057	0.8082	0.8064	0.8062
$V_{G_{47}}$	0.9235	0.9235	0.9232	0.9067	0.9078	0.9074
$V_{G_{46}}$	0.8764	0.8759	0.8757	0.7403	0.7405	0.7402
$Q_{G_{4072}}$	-0.2130	4.9683	4.9665	8.7258	8.9849	8.9826
$Q_{G_{4071}}$	2.5000	1.1419	1.1415	22.1923	2.2520	2.2519
$Q_{G_{4011}}$	5.0000	0.8662	0.8540	100	9.4523	9.4458
$Q_{G_{4012}}$	4.0000	-0.6065	-0.6119	-40.4752	1.5048	1.5037
$Q_{G_{4021}}$	1.5000	1.5000	1.5000	14.0337	11.1244	11.1261
$Q_{G_{4031}}$	1.7500	1.7500	1.7500	49.0580	23.4120	23.3409
$Q_{G_{4042}}$	3.5000	3.5000	3.5000	30.1225	34.3495	34.3127
$Q_{G_{4041}}$	2.0941	2.2167	2.1972	12.3894	15.2220	15.2365
$Q_{G_{4062}}$	1.7610	1.7601	1.7197	36.9707	10.5022	10.4566
$Q_{G_{4063}}$	2.2965	2.2905	2.3130	3.4694	5.2850	5.3054
$Q_{G_{4051}}$	3.5000	3.5000	3.5000	15.9721	16.5290	16.5068
$Q_{G_{4047}}$	3.7669	3.8447	3.8065	15.2604	15.5880	15.5650
$Q_{G_{2032}}$	1.3713	1.3802	1.3758	26.2726	4.3197	4.3239
$Q_{G_{1013}}$	2.2579	1.2057	1.2052	12.1313	2.8660	2.8643
$Q_{G_{1012}}$	-0.7905	-0.3673	-0.3678	100	1.9076	1.9058
$Q_{G_{1014}}$	-0.9999	0.4218	0.4218	0.6924	0.6075	0.6091
$Q_{G_{1022}}$	1.2500	1.2500	1.2500	31.5172	12.1901	12.1866
$Q_{G_{1021}}$	2.7510	2.7467	2.7436	11.6739	6.8142	6.8071
$Q_{G_{1043}}$	1.0000	1.0000	1.0000	20.0257	20.1360	20.0896
$Q_{G_{1042}}$	0.4923	0.5040	0.4993	2.7057	2.7233	2.7192
λ_c	0.1492	0.1476	0.1473	0.8578	0.8148	0.8144

3.4 Summary

This chapter has presented a detailed, theoretical study of an optimization method able to determine two types of fold bifurcations directly associated with voltage instabilities in power systems. It was demonstrated that the necessary and sufficient optimality conditions yield the transversality conditions for SNBs and LISBs. Thus, it has been shown that the solution of the studied optimization problem yields the same results as those obtained with the more popular CPF techniques, which is typically used to analyze these types of bifurcations in power systems.

The advantages of stating the SNB/LIB problem as an optimization problem is that optimization solution techniques can be computationally more effective than CPF methods for maximum loadability studies, particularly when using well-tested and efficient solution techniques such as IPM. Furthermore, optimization approaches are more versatile than CPF techniques, since the problem can be readily restated so that optimal control parameter values can be calculated to increase the maximum loadability margins of a system, or readily carry out a variety of sensitivity studies.

Chapter 4

Practical Solution of Voltage-Stability-Constrained Optimal Power Flows

4.1 Introduction

Chapter 3 demonstrated the feasibility of an optimization method to determine the voltage collapse point of a power flow model, namely an SNB or LIB point. This chapter proposes a novel and practical method to enforce a VS constraint in an OPF auction model, based on the MSV and minimum singular vectors of the power flow Jacobian. By ensuring that this singular value is bounded from reaching zero and guaranteeing that generators' reactive power and other security limits are met, adequate security margins in a power system can be ensured, hence preventing a voltage collapse point. The proposed technique is based on a SVD of the power flow Jacobian at a given solution point, plus an iterative process to satisfy the VS constraint. A small but realistic, 6-bus test system and a 1211-bus model of a European grid are used to analyze the performance of the proposed technique. Comparisons with previously proposed solution techniques for similar VSC-OPFs

are presented. The results obtained demonstrate the feasibility of applying the proposed VSC-OPF in practice.

4.2 Proposed Solution Method

The main objective in the development of the proposed solution method is to replace (2.24c) with an equivalent constraint that can be written explicitly in terms of the VSC-OPF optimization variables. Thus, SVD concepts and an iterative technique to deal with this constraint in practice are used in the proposed VSC-OPF method, as described below.

4.2.1 Singular Value Decomposition (SVD)

The SVD is typically used to determine the rank of a matrix, i.e., the maximum number of independent rows or columns, and it can be used as a measure of how close a matrix is to the set of singular matrices [96]. Therefore, if the Jacobian $J \in \mathbb{R}^{n\times n}$, where $n = 2n_b$ (n_b is the number of buses in (2.21b)), is invertible or nonsingular, this matrix is full rank and its orthonormal decomposition is defined as:

$$J = U\Sigma W^T = \sum_{i=1}^{n} \sigma_i u_i w_i^T \tag{4.1}$$

where the singular vectors u_i and w_i are the i^{th} columns of the unitary matrices U and W, and Σ is a diagonal matrix of positive real singular values σ_i, such that $\sigma_1 \geq \sigma_2 \geq \cdots \sigma_n$. Thus, for the i^{th} column of the unitary matrices it follows that:

$$\left.\begin{array}{c} J^T u_i = \sigma_i w_i \\ J w_i = \sigma_i u_i \end{array}\right\} \Rightarrow u_i^T J w_i = \sigma_i, \tag{4.2}$$

where $u_i^T u_i = 1$, $w_i^T w_i = 1$, and $u_i^T w_i = 0$ [96] (σ_n is zero if J is singular).

Since J becomes singular at an SNB point, the proximity to voltage collapse can be determined by monitoring the smallest singular value σ_n [13,44]. Therefore,

the following equation is proposed as an alternative formulation for (2.24c):

$$\sigma_{min}\{J\} \geq \sigma_c \;\Leftrightarrow\; u_n^T J w_n \geq \sigma_c \tag{4.3}$$

Consequently, (2.24) can be restated as follows:

$$\begin{aligned}
\max_{\substack{\delta,V_L,Q_G \\ V_G,P_S,P_D}} \quad & \sum_{j\in\mathcal{D}} C_{D_j} P_{D_j} - \sum_{i\in\mathcal{G}} C_{S_i} P_{S_i} && \text{(4.4a)}\\
\text{s.t} \quad & \widehat{G}(\delta, V_L, Q_G, V_G, P_S, P_D) = 0 && \text{(4.4b)}\\
& u_n^T J(\delta, V_L, V_G) w_n \geq \sigma_c && \text{(4.4c)}\\
& P_{S_{i_{min}}} \leq P_{S_i} \leq P_{S_{i_{max}}} \quad \forall i \in \mathcal{G} && \text{(4.4d)}\\
& P_{D_{j_{min}}} \leq P_{D_j} \leq P_{D_{j_{max}}} \quad \forall j \in \mathcal{D} && \text{(4.4e)}\\
& Q_{G_{i_{min}}} \leq Q_{G_i} \leq Q_{G_{i_{max}}} \quad \forall i \in \mathcal{G} && \text{(4.4f)}\\
& V_{i_{min}} \leq V_i \leq V_{i_{max}} \quad \forall i \in \mathcal{B} && \text{(4.4g)}\\
& I_{ij}(\delta, V) \leq I_{ij_{max}} \quad \forall (i,j) \in \mathcal{T}, i \neq j && \text{(4.4h)}
\end{aligned}$$

The main advantages of model (4.4) is that the explicit function (4.4c) does not require to approximate derivatives in the solution process, and it can be implemented using mathematical programming languages and solved with commercial solvers for large-scale nonlinear optimization problems. Furthermore, it can be applied in the solution of more realistic systems, as demonstrated later in Section 4.3.5. However, the discussed observations below lead to the development of an iterative solution method.

Observe that σ_n may not be necessarily greater or equal to σ_c at the optimal solution, since the parameters u_n and w_n come from the SVD of J at a particular power flow solution, which does not necessarily correspond to the solution of (4.4); this leads to having to update these vectors iteratively until $\sigma_n \geq \sigma_c$. Furthermore, notice that the structure of J may also differ from that at the initial point, due to some PV buses becoming PQ buses during the solution process; however, the proposed method to solve this model requires an invariant Jacobian to reduce the execution time and make it more practical. The following two sections address

these two particular issues; thus, Section 4.2.2 studies the MSV of an invariant Jacobian that is not affected by PV buses becoming PQ buses, and Section 4.2.3 describes the proposed algorithm to update the parameters u_n and w_n.

4.2.2 MSV VSI of Invariant Jacobian

The power flow model used to obtain the VSI used in (2.24) is based on the following nonlinear set of equations that define the active and reactive power mismatches at the system buses:

$$\left[\begin{array}{c} \Delta P(\delta, V_L, K_G, V_G, \lambda) \\ \Delta Q(\delta, V_L, Q_G, V_G, \lambda) \end{array} \right] = \widehat{G}(\delta, V_L, Q_G, K_G, V_G, \lambda) = 0 \tag{4.5}$$

Notice that the reactive power mismatch equations at PV buses are included in (4.5). Thus, for an n_b-bus system, there are two equations and two variables for each PQ, PV, or slack bus (SL). This allows to solve (4.5) without the need for changing the dimension of J when a Q_G-limit is reached or released, requiring only to swap variables V_G with Q_G, or viceversa.

In the "classical" way of solving the power flow problem using a Newton-Raphson method, the power flow Jacobian is associated with two equations for each PQ bus and one for each PV bus, and none for the slack bus, since only the δ and V variables for each PQ bus and the variable δ for each PV bus are considered [97]. This Jacobian is referred here as $J_{PF} \in \mathbb{R}^{n \times n}$, where $n = 2n_b - n_{PV} - 1$ (n_{PV} is the number of *original* PV buses), and is a submatrix of J as follows:

$$J = \left[\begin{array}{cc} J_{PF} & J_2 \\ J_3 & J_4 \end{array} \right] \tag{4.6}$$

Table 4.1 summarizes the number of equations and associated variables with each of the submatrices of J. In this table, $\Delta P_{PV}, \Delta P_{SL}$ and ΔP_{PQ} represent the active power mismatch equations at PV, SL, and PQ buses, respectively, and ΔQ_G

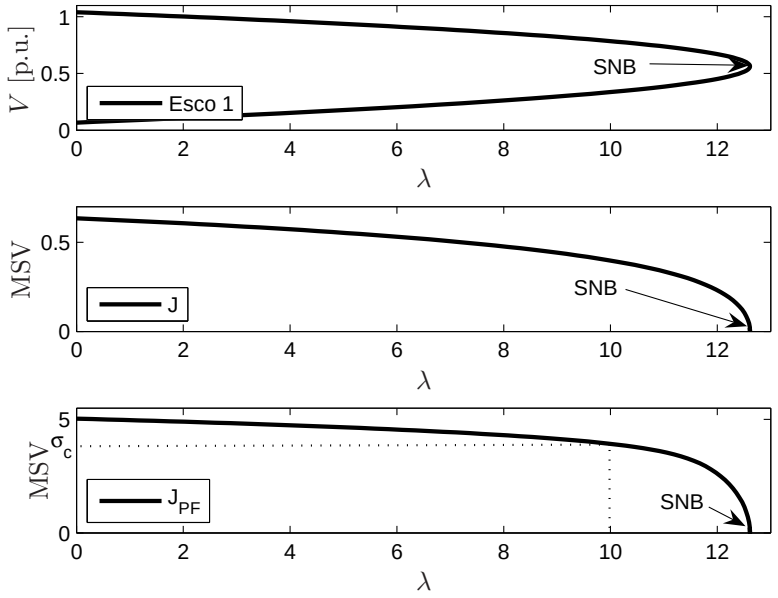

(a)

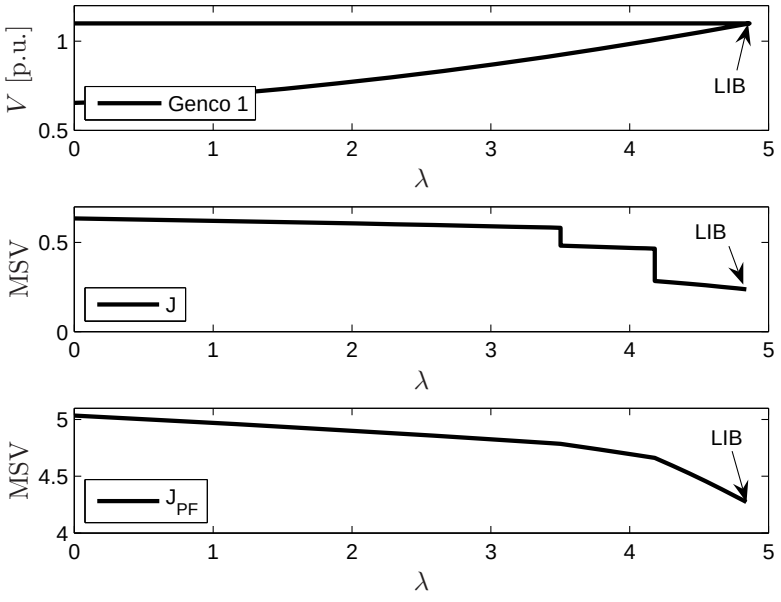

(b)

Figure 4.1: PV curves, and MSV of J and J_{PF} for a 6-bus test system: (a) SNB neglecting Q_G-limits; (b) LIB considering Q_G-limits.

Table 4.1: Structure and dimensions of J

	Equations (rows)	Variables (cols)	Dimension
J_{PF}	$\Delta P_{PV}, \Delta P_{PQ}, \Delta Q_{PQ}$	δ, V_L	$n \times n$
J_2	$\Delta P_{PV}, \Delta P_{PQ}, \Delta Q_{PQ}$	K_G, Q_G	$n \times m$
J_3	$\Delta P_{SL}, \Delta Q_G$	δ, V_L	$m \times n$
J_4	$\Delta P_{SL}, \Delta Q_G$	K_G, Q_G	$m \times m$

$n = 2n_b - n_{PV} - 2, m = n_{PV} + 2$

and ΔQ_{PQ} are the reactive power mismatch equations at generation (PV and SL buses) and PQ buses, respectively.

As λ increases, some PV buses become PQ buses as Q_G-limits are reached, and the structure of J changes to accommodate the switch between Q_G and V_G variables; hence, as λ changes, J is affected, and this fact has to be taken into consideration in the formulation of the proposed VS constraint (4.4c). However, given the matrix subdivision of J in (4.6), J_{PF} remains invariant as λ increases, i.e., the change in variables when PV buses become PQ buses does not affect it. Furthermore, through numerical tests it can be observed that the MSV of J_{PF} decreases as λ increases; there is no formal proof of this fact, but the author has observed this in all small and large systems studied. For example, consider the 6-bus test system shown in Figure A.1. Figure 4.1 depicts the MSV of J and J_{PF} obtained while calculating the PV curves using a CPF technique [72], based on (2.13)-(2.15). Figure 4.1(a) shows that the MSVs of both J and J_{PF} become zero at the SNB point if Q_G-limits are not considered. Figure 4.1(b), which corresponds to a LIB due to Q_G-limits being reached, shows that the MSV of J_{PF} is different from that of J at the maximum loading point and that it does not undergo sudden changes. The latter is an important advantage, since the convergence problems that can result from the rapid changes of the MSV of J are less likely to occur.

Note that even though the MSVs of J and J_{PF} are not the same, the MSVs

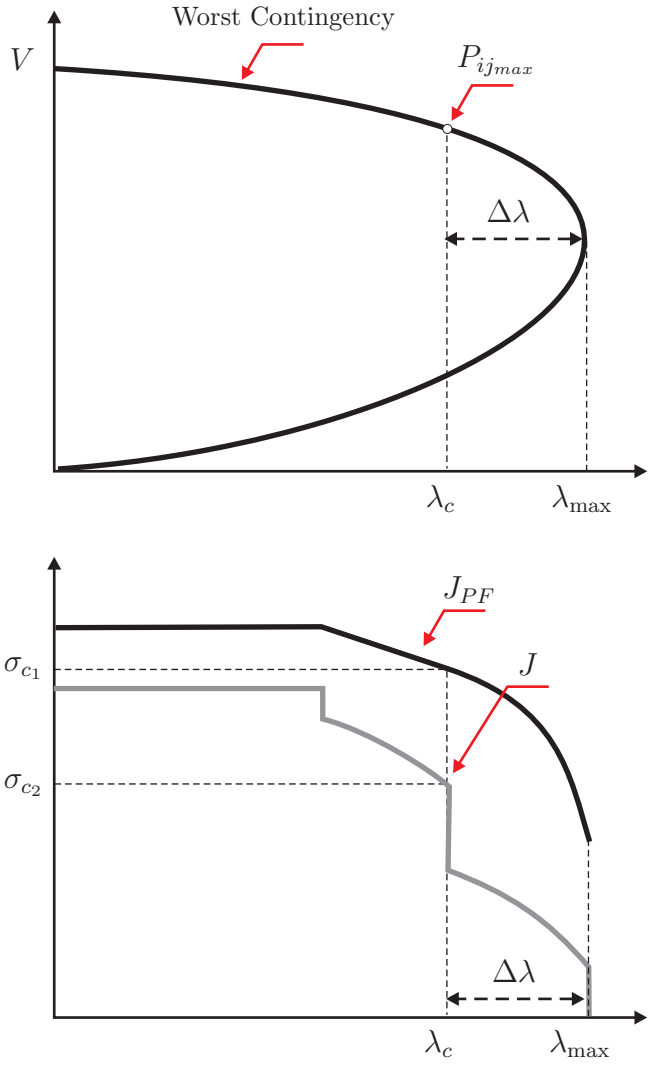

Figure 4.2: PV curve, and two critical MSV for J and J_{PF} at the the same loading point; $\Delta\lambda$ defines a security margin.

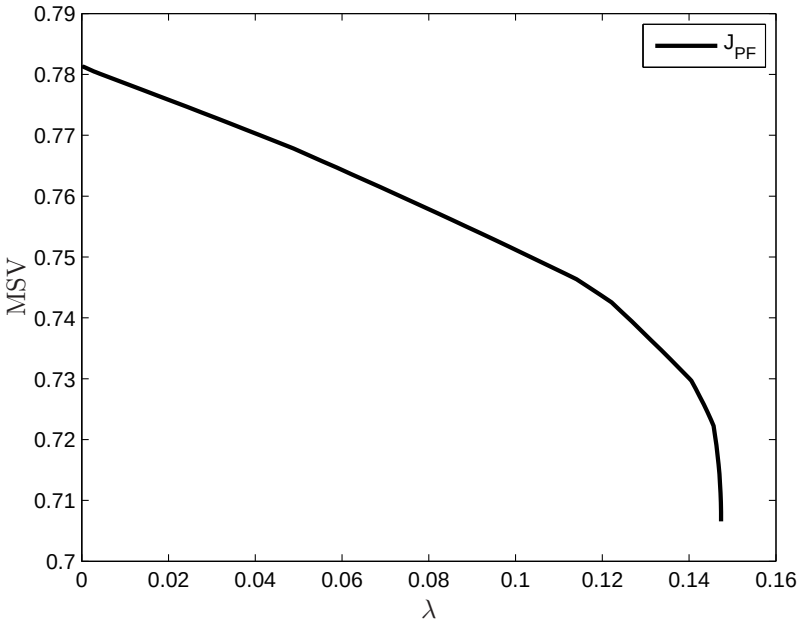

Figure 4.3: MSV of J_{PF} for the CIGRE-32 test system considering Q_G-limits.

of these Jacobians associated with any maximum loading point of interest can be used as a VSI for a particular system. This is illustrated in a more general form in Figure 4.2, where σ_{c_1} or σ_{c_2} define a "critical" MSV of a particular system at certain loading point defined by λ_c; these values are chosen off-line, so that λ_c defines a maximum loading point for a given dispatch pattern considering the worst contingency. It should be mentioned that the MSV of J_{PF} does not necessary become zero at the SNB point when Q_G-limits are considered, as observed in studies of larger test systems (e.g., the CIGRE-32 test system case shown in Figure 4.3). However, as illustrated in Figure 4.2, the MSV of J_{PF} simply defines an alternative VSI that can be used to determine the σ_c value, which is a valid value from the practical perspective of applying the proposed VSC-OPF.

4.2.3 Updating Algorithm

As previously mentioned, an iterative algorithm to update the vectors u_n and w_n during the solution process is required. The initial values for these parameters can be obtained by relaxing (4.4c), i.e., basically solving an OPF. In fact, if (4.4c) holds for the optimal solution, then the solution for this subproblem is also a solution of (4.4). Thus, the following algorithm is proposed to solve the VSC-OPF model, which calculates the SVD of J_{PF} at the OPF solution to update u_n and w_n until $\sigma_n \geq \sigma_c$:

Algorithm: Solution of the VSC-OPF using a SVD

1 **begin**
2 $\sigma_c \leftarrow$ Off-line VS study
3 $k \leftarrow 1$
4 $(\delta^*, V_L^*, V_G^*) \leftarrow$ VSC-OPF ("relaxed")
5 $(u_n, \sigma_n, w_n) \leftarrow \text{SVD}(J_{PF}|_*)$
6 **if** $\sigma_n \geq \sigma_c$ **then**
7 **end**
8 **else**
9 **repeat**
10 $k \leftarrow k + 1$
11 $(\delta^*, V_L^*, V_G^*) \leftarrow$ VSC-OPF
12 $(u_n, \sigma_n, w_n)^{(k)} \leftarrow \text{SVD}(J_{PF}|_*)$
13 **until** $\sigma_n^{(k)} \geq \sigma_c$
14 **end**
15 $(\delta^*, V_L^*, Q_G^*, V_G^*, P_S^*, P_D^*) \rightarrow$ Optimum
16 **end**

Note that in Step 4, the algorithm initially solves (4.4) without (4.4c) to obtain $(u_n, \sigma_n, w_n)^{(1)}$. Then, it verifies whether $\sigma_n \geq \sigma_c$. If true, the process stops. If not, then $(u_n, w_n)^{(k)}$ is used to solve the VSC-OPF in Step 11, with (4.4c) incorporated

into the optimization. The SVD is updated at the new solution, and k is increased. The process is repeated until $\sigma_n^{(k)} \geq \sigma_c$.

4.3 Numerical Results

This section presents and discusses numerical examples of the proposed method, concentrating first on demonstrating how the proposed VSC-OPF method (4.4) works, and comparing it to the VSC-OPF model (2.24). A comparison between the VSC-OPF (4.4) and the SC-OPF (2.21) is then presented to study the effect of the proposed VS constraint on a single 6-bus model. Finally, a 1211-bus system model representing an actual European network is used to demonstrate the feasibility of applying the proposed technique in practice.

The proposed method (4.4) was formulated using the AMPL [93] modeling language and solved with IPOPT [98], whereas Matlab [99] was used for the required SVD computations. The optimization model (2.24) was implemented in Matlab, since current mathematical programming languages are not able to handle implicit constraints.

4.3.1 Effect of Proposed VS Constraint

A numerical example to illustrate the application of the proposed method and the effect of σ_c on the results is presented here using the 6-bus test system shown in Figure A.1. Observe in Figure 4.1(b) that a small change in σ_c for this system, e.g., from 4.99 to 5.03, can have a significant effect on the loading margin (security levels), hence affecting system dispatch levels and market conditions.

Table 4.2 shows the initial values of u_n and w_n obtained at each iteration of the proposed method. Notice the progress of σ_n with respect to the values chosen for σ_c, with the starting system conditions meeting the initial value chosen for $\sigma_{c_1} = 4.99$ (in this case the proposed method did not require any iterations), and

Table 4.2: Progress of the unitary vectors and MSV when σ_c is increased from 4.99 to 5.03.

Initial values		$k=1$		$k=2$	
$u_n^{(0)}$	$w_n^{(0)}$	$u_n^{(1)}$	$w_n^{(1)}$	$u_n^{(2)}$	$w_n^{(2)}$
-0.3504	0.3556	-0.3535	0.3583	-0.3535	0.3583
-0.5266	0.5377	-0.5275	0.5375	-0.5275	0.5376
-0.2540	0.2426	-0.2557	0.2447	-0.2557	0.2448
-0.5102	0.4879	-0.5078	0.4879	-0.5055	0.4878
-0.5242	0.5167	-0.5227	0.5161	-0.5228	0.5162
0.0076	0.0659	0.0100	0.0642	0.0101	0.0642
-0.0019	0.0993	0.0043	0.0936	0.0045	0.0934
0.0086	0.0784	0.0131	0.0742	0.0132	0.0741
$\sigma_n^{(0)} = 4.99 \geq 4.99$		$\sigma_n^{(1)} = 5.0291 < 5.03$		$\sigma_n^{(2)} = 5.0302 > 5.03$	

Table 4.3: Comparison of voltage, power dispatch, and LMPs at the solution of the VSC-OPF when σ_c is increased from 4.99 to 5.03.

Participant	VSC-OPF ($\sigma_c = 4.99$)			VSC-OPF ($\sigma_c = 5.0302$)		
	V [p.u.]	P_S/P_D [MW]	LMP [$/MWh]	V [p.u.]	P_S/P_D [MW]	LMP [$/MWh]
GENCO 1	1.1	0	8.95	1.1	0	9.06
GENCO 2	1.1	25	8.90	1.1	6.0	8.80
GENCO 3	1.1	20	9.07	1.1	20	9.33
ESCO 1	1.021	25	9.48	1.022	25	9.60
ESCO 2	1.012	10	9.58	1.020	0.85	9.98
ESCO 3	1.038	8.0	9.35	1.044	0	9.73

after two iterations the method converged to $\sigma_n > \sigma_{c_2} = 5.03$. Table 4.3 shows that the voltage profile at load buses improves by increasing σ_c; however, the LMPs increase, and the power dispatch levels are reduced. This is to be expected, since the system security levels rise with an increase in σ_c, thus positively affecting system operating conditions, and negatively affecting market conditions.

4.3.2 Efficiency of the Proposed Method

A small change in σ_c was used in the last section to see the effect of increasing system security on the market and system conditions. This section presents a similar test to determine how the proposed method performs when it is subject to a σ_c value considerably different from that at a given power flow solution. The following two cases are studied: the current operating point is close to an SNB, and the operating point is close to a LIB point. Thus, $\sigma_c = 4.98$ is used to force the VSC constraint to become active and determine how fast the method converges to this value. Note that $\sigma_n \approx 0$ at the SNB point, and that $\sigma_n = 4.262$ at the LIB point in Figure 4.1(b).

Figure 4.4 shows σ_n at every iteration for the two cases. Observe that in both cases the proposed method required only one iteration to increase σ_n to approximately 4.98, plus one iteration to converge. The author's experience with different test cases shows that, in general, the proposed method requires less than three iterations to converge regardless of the difference between the σ_c and σ_n. These results permit one to conclude that the proposed method can handle large increments of σ_n during the solution process, allowing a quick and efficient solution of the VSC-OPF.

4.3.3 Comparison of VSC-OPF Formulations

Although the VSC-OPF models (2.24) and (4.4) are somewhat equivalent, their corresponding stability constraints (2.24c) and (4.4c) require different solution ap-

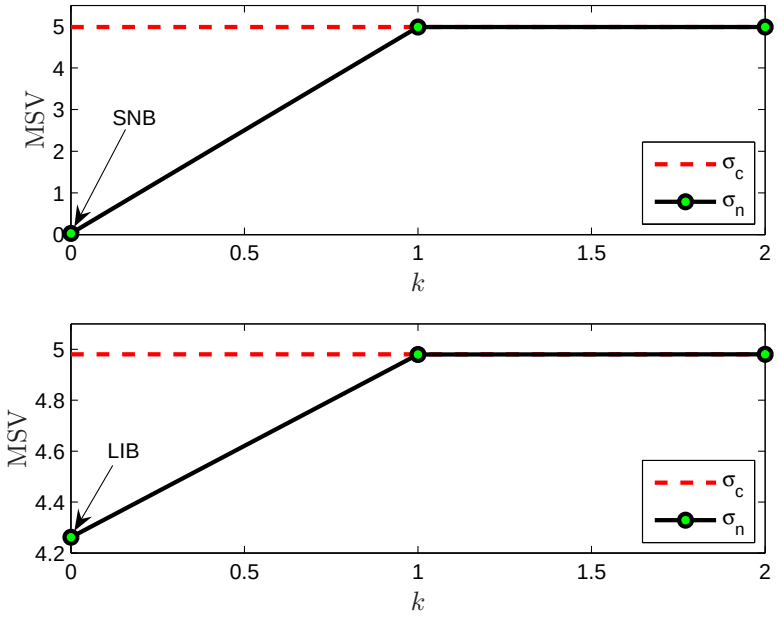

Figure 4.4: MSV at every iteration when σ_c is increased from 0 to 4.98, and when increased from 4.262 to 4.98.

proaches. In (2.24), approximate derivatives of the constraint are needed in the IPM solution process [34], whereas an iterative procedure is used in (4.4). Therefore, a comprehensive comparison of both methods to understand their properties is of interest.

In order to better understand the differences between different VSC-OPF solution methods, neither thermal nor generation reactive power limits are considered here, thus concentrating on the effect and handling of the MSV constraint without lost of generality. The highly nonlinear nature of the MSV as it approaches maximum loading condition is the main disadvantage of this index [13], and this feature may result in convergence problems. Therefore, in order to study this issue, the operating point at $\lambda_c = 10$ in Figure 4.1(a), which is closer to the maximum loading point and hence results in large changes of the MSV with only small loading level changes, is considered to be the base loading condition. Thus, the MSV associated with this loading level is used as the σ_c value, i.e., $\sigma_c = 3.8603$. The tests then

consist of increasing λ from 10 following the directions shown in (2.13)-(2.15) until both (2.24) and (4.4) become unfeasible. This allows a comparison of solutions obtained with these methods and their overall performance.

Figures 4.5(a) and 4.5(b) show the most significant results from the test, i.e., the final MSV of the power flow Jacobian at the optimum in p.u. with respect to σ_c, and the number of iterations required to converge. The values of the MSV are normalized in these two figures due to the fact that (2.24) and (4.4) are not based on the same Jacobian (as discussed in detail in Section 4.2.2). Figure 4.5(a) demonstrates that the proposed method successfully meets the MSV constraint for all the feasible values of λ. A consistent number of iterations to attain convergence is obtained, where k is the number of iterations in the proposed algorithm (as discussed in Section 4.2.3), and k_s is the number of iterations needed by the IPOPT solver for each k ($k \leq 2$ in all cases). Notice that this behavior is observed even when close to the point where the optimization becomes unfeasible at $\lambda = 10.21$.

Figure 4.5(b) reveals two important characteristics of the VSC-OPF model (2.24). First, observe that σ_{min} is slightly below σ_c for most of the feasible values of λ; and second, the feasible values of λ are larger (for (2.24), $\lambda_{max} = 10.72$, whereas $\lambda_{max} = 10.21$ for (4.4)). These differences are due to the fact that the VS constraint in (2.24) is handled approximately within the solution technique in [34, 45], i.e., it is basically a "soft" constraint; this is not the case in (4.4), where this constraint is "hard". With respect to the number of iterations, (2.24) requires a comparatively larger number of total iterations to converge than (4.4). It is important to highlight that although both methods were implemented using different computational environments, the number of iterations should provide a reasonable comparison of the performance. Thus (4.4) is significantly more efficient than (2.24).

The differences in the handling of the VS constraint by these two models have a significant impact in the system and market conditions, obtaining different dispatch and voltage levels as well as LMPs for both methods as λ is increased. Notice, for instance, that the power dispatch for ESCO 3 and GENCO 3, shown in Figure 4.6 and Figure 4.7, respectively, is significantly different when using (4.4) or (2.24).

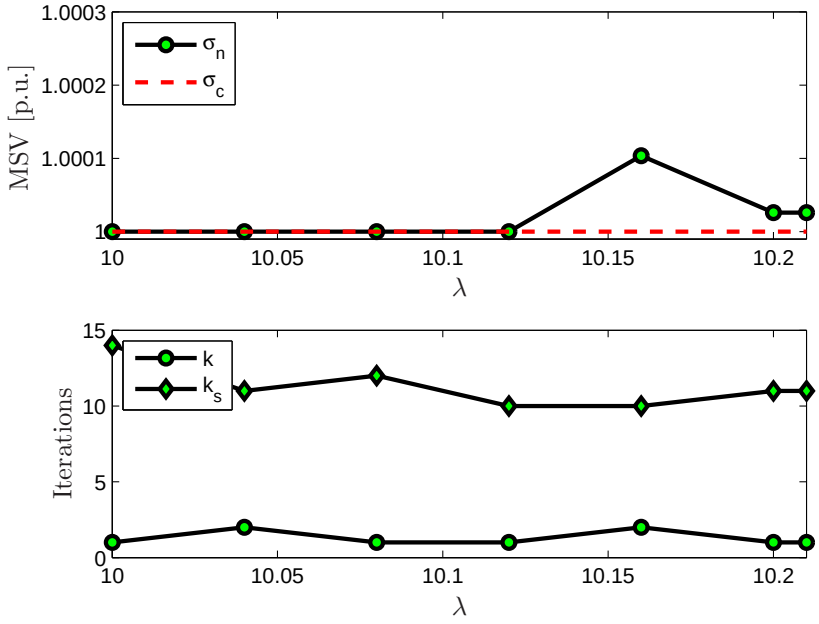

(a)

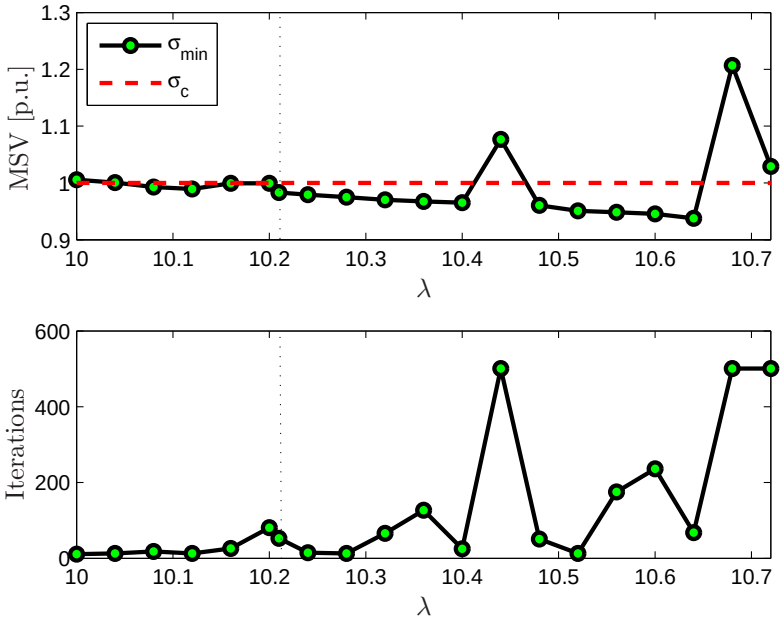

(b)

Figure 4.5: MSV at the optimum with respect to the loading factor (a) for (4.4), and (b) for (2.24).

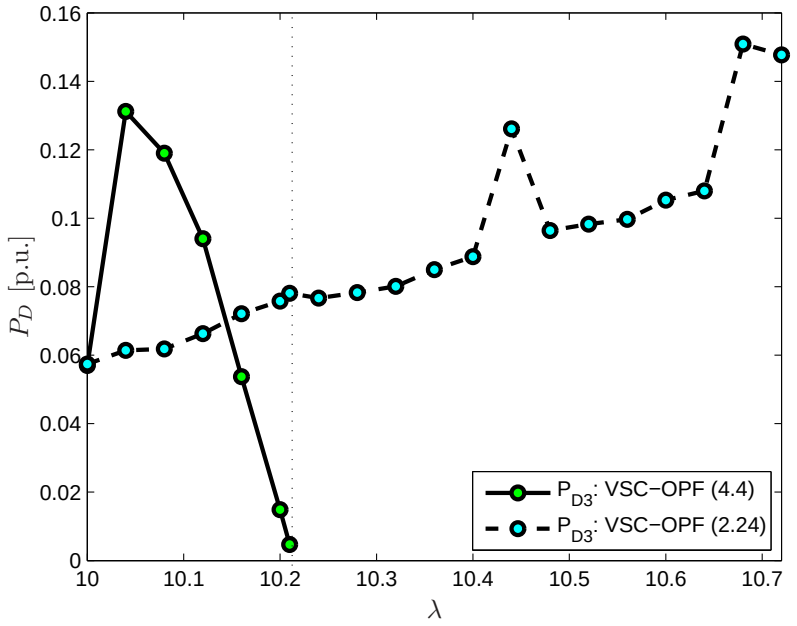

Figure 4.6: ESCO 3 power with respect to the loading factor for the 6-bus system.

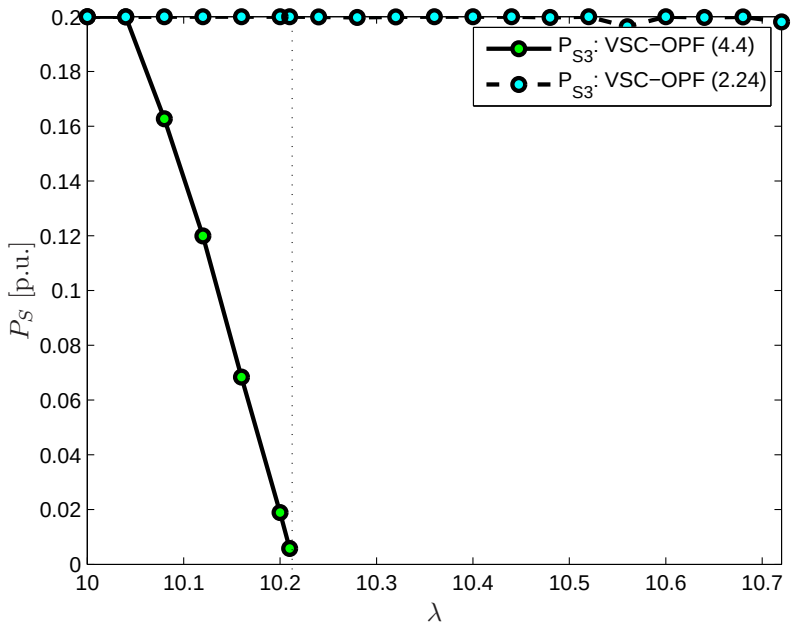

Figure 4.7: GENCO 3 power with respect to the loading factor for the 6-bus system.

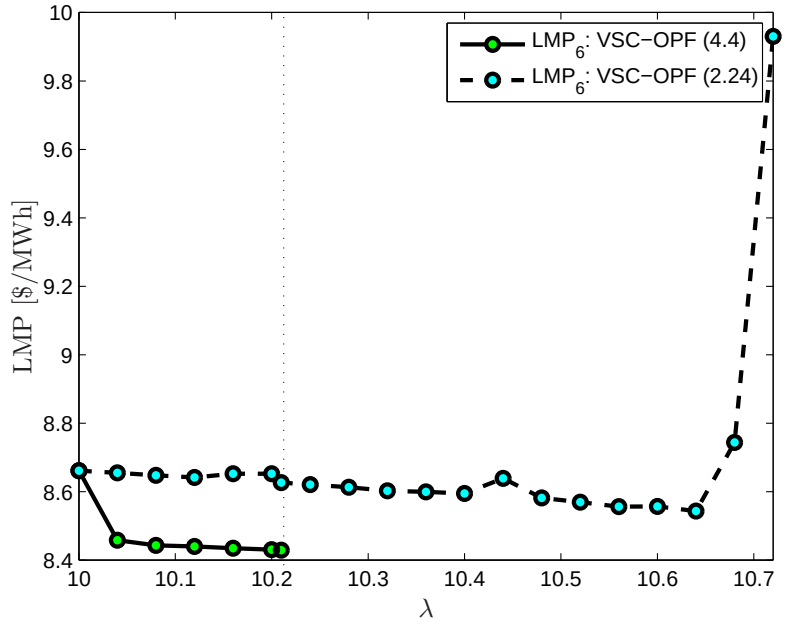

Figure 4.8: LMP 6 with respect to the loading factor for the 6-bus system.

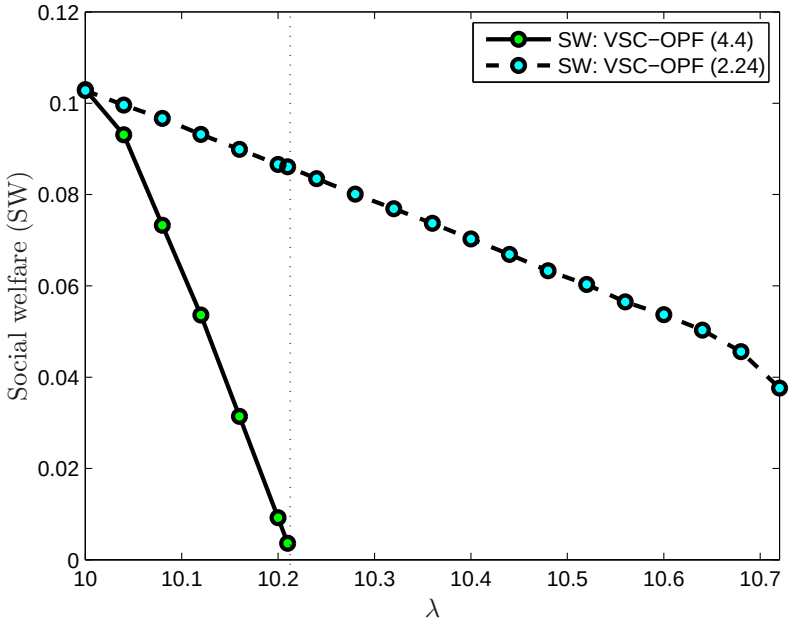

Figure 4.9: Objective function with respect to the loading factor for the 6-bus system.

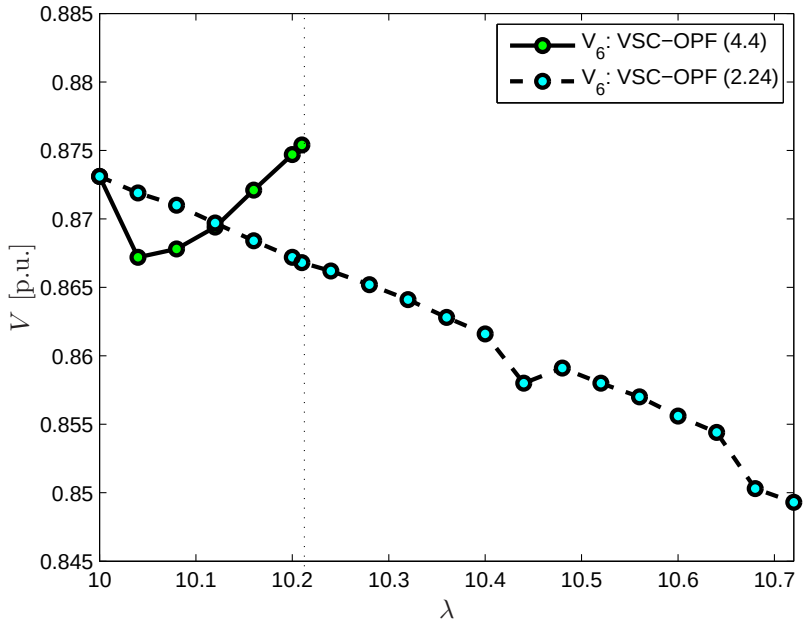

Figure 4.10: ESCO 3 voltage with respect to the loading factor for the 6-bus system.

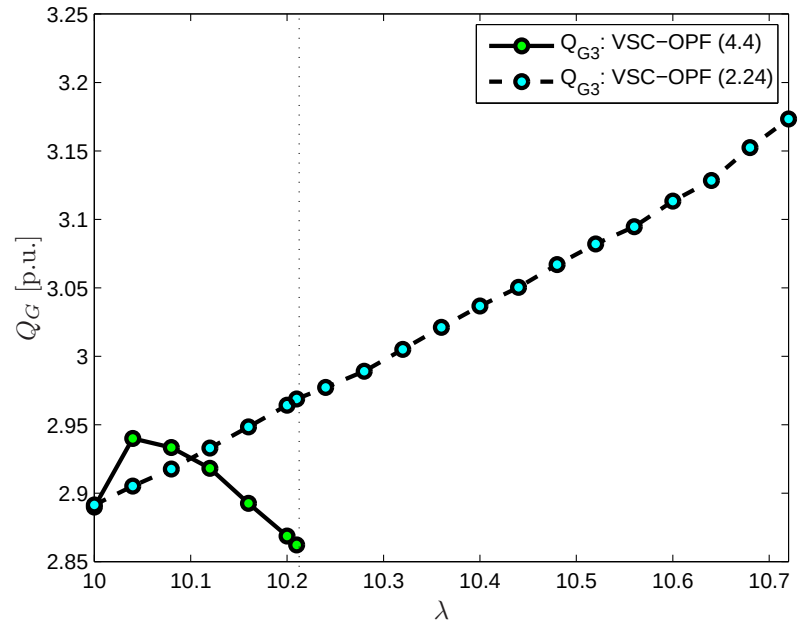

Figure 4.11: GENCO 3 reactive power with respect to the loading factor for the 6-bus system.

This difference is reflected in the corresponding LMP shown in Figure 4.8. The social welfare depicted in Figure 4.9 shows that the power dispatch obtained using (4.4) is practically zero at the maximum loading point. This result permits one to conclude that the proposed model tends to reduce the dispatchable loads in order to satisfy the VS constraint until it becomes unfeasible. In contrast, the model (2.24) continues to dispatch power until it becomes unfeasible due to convergence problems, as concluded from the large number of iterations shown in Figure 4.5(b).

Notice that Figure 4.10 is in accordance with the differences in the market conditions, i.e., the voltage increases at the buses where the power dispatch is reduced using (4.4) as expected, since the VS constraint is closely related to the voltage levels. Similarly, Figure 4.11 corroborates that the proposed model tends to reduce the dispatchable loads when the system is under stressed security conditions, since reactive power is still available. However, the proposed model is also able to readjust other control variables when the load is inelastic, as discussed in Section 4.3.5.

4.3.4 Proposed VSC-OPF vs SC-OPF

The results presented in the previous section demonstrate that the proposed method successfully and efficiently guarantees the required VS constraint. This section presents a comparison between the VSC-OPF model (4.4) and the SC-OPF model (2.21) to study how the corresponding VS constraint affects both the system and market conditions.

The stability limits $P_{ij_{max}}$ in (2.21) were obtained by means of off-line maximum loadability analysis using a CPF method and considering an N-1 contingency criterion. At the same time, σ_c in (4.4) corresponds to the value of $\sigma_{min}(J_{PF})$ at the same loading level λ_c corresponding to $P_{ij_{max}}$.

The results presented in Tables 4.4 and 4.5 correspond to the solution of the SC-OPF as well as the proposed VSC-OPF models at the base loading condition, respectively. This comparison shows that the VSC-OPF auction model provides

Table 4.4: SC-OPF Results for 6-bus Test System.

Participant	V [p.u.]	LMP [$/MWh]	P_S [MW]	P_D [MW]	Q_G [Mvar]
GENCO 1	1.1	9.7	5.41	-	39.91
GENCO 2	1.1	8.8	21.24	-	78.83
GENCO 3	1.1	7.85	20	-	78.08
ESCO 1	1.022	10	-	25	0
ESCO 2	1.018	12.12	-	0	0
ESCO 3	1.033	6.33	-	20	0
TTC = 548.59 MW					

Table 4.5: VSC-OPF Results for 6-bus Test System.

Participant	V [p.u.]	LMP [$/MWh]	P_S [MW]	P_D [MW]	Q_G [Mvar]
GENCO 1	1.1	8.94	0	-	44.78
GENCO 2	1.1	8.90	25	-	72.20
GENCO 3	1.1	9.07	20	-	73.94
ESCO 1	1.021	9.48	-	25	0
ESCO 2	1.012	9.57	-	10	0
ESCO 3	1.038	9.35	-	8.12	0
TTC = 549.47 MW					

lower and more uniform LMPs than the SC-OPF; furthermore, the TTC level obtained using a continuation method and the corresponding dispatch directions in (2.13)-(2.15) are slightly higher than in the SC-OPF. These results show that the VSC-OPF yields better market and system conditions than the SC-OPF, while meeting the required security constraints. Thus, the proposed representation of system security is better overall than simply using fixed limits on power flows.

The base loading level was then increased following the power directions shown in (2.13)-(2.15) to determine the maximum feasible point of these two models. For these studies, the differences in the power dispatch at every bus for both models are shown in Figures 4.12-4.14, for ESCOs, and in Figures 4.15-4.17, for GENCOs. These figures show that the use of a more "relaxed" stability constraint in the proposed VSC-OPF than in the SC-OPF yields higher dispatch levels and consequently better objective function values, as shown in Figure 4.18. Observe that the maximum feasible point for both models occurs at $\lambda = \lambda_c = 1.98$, as expected, since this value corresponds to the loading level defining $P_{ij_{max}}$ and σ_c. However, notice also that the dispatch in the SC-OPF starts to decrease earlier than in the VSC-OPF, becoming practically zero at λ_c. Figures 4.19-4.24 show that the LMPs obtained using the VSC-OPF have a better profile than the LMPs obtained using the SC-OPF as the load increases, as expected from the results shown in Tables 4.4 and 4.5. Observe the drastic change in the LMP values as these models approach the maximum feasible point.

Observe in Figures 4.25 and 4.26 (corresponding to the most representative buses as well) that the bus voltage levels are within limits, and more reactive power can be supplied. However, the lower voltage and higher reactive power values obtained in the VSC-OPF indicate that this model allows a greater power supply than in the SC-OPF within the same operational limits.

Figure 4.27 shows the MSV for both SC-OPF and VSC-OPF, as well as the value of σ_c used in (4.4). Observe that the MSV constraint in the VSC-OPF becomes active at $\lambda = 1.6$. Furthermore, the SC-OPF is shown to be more secure than the VSC-OPF as the loading increases, since its corresponding σ_{min} value is higher

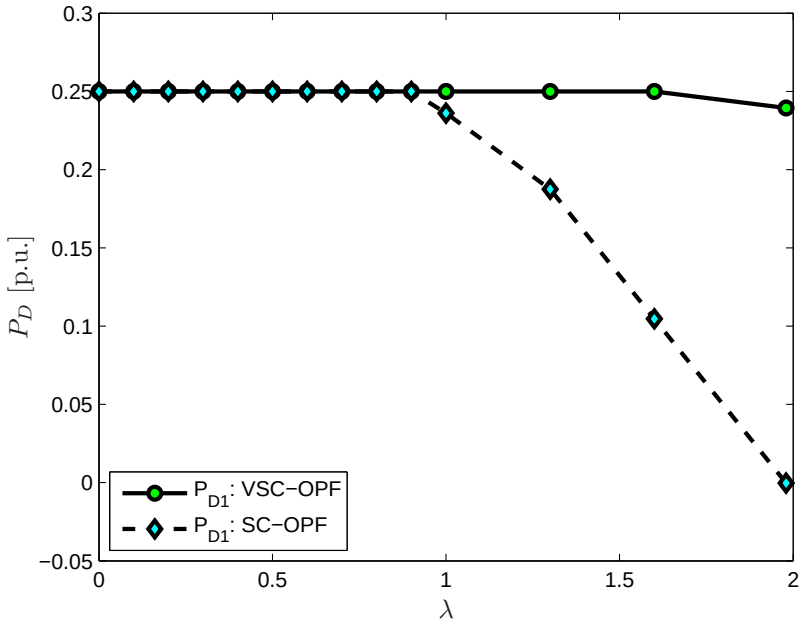

Figure 4.12: ESCO 1 power with respect to the loading factor for the 6-bus system.

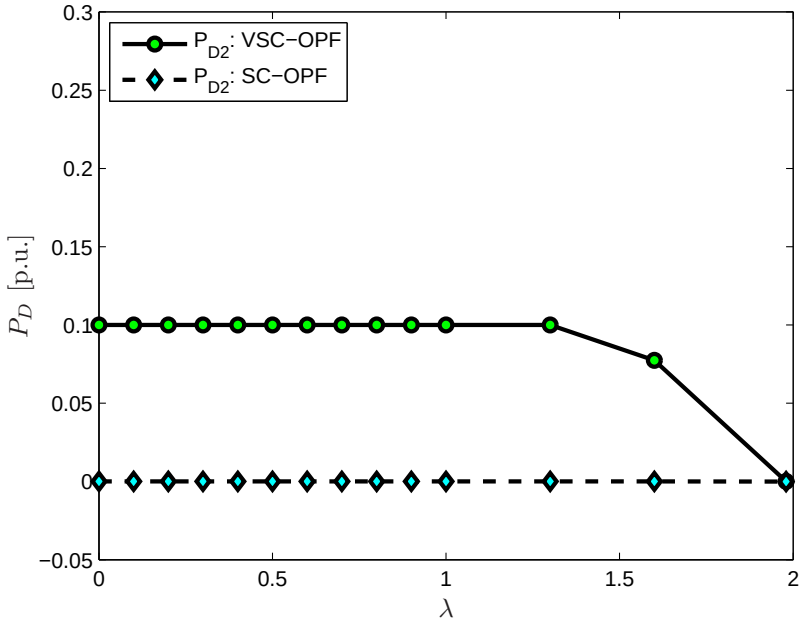

Figure 4.13: ESCO 2 power with respect to the loading factor for the 6-bus system.

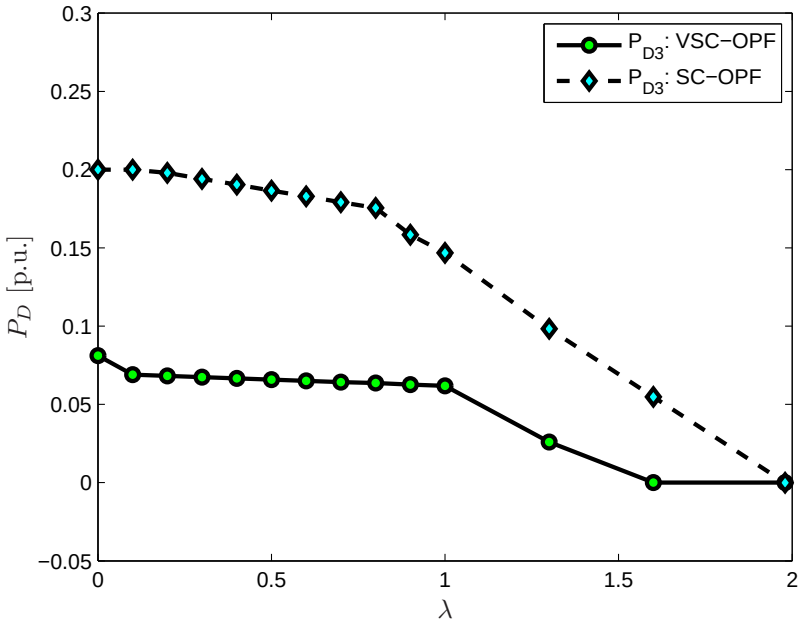

Figure 4.14: ESCO 3 power with respect to the loading factor for the 6-bus system.

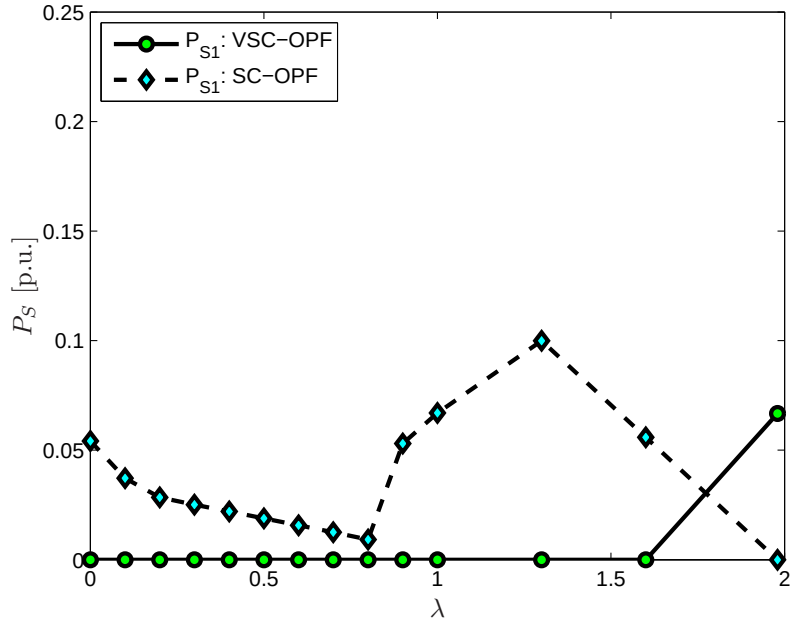

Figure 4.15: GENCO 1 power with respect to the loading factor for the 6-bus system.

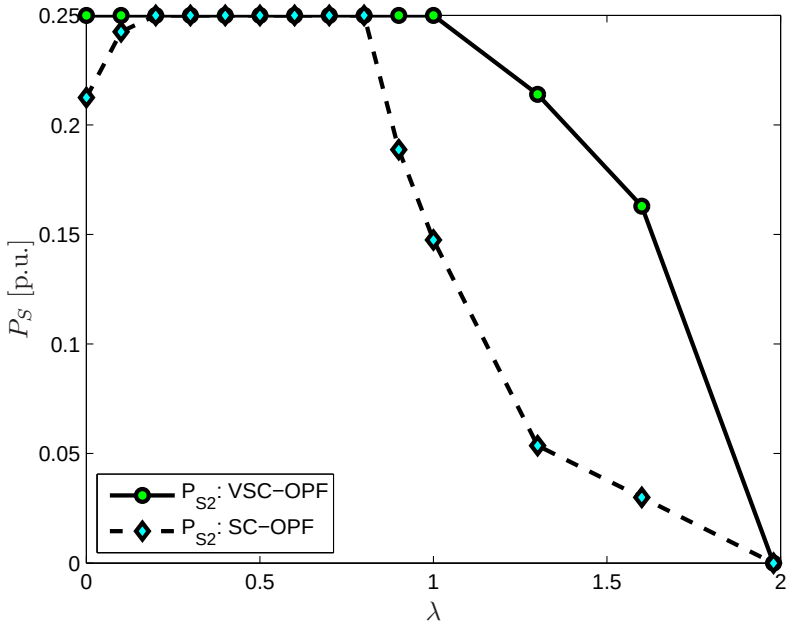

Figure 4.16: GENCO 2 power with respect to the loading factor for the 6-bus system.

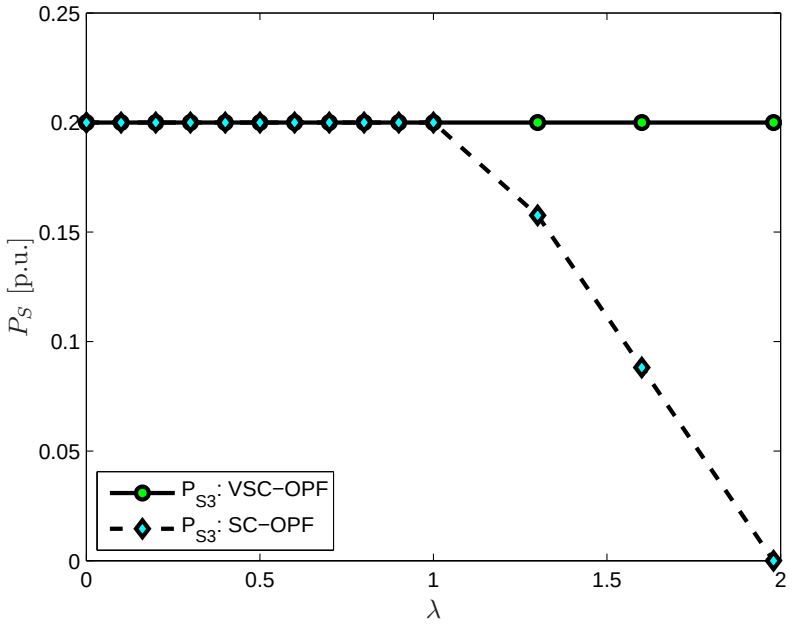

Figure 4.17: GENCO 3 power with respect to the loading factor for the 6-bus system.

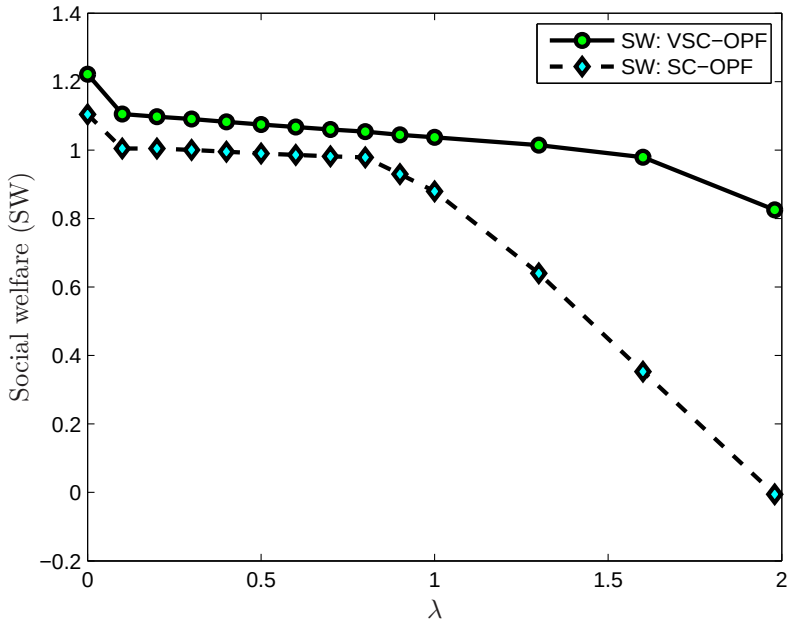

Figure 4.18: Objective function with respect to the loading factor for the 6-bus system.

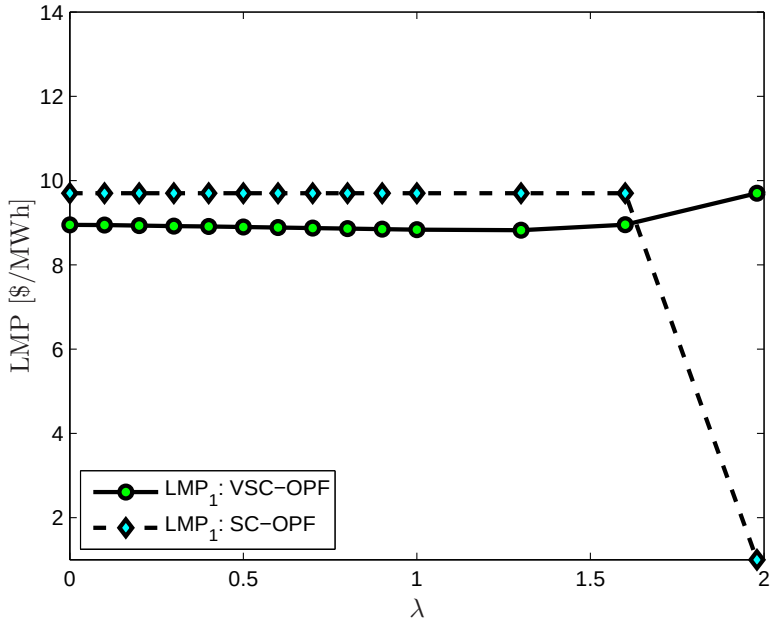

Figure 4.19: Locational Marginal Price (LMP) at bus 1 with respect to the loading factor for the 6-bus system.

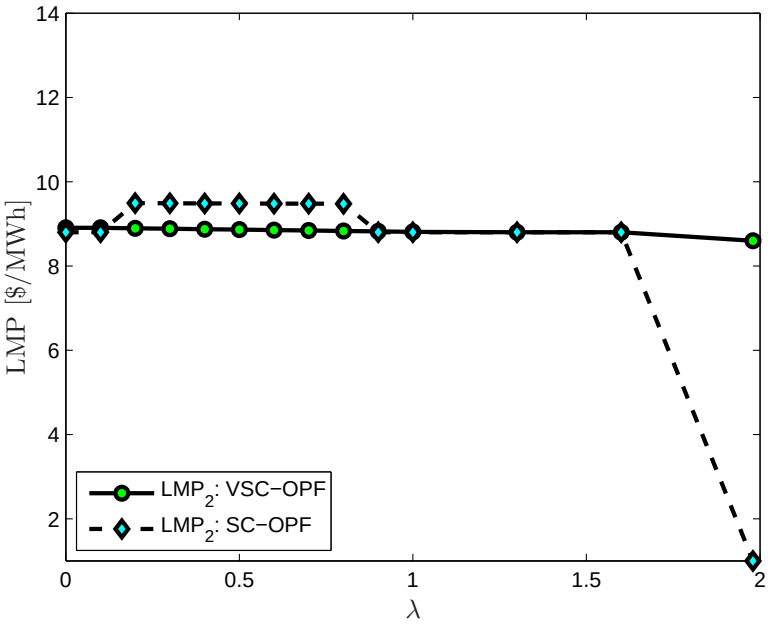

Figure 4.20: Locational Marginal Price (LMP) at bus 2 with respect to the loading factor for the 6-bus system.

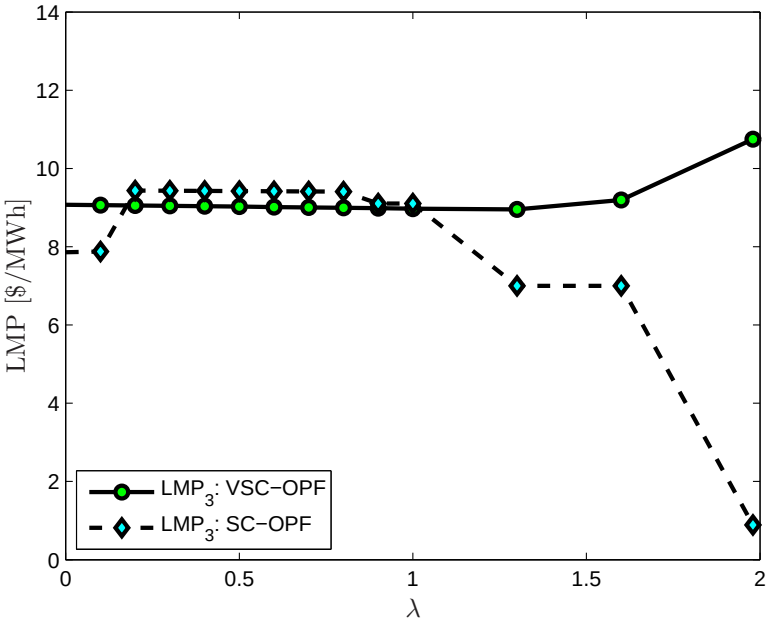

Figure 4.21: Locational Marginal Price (LMP) at bus 3 with respect to the loading factor for the 6-bus system.

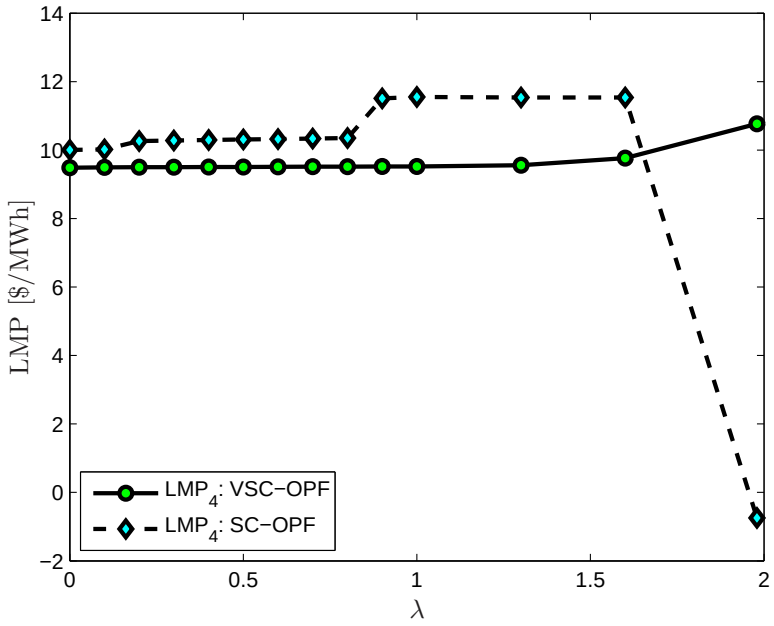

Figure 4.22: Locational Marginal Price (LMP) at bus 4 with respect to the loading factor for the 6-bus system.

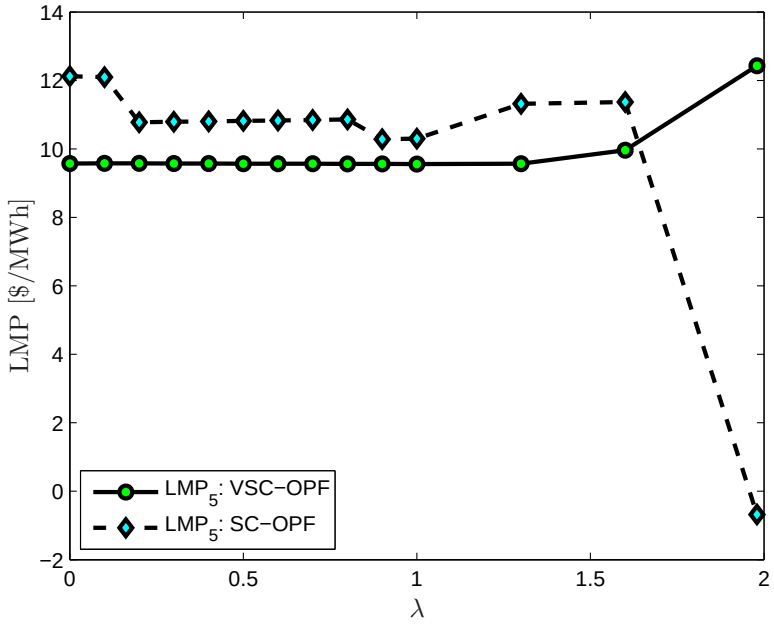

Figure 4.23: Locational Marginal Price (LMP) at bus 5 with respect to the loading factor for the 6-bus system.

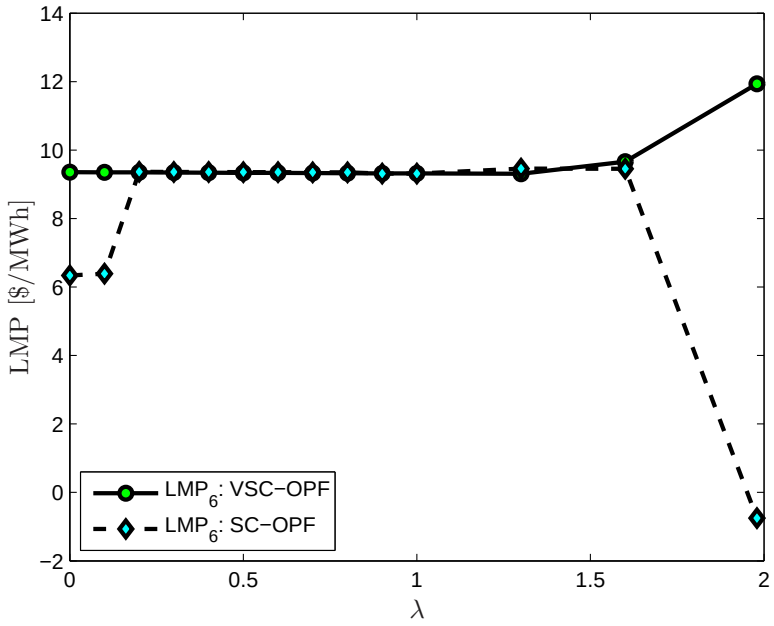

Figure 4.24: Locational Marginal Price (LMP) at bus 6 with respect to the loading factor for the 6-bus system.

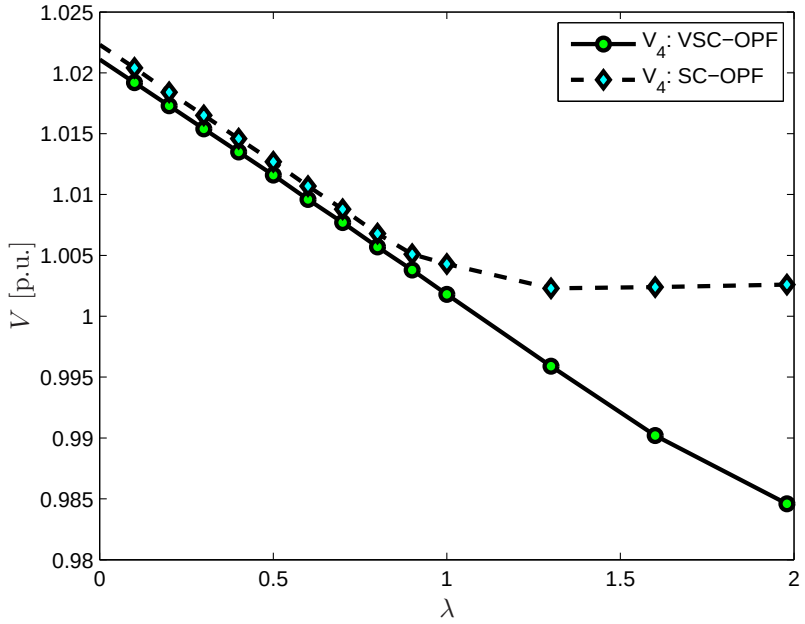

Figure 4.25: ESCO 2 voltage level with respect to the loading factor for the 6-bus system.

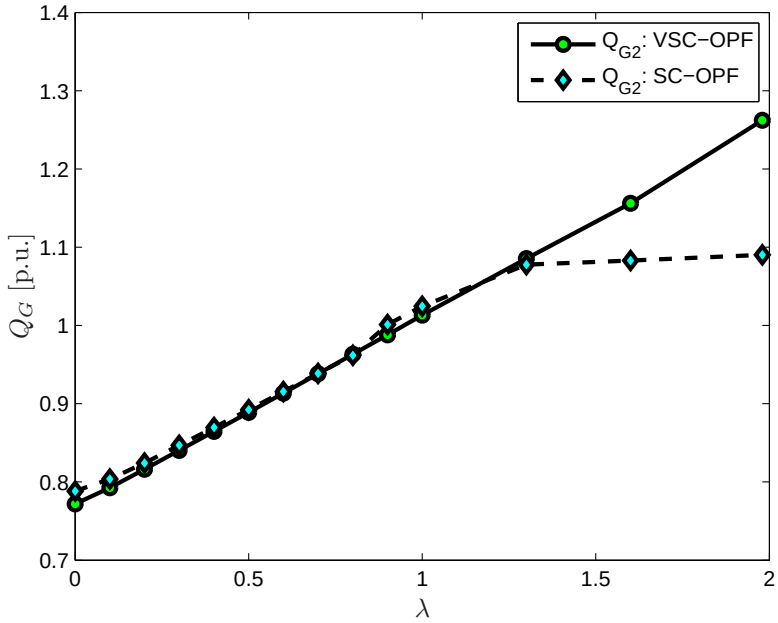

Figure 4.26: GENCO 2 reactive power with respect to the loading factor for the 6-bus system.

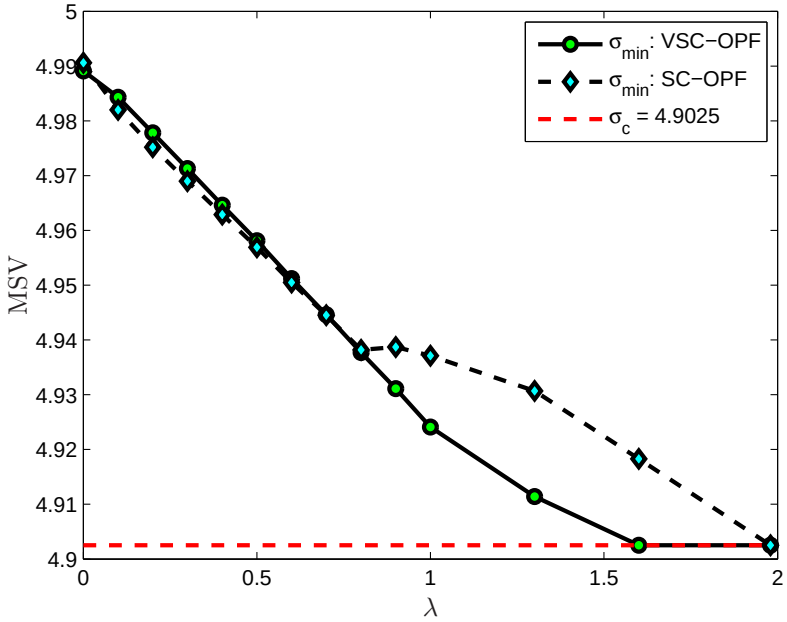

Figure 4.27: MSV at the optimum of the VSC-OPF and SC-OPF.

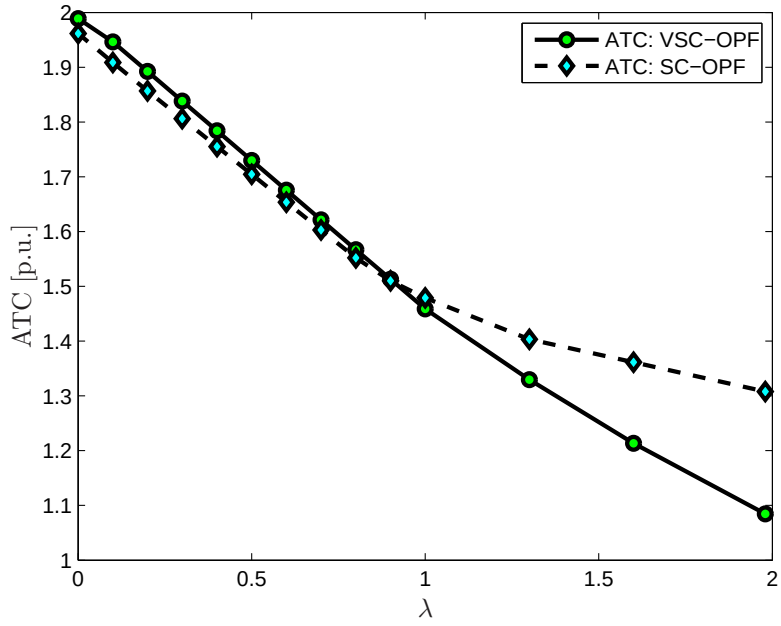

Figure 4.28: ATC with respect to system loading for the 6-bus system.

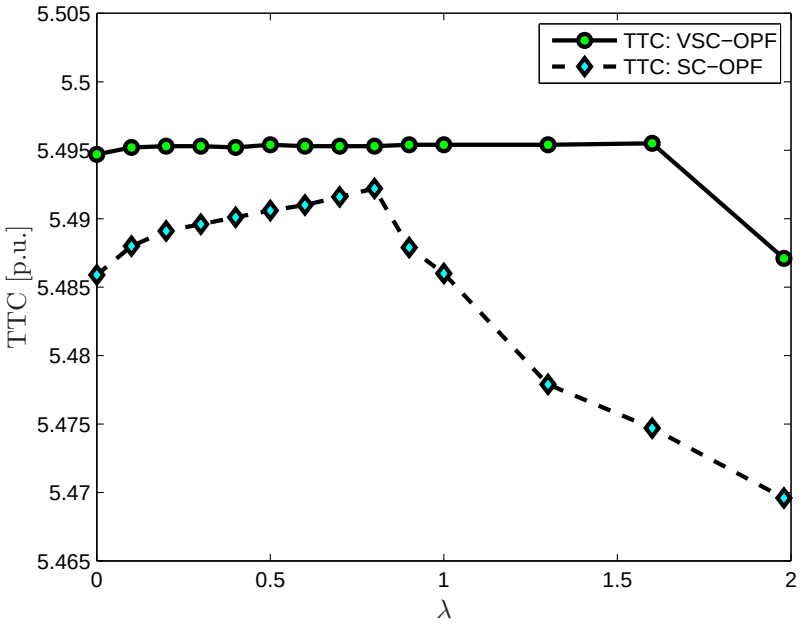

Figure 4.29: TTC with respect to system loading for the 6-bus system.

Table 4.6: Solution statistics when increasing σ_c from 2.6762 to 2.7 in the 1211-bus test system.

	VSC-OPF (base case)	VSC-OPF (increased security)
C	266,555	267,222
σ_c	2.6762	2.7001
k_s	158	159
k	1	1
CPU (s)	11.53	45.059

than that of the VSC-OPF. This is further corroborated by the ATC shown in Figure 4.28, which shows that the SC-OPF is more secure overall than the VSC-OPF. The TTC value shown in Figure 4.29 clearly demonstrates that the SC-OPF becomes more restrictive as the load increases, allowing fewer market transactions. These results show that, while both models (2.21) and (4.4) meet required security limits, the $P_{ij_{max}}$ security constraints in the SC-OPF model are more restrictive than the σ_{min} constraint in the VSC-OPF formulation, thus demonstrating that the latter is a better auction model overall.

4.3.5 Generation Cost Minimization in a Real System

Generally, solving an OPF with inelastic demand is computationally more difficult, since the degrees of freedom are reduced. Thus, to test the feasibility and efficiency of the proposed VSC-OPF method, the VSC-OPF model (4.4) is solved using a European test system of 1211 buses. A classical OPF formulation is used in this case, i.e., the objective function is to minimize a quadratic cost function C, with an inelastic demand. It should be mentioned that thermal limits on transmission lines were not used, since the objective of these studies is to analyze the practical

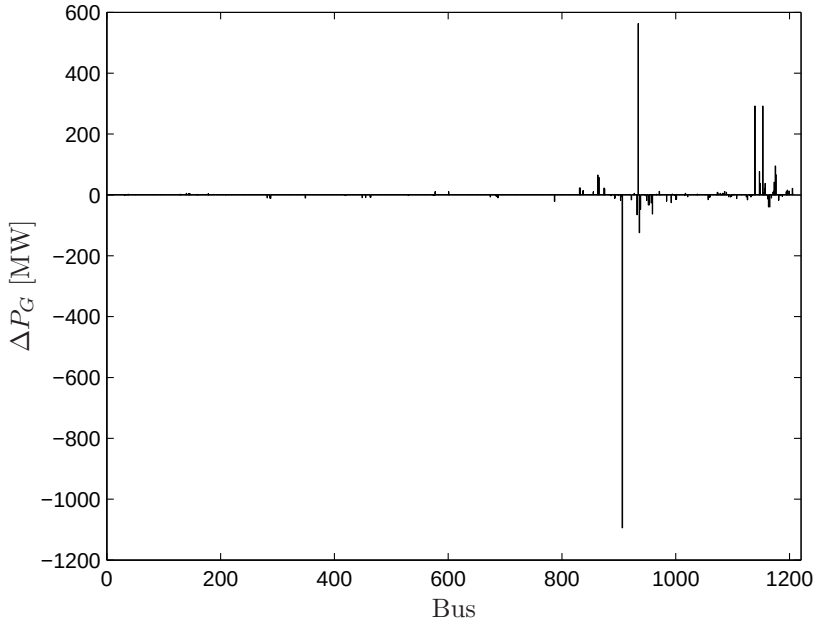

Figure 4.30: Generation re-dispatch when the VSC-OPF is applied to a 1211-bus test system.

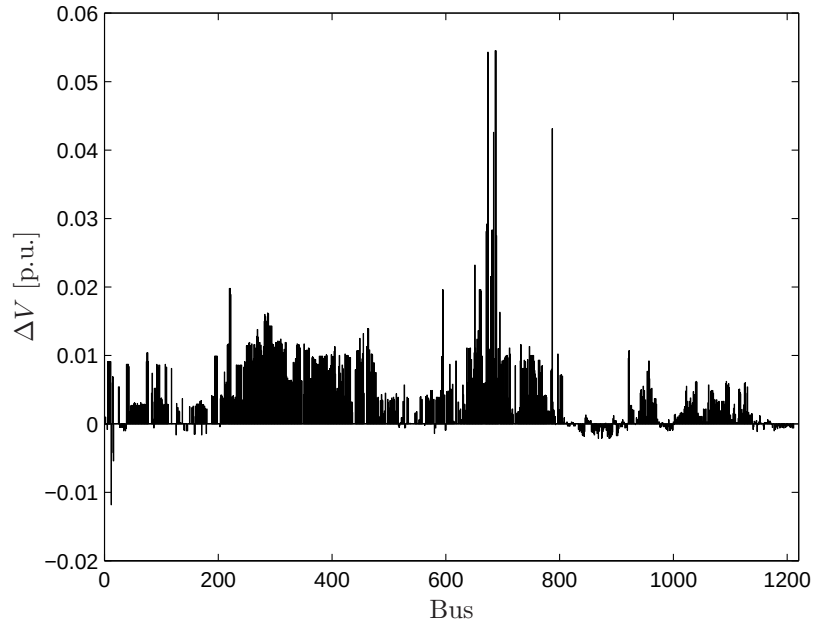

Figure 4.31: Increment in bus voltages when the VSC-OPF is applied to a 1211-bus test system.

feasibility and performance of the proposed VSC-OPF. Thus, the VSC-OPF (4.4) was solved first under normal operating conditions without the MSV constraint (base case), and a $\sigma_{min}(J_{PF})$ was obtained for this solution. Then, to force the MSV constraint (4.4c) to become active, a slightly larger value than σ_{min} was used as the σ_c value in the solution of (4.4).

Figure 4.30 shows that a generation re-dispatch with respect to the base case solution is required to meet the required security constraint, improving the voltage profile at most of the buses, as expected and depicted in Figure 4.31. However, this corrective action is accompanied by an increase in the total generation costs, as shown in Table 4.6; this increase in the total cost can be seen as the cost of improving system security.

The results presented in Table 4.6 demonstrate the feasibility of the proposed method in practice, since for this large system, it only required one iteration and 45s of CPU time for the method to converge using a (Intel Xeon 2.83GHz with 3.00 GB of RAM). In general, the author's experience with different test systems shows that the proposed method converges in less than three iterations ($k \leq 3$), regardless of the system size.

4.4 Summary

In this chapter, a novel and practical solution method to solve a VSC-OPF model that includes a VS constraint based on a MSV index is proposed. The method consists of solving the VSC-OPF iteratively to update the SVD of the power flow Jacobian until the MSV constraint is satisfied. The proposed method is shown to have better numerical characteristics than a previously proposed VSC-OPF model based on a similar VS constraint.

The advantages of using the proposed method with respect to "standard" SC-OPF are highlighted by means of numerical comparisons. In this context, it is demonstrated that the VSC-OPF model provides better system and market conditions when compared to the SC-OPF. It is shown that the proposed method performs well in large systems, demonstrating its practical feasibility by applying it to a real European system. One of the main advantages of the proposed model is that commercial mathematical programming languages and solvers can be used to formulate it, making it easier to implement and more practical. Overall, the proposed method is shown to be a good alternative to SC-OPFs.

Chapter 5

Other Approaches to Solving the VSC-OPF

5.1 Introduction

This chapter proposes two alternative methods to solving the MSV-based VSC-OPF model, besides the method discussed in the previous chapter. The first method is a modified primal-dual IPM which handles the MSV constraint using a CP technique at every iteration. The second method attempts to reformulate the VSC-OPF as a SDP relaxation.

5.2 Solving the VSC-OPF via CP/IPM

Although the CP method is commonly used to solve mixed-integer problems in linear programming, the basic idea of adding linear constraints (cuts) until the optimal solution reaches desired values is extended here to solve the VSC-OPF. Thus, a modified primal-dual IPM algorithm is proposed in this section to incorporate a CP step to modify the upper limits of the demand block bids at a particular

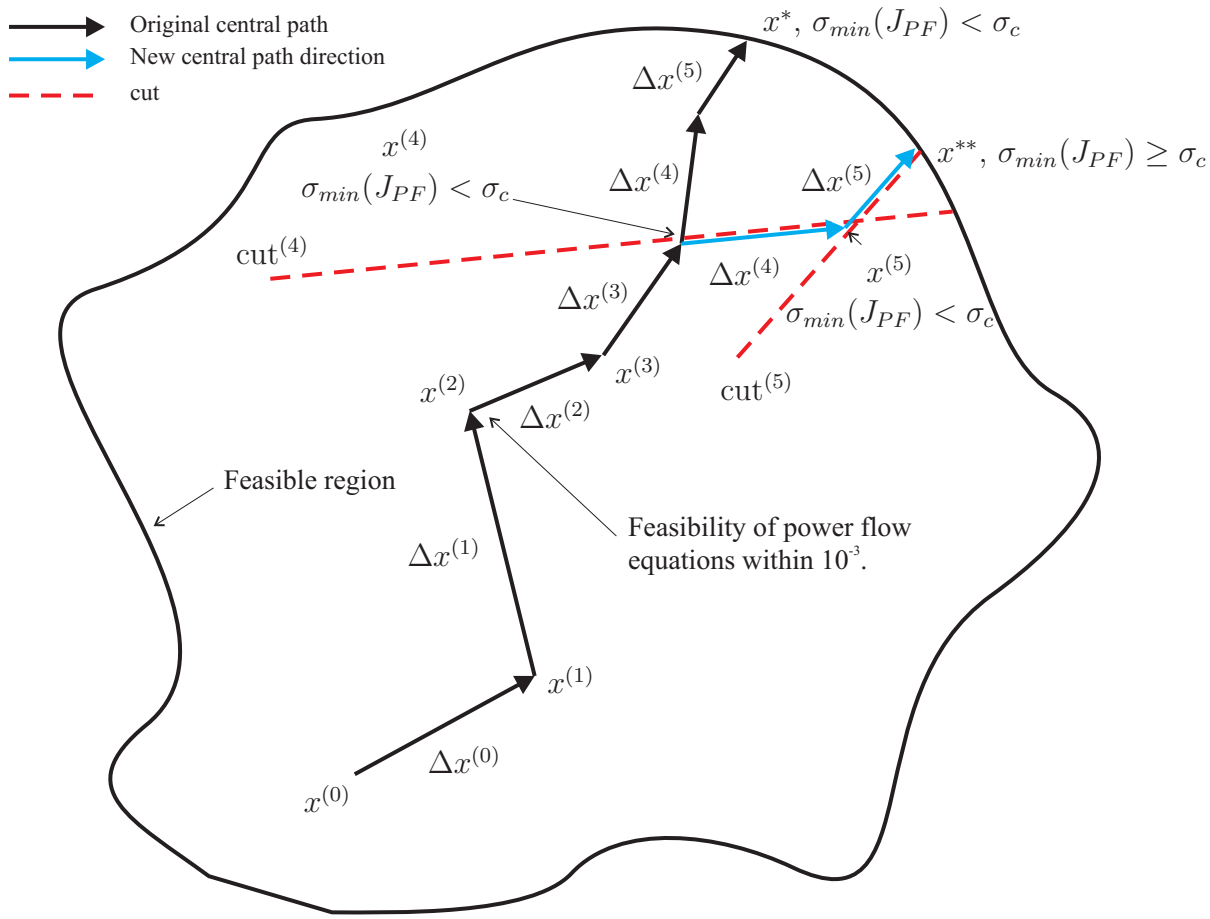

Figure 5.1: Graphic representation of the proposed CP/IPM algorithm.

iteration, so that the optimal power dispatch satisfies the MSV constraint. Two test systems are used to study the proposed CP/IPM algorithm.

5.2.1 Proposed Technique

Refer to Figure 5.1, and suppose that the constraint $\sigma_{min}\{J_{PF}\} \geq \sigma_c$ in (2.24) is not included in the model, i.e., the problem is "relaxed". Thus, the optimal point denoted by x^* is reached by taking Newton steps along the central path using an IPM scheme. At this solution point $\sigma_{min}(J_{PF}|_*) < \sigma_c$. Therefore, the optimization

model must be re-solved with this constraint included in the problem, so that $\sigma_{min}(J_{PF}|_*) \geq \sigma_c$.

In the proposed algorithm, the constraint on the MSV is handled in the IPM by monitoring σ_{min} at every iteration k, and by adding "cuts" when $\sigma_{min}^{(k)} < \sigma_c$. This idea is also illustrated in Figure 5.1 and can be described as follows: Let $x^{(0)}$ be the initial point, let $\Delta x^{(k)}$ be a Newton step at iteration k, and let $x^{(k)}$ be the solution point at which $\sigma_{min}^{(k)} < \sigma_c$. Suppose that at $k = 4$, $\sigma_{min}^{(k)} < \sigma_c$. Then, the upper limit of P_D in (2.24) is modified by adding a cut$^{(k)}$. The cut basically modifies the line search or central path for subsequent iterations, leading the Newton steps towards another local optimal point x^{**} where $\sigma_{min} \geq \sigma_c$, as illustrated in Figure 5.1.

Given the characteristics of the aforementioned approach, it must be noticed that adding the first cut at $k \neq 4$ may result in different lines search. Consequently, the algorithm would either find another local optimum, or it may not be able to find any. The proposed algorithm deals with these two main problems when adding the cut as follows:

1. Define the cut magnitude (a constraint in P_D).

2. Determine the iteration at which the cut has to be added.

Calculating the Cut Magnitude

The particular characteristics of the VSC-OPF can be exploited to determine the cut. Thus, σ_{min} tends to zero as the load increases, and a power flow solution must exist for this value to have a practical meaning from the VS point of view. Based on these characteristics, the following formula to modify the upper limit of P_D is introduced:

$$P_{D_{max}}^{(k+1)} = P_D^{(k)} - \hat{a} \circ \alpha P_D^{(k)} \tag{5.1}$$

where

$$\hat{a} = \frac{\Delta P_D^{(k)}}{|\Delta P_D^{(k)}|} \tag{5.2}$$

is a unit vector with the same direction of the Newton step at iteration k; $\alpha \in (0, 1)$ is a scaling factor for tuning purposes and is explained in more detail below, and

$$0 \leq P_{D_{max}}^{(k+1)} \leq P_{D_{max}} \tag{5.3}$$

Note that the second term in (5.1) defines a step backward from the current solution point, taken in a component-wise basis of the last Newton direction. The vectors $\hat{a}$ and αP_D are the Newton step and step length, respectively. This equation along with (5.3) allows P_D to either recover its actual maximum limit, or to reduce it when a cut is added.

Determining the Cut Iteration

The cut must be added at the iteration where the feasibility of the power flow equations is within a tolerance ξ. However, notice that a small value of ξ implies that the magnitude of the Newton step is also small. Therefore, this value would directly affect the ability of the algorithm to recover from an undesired point where $\sigma_{min}^{(k)} < \sigma_c$, as inferred from (5.1). In other words, if the cut is added when the algorithm is "too close" to an optimal where $\sigma_{min}^{*} < \sigma_c$, then it may be "too late" to find another one where $\sigma_{min}^{*} \geq \sigma_c$. Similarly, if the cut is added regardless of the feasibility of the power flow equations, the algorithm may not yet have enough accurate information to find a better solution. Therefore, it is necessary to tune ξ, and the step length which defines how much the upper limit of P_D must be modified. For this purpose, the scalar α has been included in (5.1) to determine the fraction of the step length that would result in better solutions and greater performance of the algorithm. These parameters are determined by means of experimental results, as described in Section 5.2.1.

CP/IPM Algorithm

The method described above is formally stated in the flow chart shown in Figure 5.2, which is basically a modified primal-dual IPM with standard Newton method or

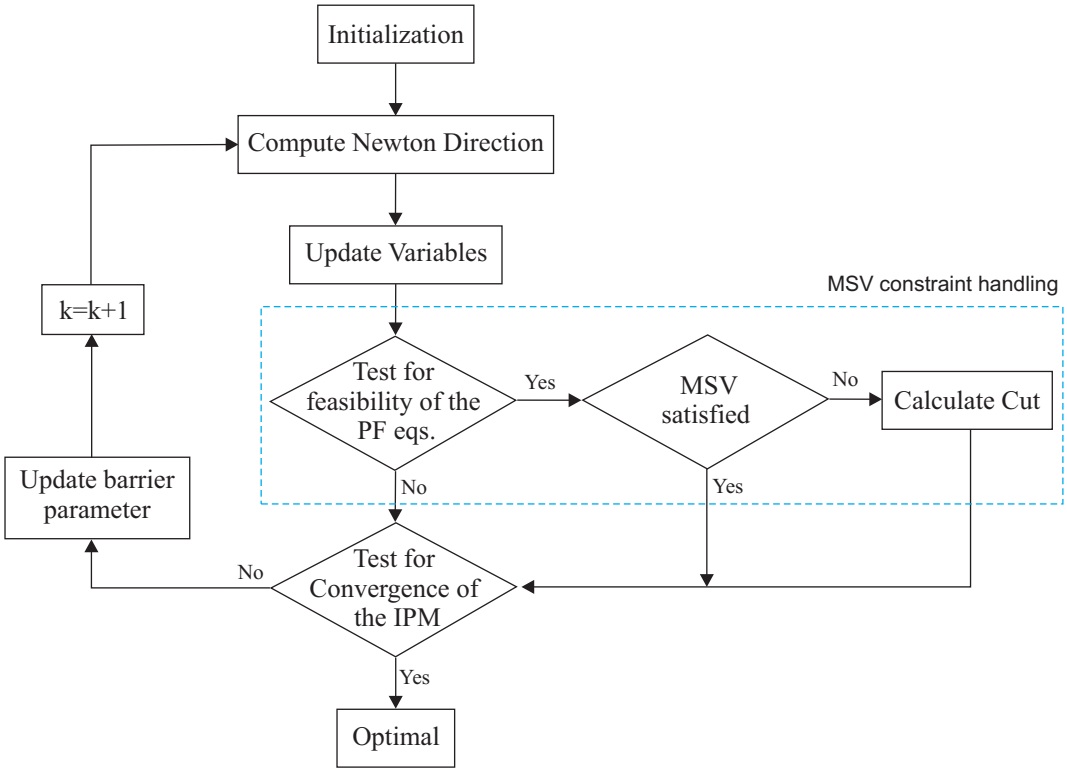

Figure 5.2: CP/IPM flow chart to solve the VSC-OPF

predictor-corrector method to solve the Newton direction [80]. The proposed algorithm steps can be then described as follows:

1. *Initialization:*
   - Set $k = 0$.
   - Define the barrier parameter $\bar{\mu}^0$.
   - Choose a starting point that satisfies the strict positivity conditions (e.g., a power flow solution or a flat start).
   - Set $P^{bk}_{D_{max}} = P_{D_{max}}$ and $P^{bk}_{D_{min}} = P_{D_{min}}$.
2. *Compute Newton Direction:* The Newton direction can be obtained by solving the system (2.34) using the standard Newton method, or a predictor-corrector

method.

3. *Update Variables:* Compute the step length parameters for primal and dual variables using (2.38)-(2.39), and update the variables using (2.40).

4. *Test for Feasibility of the Power Flow Equations:* If the feasibility is within a predetermined tolerance ξ, then start monitoring σ_{min} using a SVD.

   - If $\sigma_{min}^{(k)} < \sigma_c$, i.e., the MSV constraint is not satisfied, then proceed to calculate the cut as follows: Use equation (5.1), and verify if $0 \leq P_{D_{max}}^{(k+1)} \leq P_{D_{max}}$. If $P_{D_{max}}^{(k+1)} > P_{D_{max}}$, then set $P_{D_{max}}^{(k+1)} = P_{D_{max}}^{bk}$. A similar process for the lower limit is followed.
   - Otherwise, continue the iterative process.

5. *Test for Convergence:* If the new point satisfies the convergence criteria, stop. Otherwise, set $k = k + 1$, update the barrier parameter $\bar{\mu}^k$, and return to Step 1.

Tuning of the Algorithm

As in many iterative solution methods such as the Newton method, determining the step length parameters is one of the most important issues to ensure a good performance of the algorithm. Different approaches to calculate these parameters have been proposed. For instance, separate step lengths for primal and dual variables are used to update the variables in the IPM [80]; dynamic adjustments of step sizes and tolerances have been proposed in [100]. One common practice is to calculate these parameters based on heuristic methods.

In the proposed algorithm, choosing an adequate value for ξ and α is a problem independent of determining the step length parameters of the Newton direction. It also requires a heuristic type of method to ensure that the algorithm converges to a desired solution point in a reasonable number of iterations. Thus, experimental

results are needed to study how the algorithm performs when the cut is added at different iterations, in combination with different step sizes.

Let $\xi = \{\text{NPF}, 1 \times 10^{-1}, 1 \times 10^{-2}, 1 \times 10^{-3}, 1 \times 10^{-4}\}$ be a set of threshold values to test the feasibility of the power flow equations at iteration k. If $\xi = \text{NPF}$ no test is carried out and the cut is added at any iteration where $\sigma_{min}^{(k)} < \sigma_c$. If $\xi \neq \text{NPF}$ and if $\sigma_{min}^{(k)} < \sigma_c$, then a cut is added at iteration k. On the other hand, $\alpha \in (0, 1)$ is used to take a fraction of the Newton step at the current iteration. If $\alpha = 0$, then $P_{D_{max}}^{(k+1)} = P_D^{(k)}$; whereas, $\alpha = 1$ takes a full step backwards in the same direction of the last Newton step in order to avoid the point $P_D^{(k)}$, as this value results in a violation of the MSV constraint.

Figures 5.3-5.10 show different optimal solutions for different combinations of ξ and α, using an IPM with a Newton or predictor-corrector method, initialized using a flat start or a power flow solution start. The 6-bus test system and the CIGRE-32 test system presented in Appendix A were used to test the proposed algorithm. The CP/IPM algorithm was implemented in Matlab.

Figures 5.3(a), 5.3(b), 5.4(a) and 5.4(b) show the MSV of the power flow Jacobian at the optimal solution for various values of α and ξ; the results correspond to the 6-bus system for $\sigma_c = 5.0$. These figures show that for various (α, ξ) values, the algorithm satisfies $\sigma_{min} \geq \sigma_c$, while it fails for others. One of the most significant results is that if the cut is added at any iteration where the MSV constraint is violated ($\xi = \text{NPF}$), a higher value of the MSV is obtained; thus, observe that the (α, NPF) values provide a solution with a higher MSV than other cases where the feasibility of the power flow equations is tested at every iteration before adding a cut. For instance, the combination $(1, \text{NPF})$ generally results in the highest MSV values, which means that if a full Newton step is taken backwards whenever the MSV constraint is violated, the algorithm encounters a wider feasible region where it can find the desired optimal point. From these results, it could be concluded that the best values are $\alpha = 1$ and $\xi = \text{NPF}$; thus, let the algorithm add the cut at any iteration where $\sigma_{min}^{(k)} < \sigma_c$, and take a full Newton step backward to calculate $P_{D_{max}}^{(k+1)}$. However, observe in Figures 5.5(a), 5.5(b), 5.6(a) and 5.6(b), that if such

criteria are used, the lowest transaction levels ($T = \sum P_{L_{o_i}} + P_{D_i}$) are obtained, which yields a lower objective function (SW) value, as shown in Figures 5.7(a), 5.7(b), 5.8(a) and 5.8(b). This is to be expected, since a higher MSV requires a lower demand levels, since the security margins are higher. Therefore, adding a cut is equivalent to shedding load from the demand block bids represented by P_D to maintain the required security levels given by the constraint $\sigma_{min} \geq \sigma_c$.

Notice that the combinations $(0, \xi)$ represent a cut $P_D^{(k+1)} = P_D^{(k)}$. This results in the algorithm getting "stuck" trying to avoid the solution point $x^{(k)}$. This can be observed in Figures 5.9(a), 5.9(b), 5.10(a) and 5.10(b), where it is shown that the maximum number of iterations ($k = 250$) is reached. Observe in these figures that the algorithm performs very well for all ξ, and for all α close to one.

Figures 5.11(a), 5.11(b), 5.12(a) and 5.12(b) show the cuts calculated at every iteration for different solution methods and starting points. These figures correspond to the case where the cut is added only if the feasibility of the power flow equations is within $\xi = 1 \times 10^{-3}$. Observe that the limits do not change during the first iterations, thus some cuts are added until the algorithm finds a feasible point where $\sigma_{min}^{(k)} \geq \sigma_c$, and then converges to an optimal point. Notice that (5.3) holds during the solution process, as required. However, the results in these figures along with those described above, show that the algorithm is highly dependent on both the solution method and on the starting point, since (5.1) is different in all four cases, yielding different optimal solutions. This problem is also observed in Figure 5.13, which shows $\sigma_{min}^{(k)}$ using different solution methods and starting points, as well as the application of the cut for the criteria $\xi = \text{NPF}$ or $\xi = 1 \times 10^{-3}$. Notice that the final value of $\sigma_{min}^{(k)}$ is closer to σ_c if the cut is applied only if the feasibility of the power flow equations is within $\xi = 1 \times 10^{-3}$. This is the desired final value of the MSV, since the power dispatch and transaction levels are better when it is closer to σ_c.

Figure 5.14 shows the most representative result for the CIGRE-32 test system. Observe that a similar response of the algorithm for this larger and heavily loaded system.

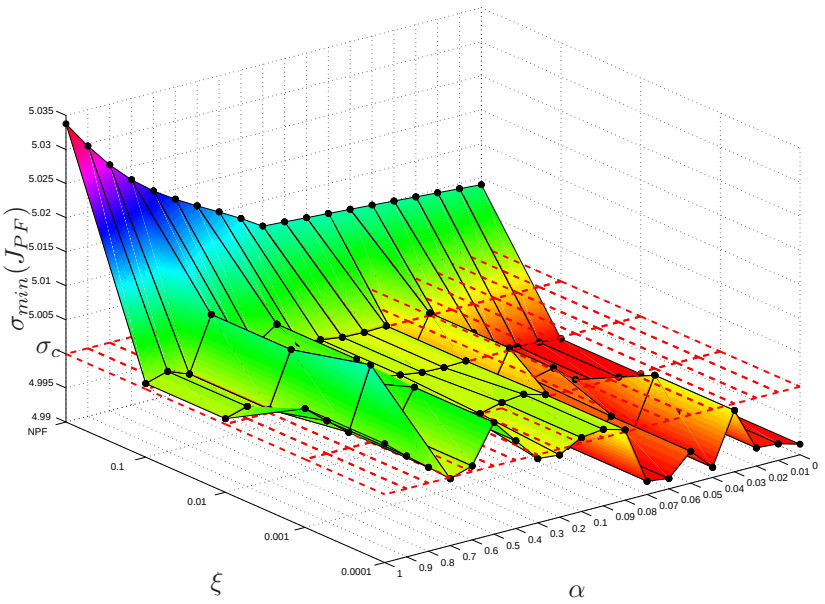

(a)

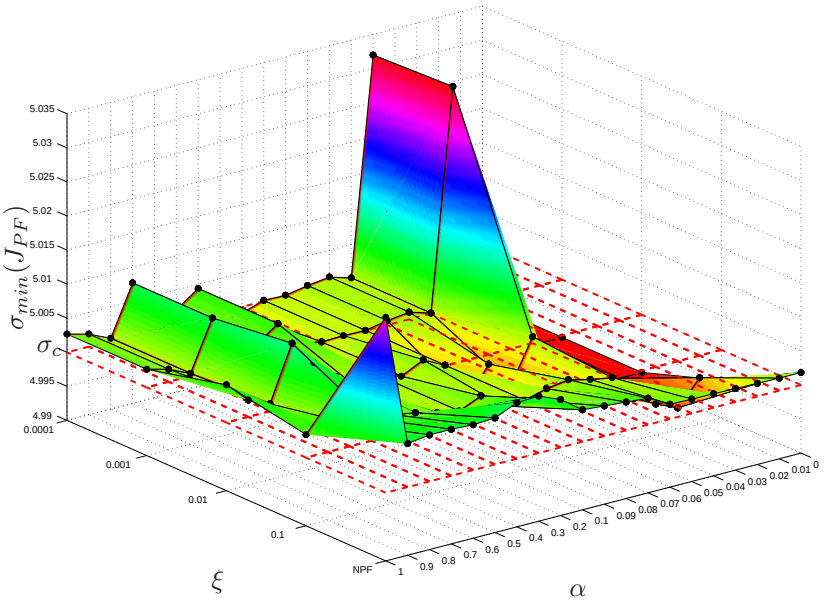

(b)

Figure 5.3: MSV of the power flow Jacobian using a Newton method: (a) flat start; (b) power flow start.

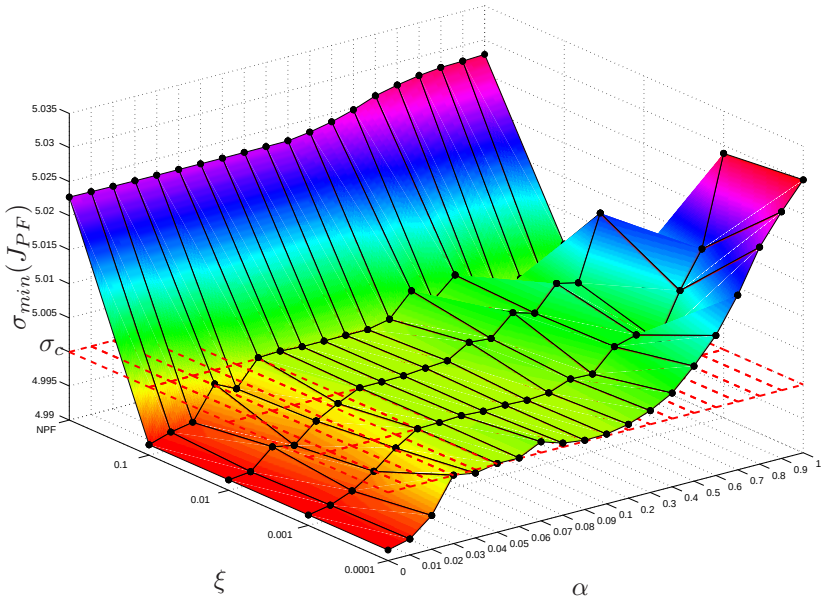

(a)

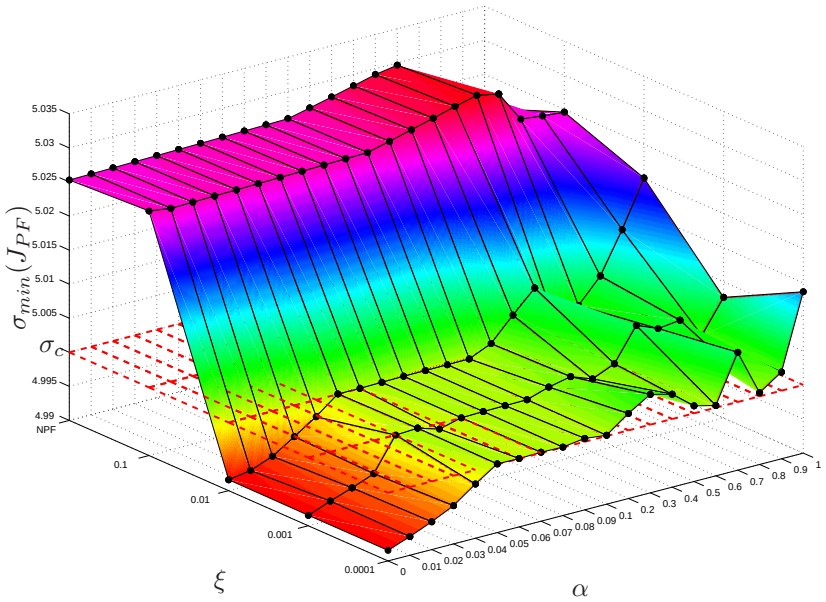

(b)

Figure 5.4: MSV of the power flow Jacobian using a predictor-corrector method: (a) flat start; (b) power flow start.

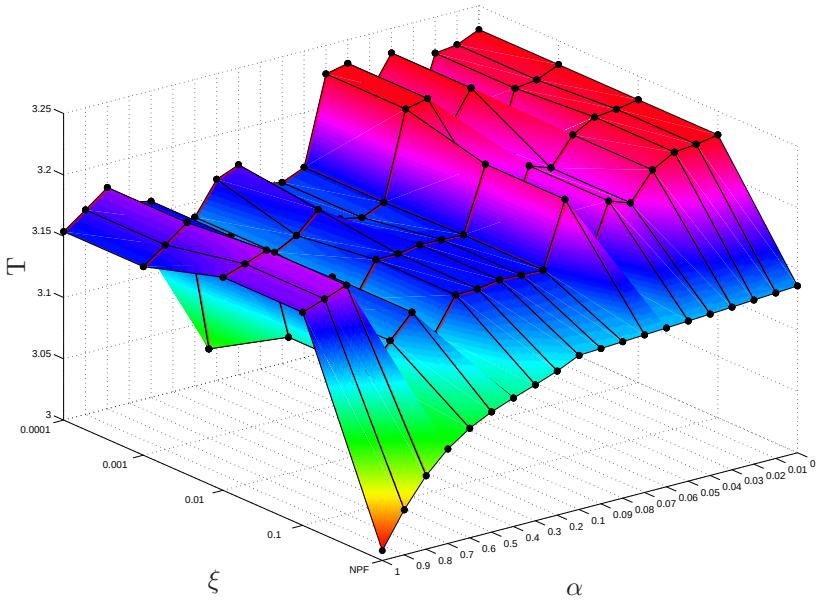

(a)

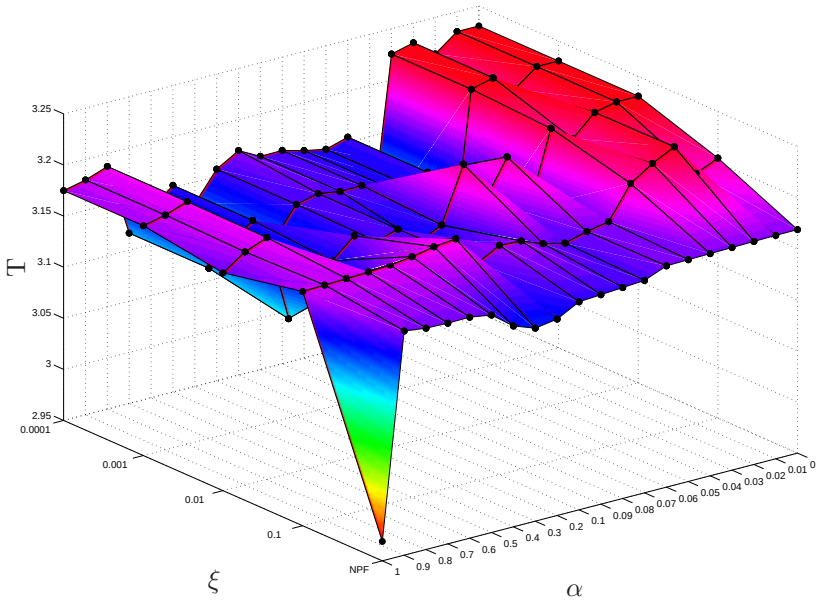

(b)

Figure 5.5: Total transaction level using a Newton method: (a) flat start; (b) power flow start.

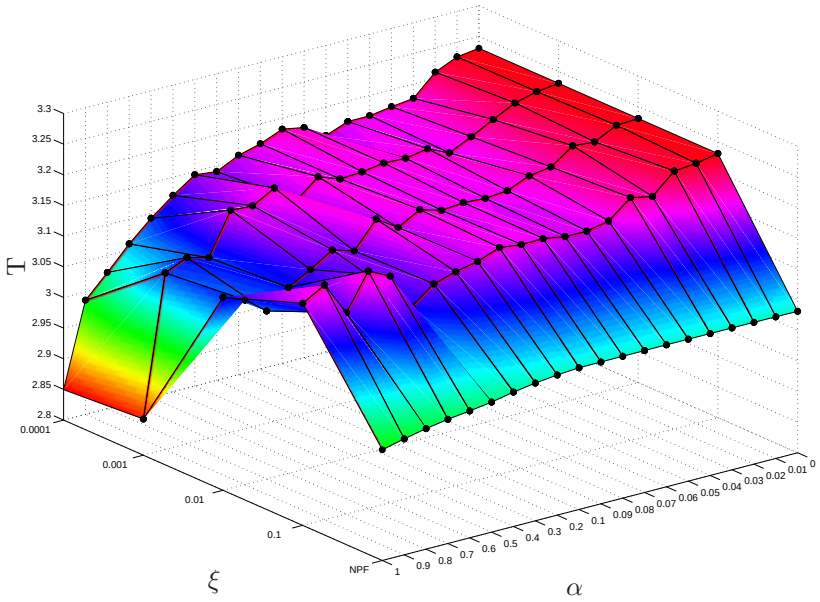

(a)

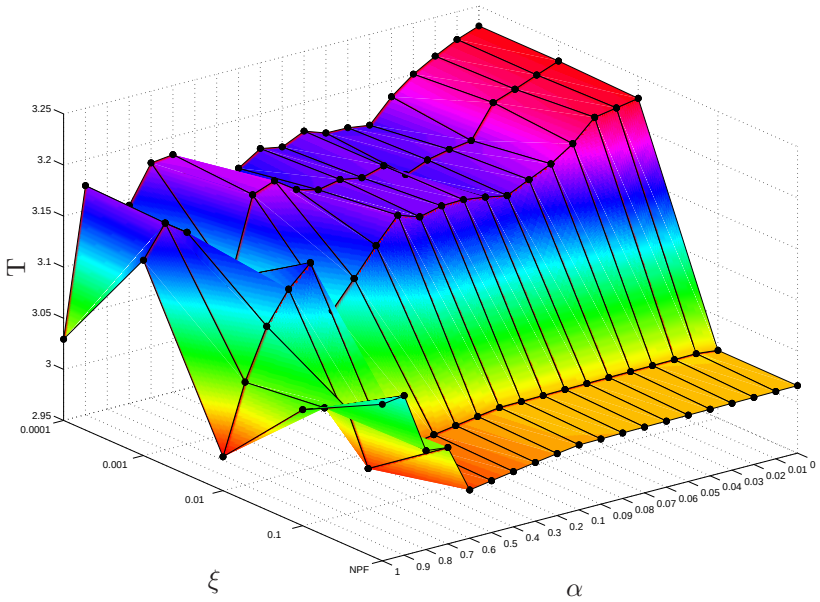

(b)

Figure 5.6: Total transaction level using a predictor-corrector method: (a) flat start; (b) power flow start.

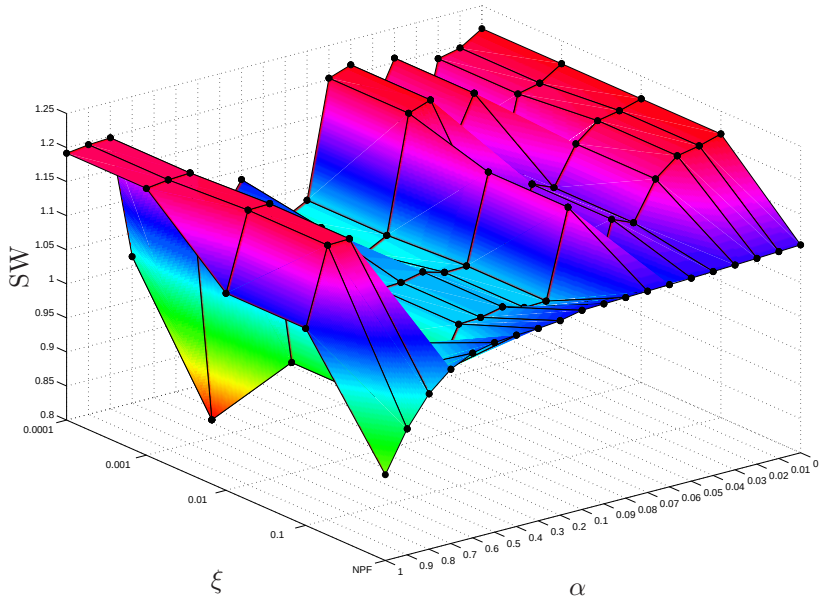

(a)

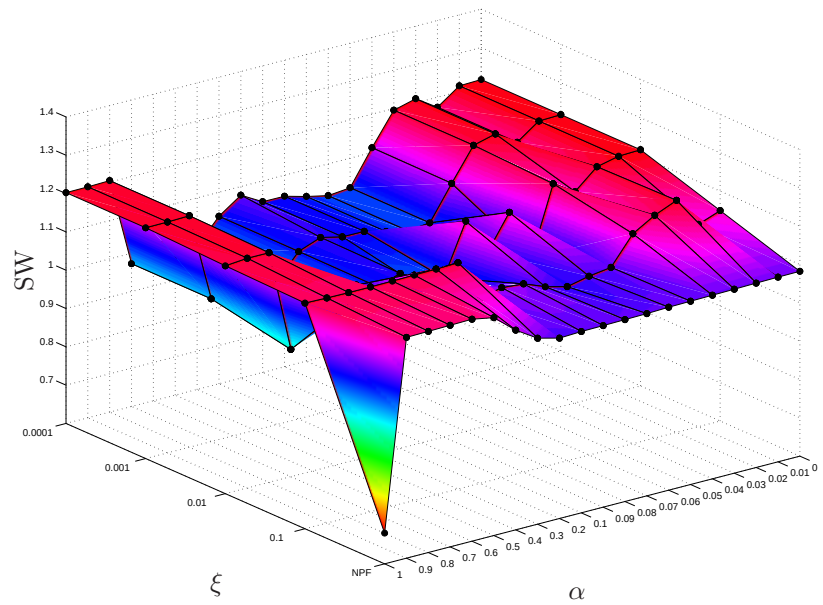

(b)

Figure 5.7: Objective function using a Newton method: (a) flat start; (b) power flow start.

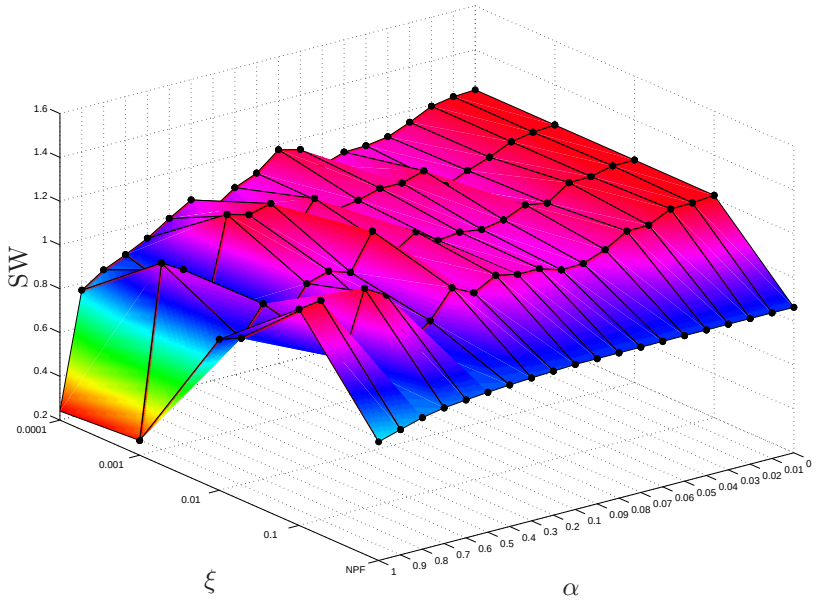

(a)

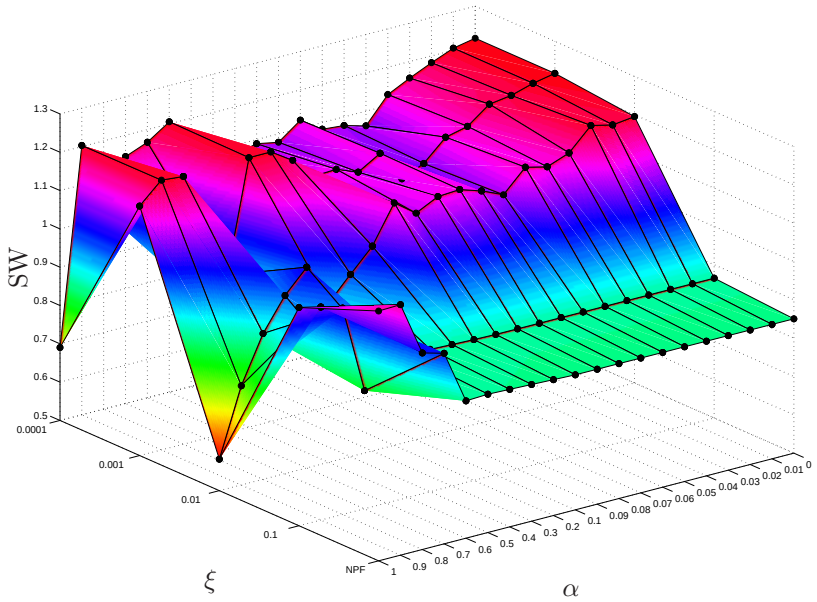

(b)

Figure 5.8: Objective function using a predictor-corrector method: (a) flat start; (b) power flow start.

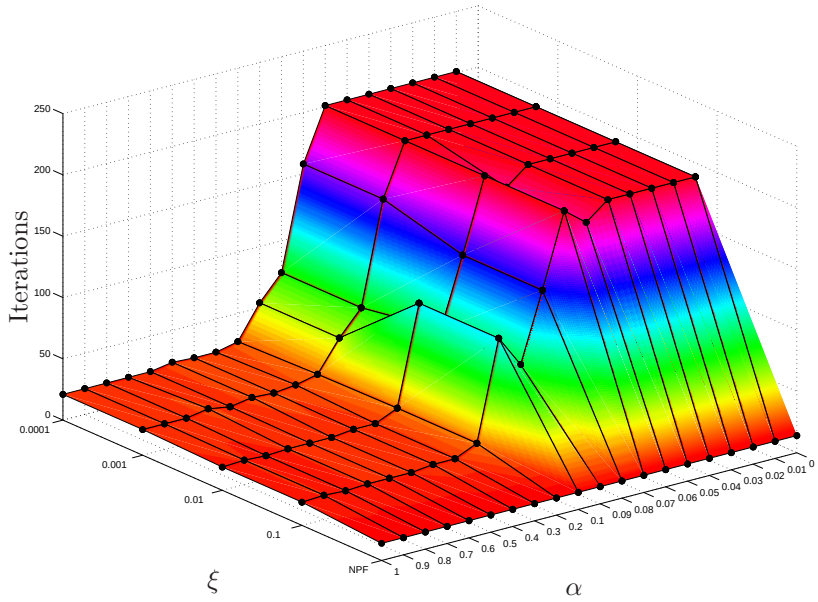

(a)

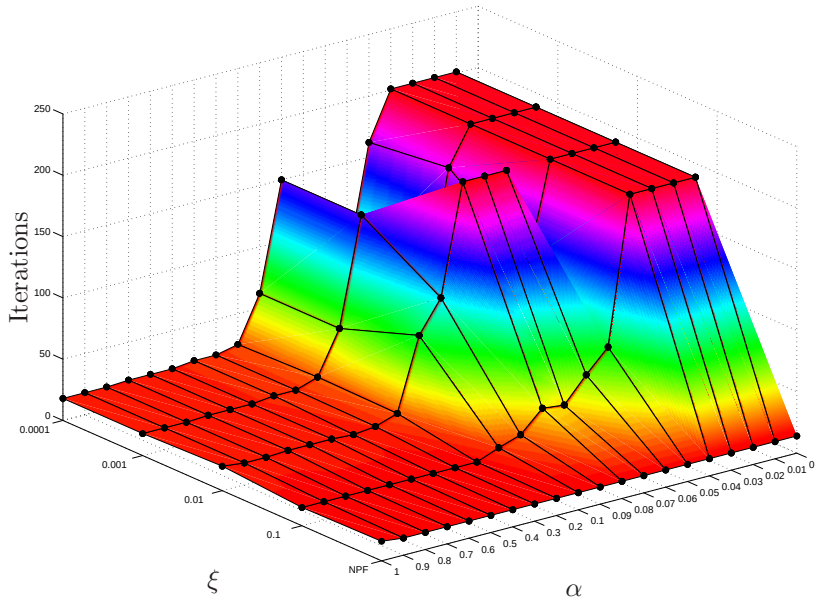

(b)

Figure 5.9: Number of iterations using a Newton method: (a) flat start; (b) power flow start.

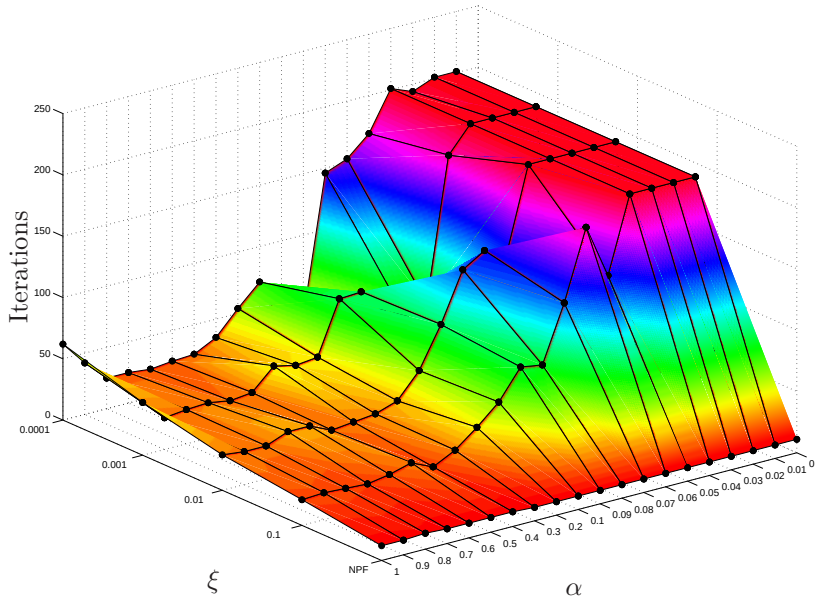

(a)

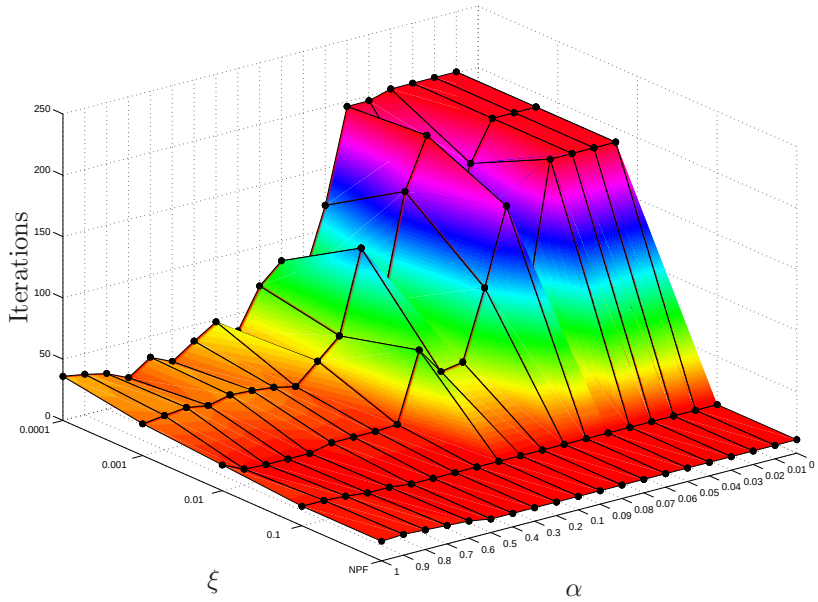

(b)

Figure 5.10: Number of iterations using a predictor-corrector method: (a) flat start; (b) power flow start.

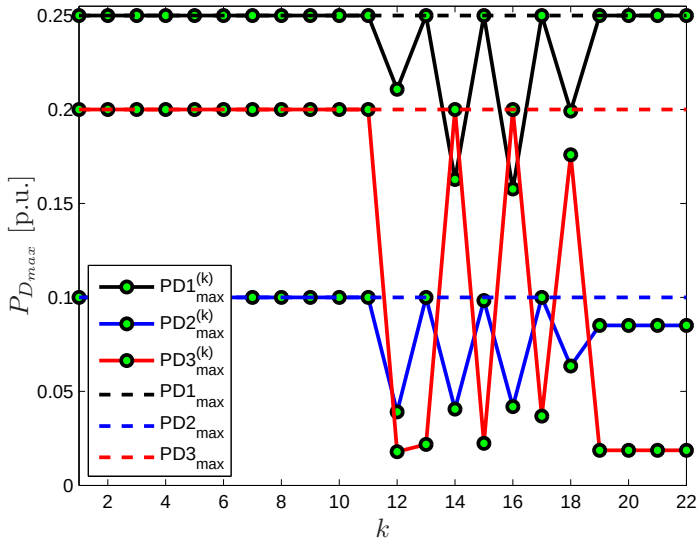

(a)

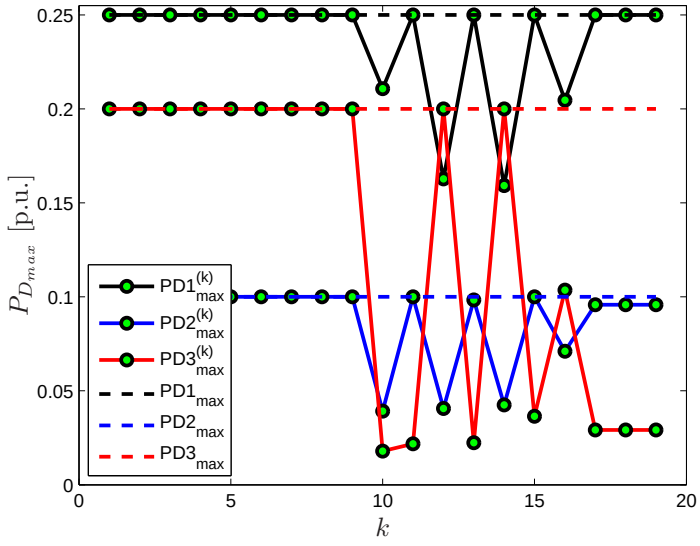

(b)

Figure 5.11: Cuts at every iteration using a Newton method: (a) flat start; (b) power flow start.

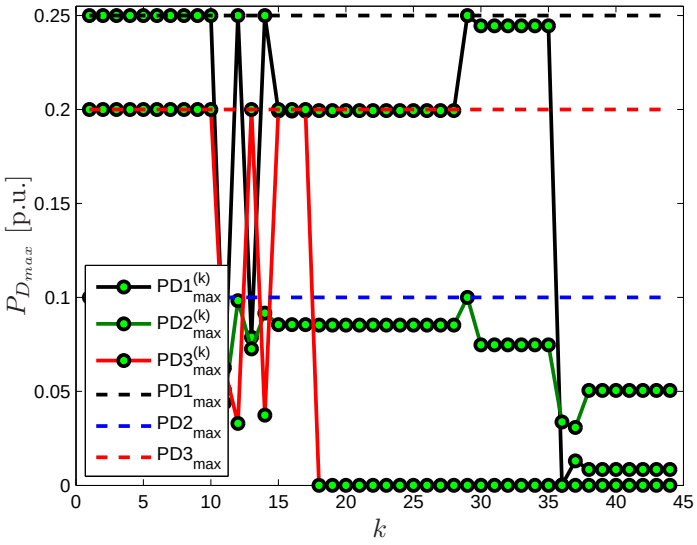

(a)

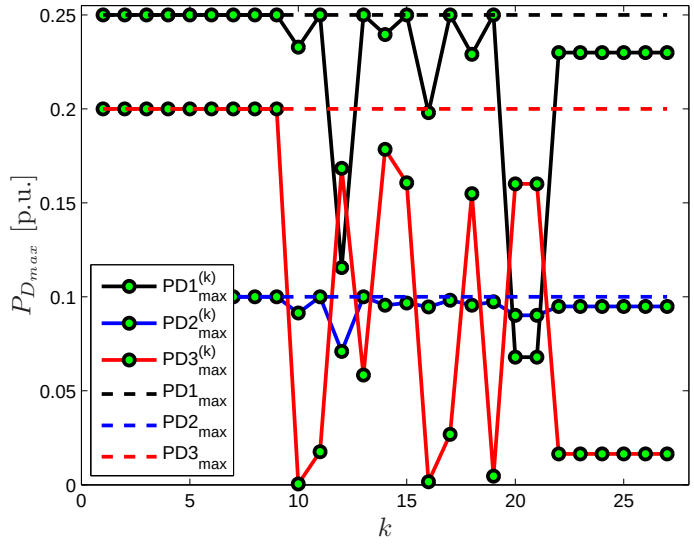

(b)

Figure 5.12: Cuts at every iteration using a Predictor-corrector method: (a) flat start; (b) power flow start.

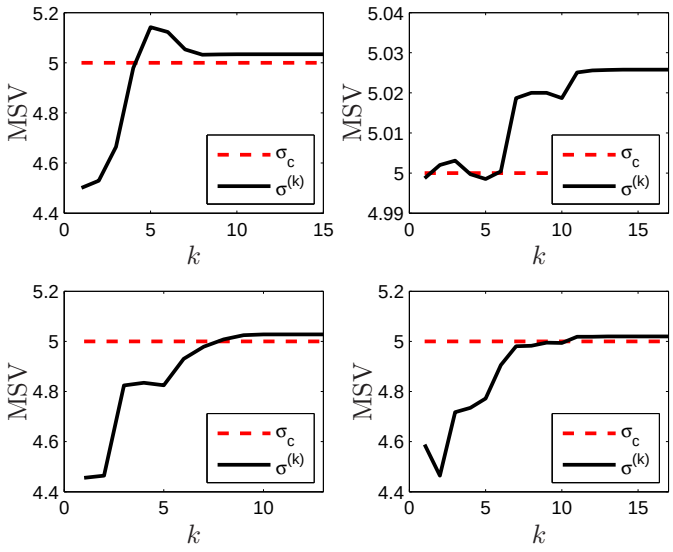

(a)

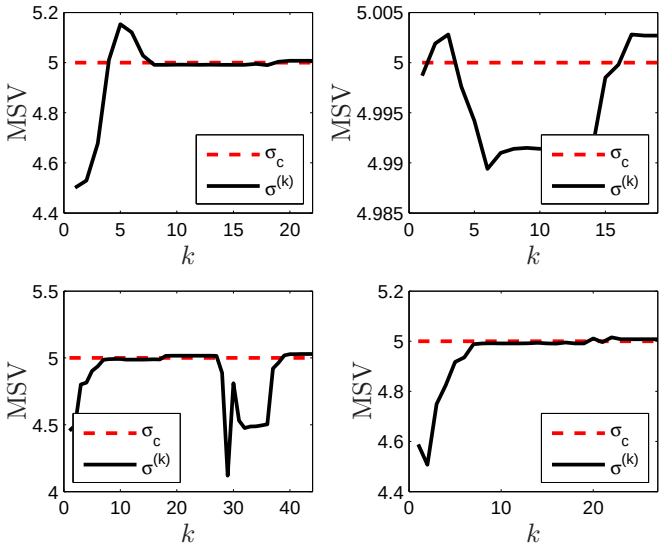

(b)

Figure 5.13: Final value of $\sigma^{(k)}$ when the cut is added using different criteria: (a) ξ = NPF (b) $\xi = 1 \times 10^{-3}$. In each case, the top two figures correspond to the Newton method; the two in the bottom correspond to the predictor-corrector method; the two on the left correspond to flat start, and power flow start is on the right.

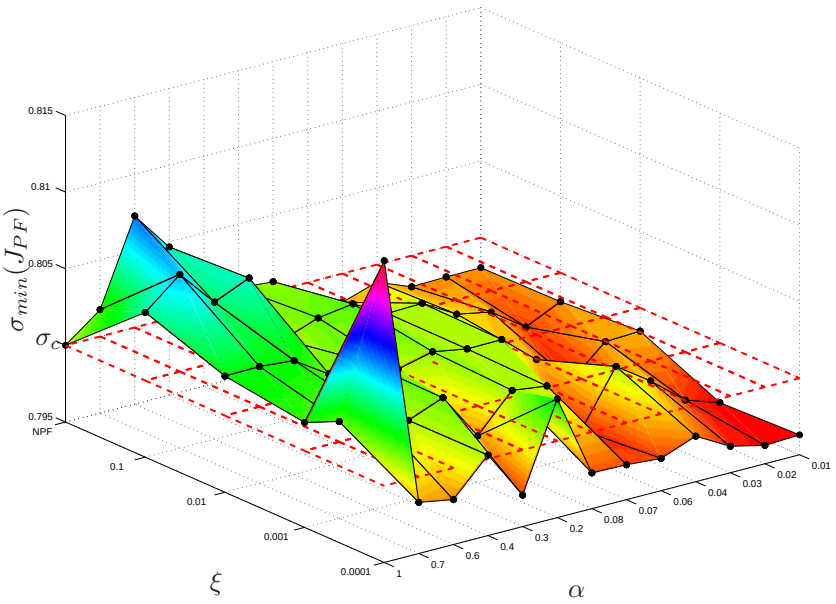

Figure 5.14: MSV of the power flow Jacobian using a predictor-corrector method with a power flow start for the CIGRE-32 test system.

After several tests, it was concluded that the best values in general are $\alpha = 1$ and $\xi = 1 \times 10^{-3}$. It was also observed that the algorithm performs well using either the Newton method or the predictor-corrector method; however, the later usually required less iterations.

5.2.2 Numerical Results

Having studied and tuned the algorithm, a comparison between the CP/IPM algorithm and the proposed method presented in Chapter 4 to solve the VSC-OPF model (2.24) is presented in this section. These methods are applied to the same 6-bus test system, and the CIGRE-32 system. The σ_c value used in the MSV constraint for each system is $\sigma_c = 5.0$ and $\sigma_c = 0.8$, respectively. The CP/IPM algorithm was solved using the Newton method with a power flow start, $\xi = 1 \times 10^{-3}$ and $\alpha = 1$.

The results presented in Table 5.1, corresponding to the 6-bus system, show

Table 5.1: Comparison of solution methods for the VSC-OPF for the 6-bus test system and $\sigma_c = 5.0$.

Participant	Model (4.4) ($\sigma_n = 5.0003 > \sigma_c$)			CP/IPM ($\sigma_{min} = 5.003 > \sigma_c$)		
	V [p.u.]	P_S/P_D [MW]	LMP [$/MWh]	V [p.u.]	P_S/P_D [MW]	LMP [$/MWh]
GENCO 1	1.1	0	8.88	1.1	0	8.83
GENCO 2	1.1	19.59	8.8	1.1	19.1	8.8
GENCO 3	1.1	20	9.02	1.1	20	8.94
ESCO 1	1.021	25	9.41	1.021	25	9.36
ESCO 2	1.013	10	9.56	1.014	9.6	9.44
ESCO 3	1.041	3.04	9.31	1.042	2.9	9.21

that the proposed CP/IPM algorithm yields similar results to the proposed VSC-OPF model (4.4). Notice that the CP/IPM is more secure than the latter, i.e., $\sigma_{min} > \sigma_n > 5.0$; therefore, the power dispatch and LMPs are less than the ones obtained using (4.4), with the voltage levels being slightly better, as expected.

It is also interesting to analyze how the CP/IPM algorithm attains optimality when solving a larger and heavily loaded system. Figure 5.15 shows $\sigma_{min}^{(k)}$ during the solution process for the CIGRE-32 system. Notice that this value starts to be monitored from $k = 172$, accordingly with the feasibility of the power flow equations criterion shown in Figure 5.16(b). Observe in Figure 5.17 that the upper limit of P_D is modified only if the MSV constraint is violated and if the feasibility of the power flow equations is within 1×10^{-3}, ($\xi_1 \leq \xi$) in (2.45). Figure 5.18 shows the feasibility of the IPM; thus, the step length parameters converge to 1, the centering parameter is close to 0, and the complementarity gap and barrier parameter are within the expected tolerances.

Table 5.2 shows a numerical comparison between the solution technique de-

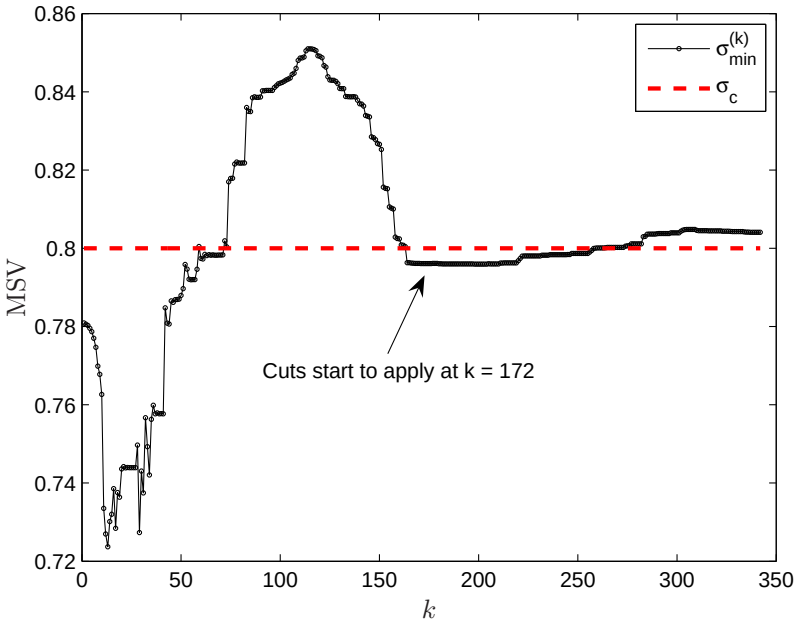

Figure 5.15: MSV at every iteration in the CP/IPM when solving the CIGRE-32 system.

scribed in Chapter 4 and the proposed CP/IPM approach. Notice that the small difference between the σ_{min} values obtained from these two techniques, i.e., 0.00409, has a significant effect on the power dispatch and LMPs at some buses. This is to be expected, since a big increase in system demand may result in a very small change in the MSV; however, this difference can be also attributed to the fact that these methods just converge to different local optimal. Finally, these results show that the two proposed methods can successfully solve the VSC-OPF model (2.24). Nevertheless, in general, the proposed model (4.4) and its solution technique is better than the CP/IPM algorithm, because:

- The CP/IPM method depends on the starting point and on the solution technique, yielding different solutions, whereas (4.4) does not.
- The CP/IPM method requires elastic demand bids, which limits its application to other OPF problems, since in most electricity markets, demand is

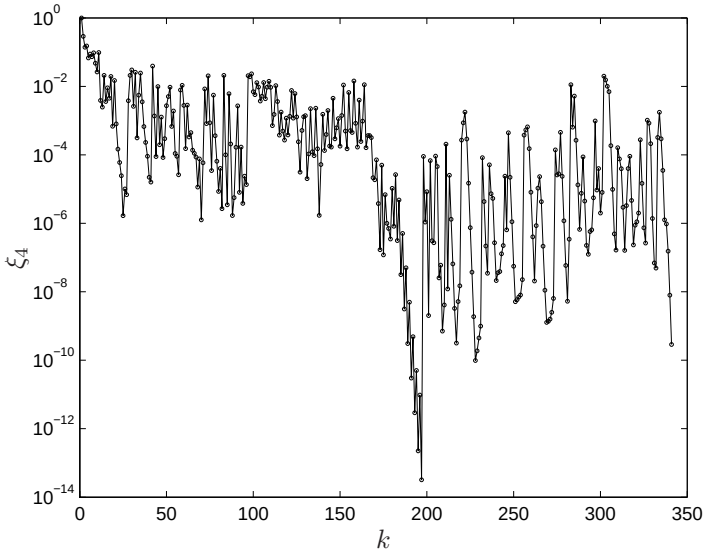

(a)

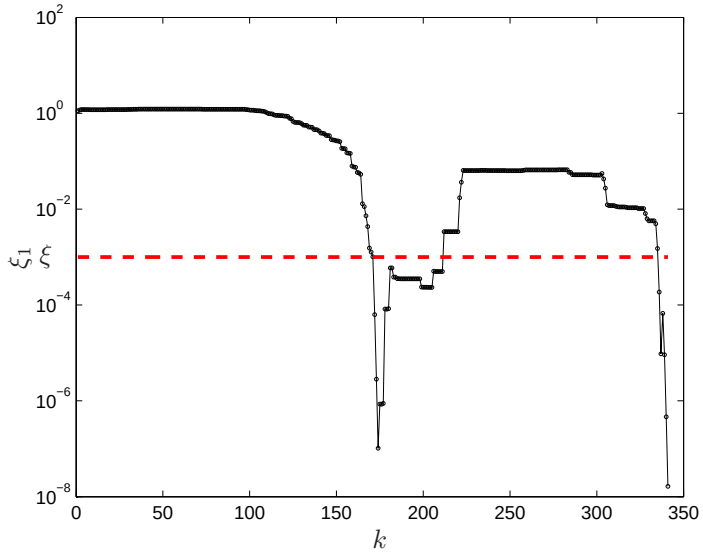

(b)

Figure 5.16: Feasibility of (a) the objective function and (b) the power flow equations (equality constraints) in the CP/IPM when solving the CIGRE-32 system.

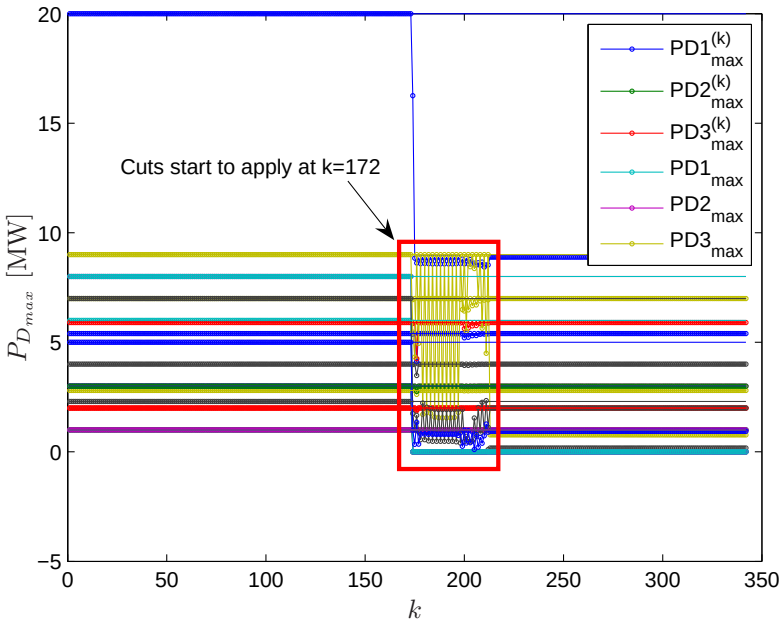

Figure 5.17: The box encloses the iterations at which some cuts are added in the CP/IPM when solving CIGRE-32 system.

inelastic. This is not the case for (4.4), which works for any type of load demand.

Table 5.2: Comparison of the proposed solution methods for the VSC-OPF using the CIGRE-32 test system, for $\sigma_c = 0.8$.

Bus	Model (4.4) ($\sigma_n = \sigma_c = 0.8$)				CP/IPM ($\sigma_{min} = 0.80409 > \sigma_c$)			
	V [p.u.]	P_S [MW]	P_D [MW]	LMP [$/MWh]	V [p.u.]	P_S [MW]	P_D [MW]	LMP [$/MWh]
4072	0.972	0	845.224	10.000	0.985	0	856.5	9.950
4071	0.964	0	0	9.499	0.972	0	0	9.360
4011	1.016	227.548	0	9.000	1.017	0	0	8.724
4012	1.009	600.6	0	8.734	1.009	573.06	0	8.500

Continued on next page

Table 5.2 – continued from previous page

Bus	Model (4.4) ($\sigma_n = \sigma_c = 0.8$)				CP/IPM ($\sigma_{min} = 0.80409 > \sigma_c$)			
	V [p.u.]	P_S [MW]	P_D [MW]	LMP [$/MWh]	V [p.u.]	P_S [MW]	P_D [MW]	LMP [$/MWh]
4021	1.100	0	0	6.517	1.100	0	0	6.861
4031	1.001	19.333	0	7.500	0.994	256.39	0	7.500
4042	0.978	658	0	7.289	0.971	0	0	6.761
4041	1.018	282	0	7.888	0.992	282	0	7.421
4062	1.094	564	0	6.388	1.009	564	0	6.171
4063	1.098	884.778	0	5.500	1.006	878.84	0	5.500
4051	1.009	658	0	8.257	0.979	658	0	7.215
4047	1.002	769.6	0	7.841	0.963	769.6	0	6.983
2032	0.968	728.277	200	4.000	0.977	694.06	200	4.000
1013	1.011	543.2	100	7.869	1.011	543.2	99.995	7.582
1012	0.900	0	300	8.717	0.900	0	300	8.473
1014	1.031	0	0	7.962	1.031	0	0	7.692
1022	0.920	0	280	8.202	0.900	0	280	8.118
1021	1.100	0	0	6.841	1.057	0	0	6.819
1043	0.964	0	0	9.677	0.932	0	17.088	8.363
1042	1.100	0	0	8.302	1.100	0	0	7.143
4022	1.004	0	0	8.200	0.996	0	0	8.104
4032	1.035	0	0	6.960	1.029	0	0	7.072
4043	0.946	0	0	8.384	0.947	0	0	7.077
4044	0.969	0	0	8.264	0.955	0	0	7.203

Continued on next page

Table 5.2 – continued from previous page

Bus	Model (4.4) ($\sigma_n = \sigma_c = 0.8$)				CP/IPM ($\sigma_{min} = 0.80409 > \sigma_c$)			
	V [p.u.]	P_S [MW]	P_D [MW]	LMP [$/MWh]	V [p.u.]	P_S [MW]	P_D [MW]	LMP [$/MWh]
4045	0.962	0	0	8.852	0.934	0	0	7.568
4046	0.949	0	0	8.470	0.933	0	0	7.160
4061	1.069	0	0	7.292	0.991	0	0	6.887
2031	0.900	0	100	7.390	0.900	0	99.995	7.397
1011	0.900	0	200	9.011	0.900	0	200	8.732
1041	0.927	0	0	10.732	0.890	0	0	9.792
1044	0.968	0	0	8.451	0.952	0	0	7.206
1045	0.946	0	700	9.261	0.915	0	700	7.772
42	0.937	0	400	7.094	0.930	0	400	6.295
41	0.986	0	540	8.143	0.959	0	540	7.421
62	1.058	0	300	7.192	0.968	0	300	6.716
63	1.043	0	590	6.388	0.944	0	590	6.152
51	0.990	0	0	8.507	0.958	0	0	7.320
47	0.961	0	100	8.155	0.920	0	99.995	6.983
43	0.900	0	837.795	9.131	0.924	0	77.584	7.020
46	0.918	0	186.956	8.899	0.900	0	199.570	7.309
61	1.052	0	55.512	7.727	0.970	0	93.825	7.176
Totals		5935.36	5735.47			5219.15	5054.52	
Iterations	234				341			

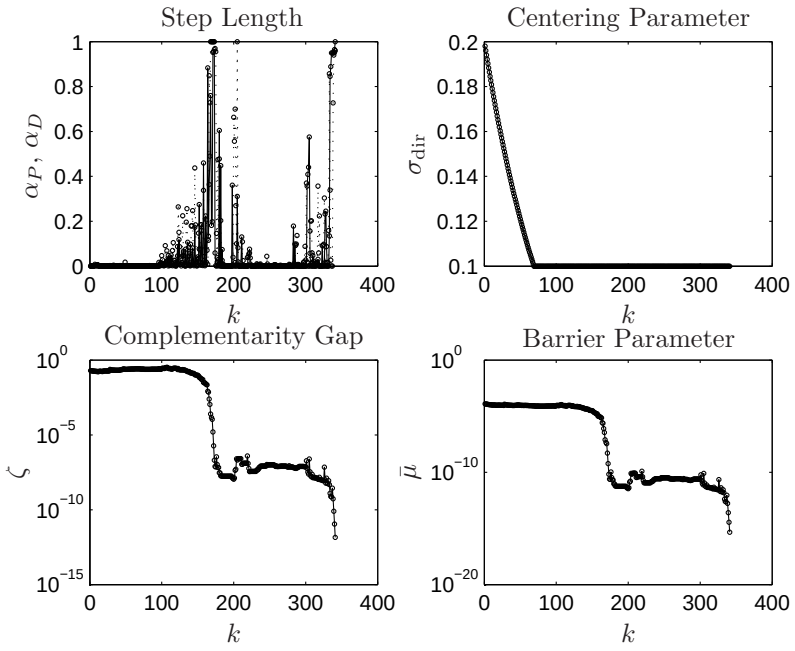

Figure 5.18: Feasibility parameters in the CP/IPM when solving the CIGRE-32 system.

5.3 Solving the VSC-OPF via SDP

This section discusses the possible application of SDP to the VSC-OPF problem, demonstrating that this optimization problem cannot really be casted as a SDP relaxation. Thus, consider the 2-bus test system with one generator and one load at each bus shown in Figure 5.19, and the OPF model (2.21). In order to obtain an equivalent SDP relaxation of this OPF, and since in general, optimization problems that can be solved using SDP have a quadratic form, the power flow equations in rectangular coordinates shown in (3.7) are used in this section with $n_b = 2$, $P_i = P_{S_i} - P_{D_i}$, and $Q_i = Q_{G_i} - K_L P_{D_i}$.

Notice that C, A, and X in a SDP problem are matrices, as explained in Section 2.6.2. Therefore, the power flow equations (3.7), along with the objective function (2.21a), can be arranged in such a way that the inner products $C \cdot X$ and $A \cdot X$ yield these sets of quadratic and linear equations, respectively. In this case, C is a

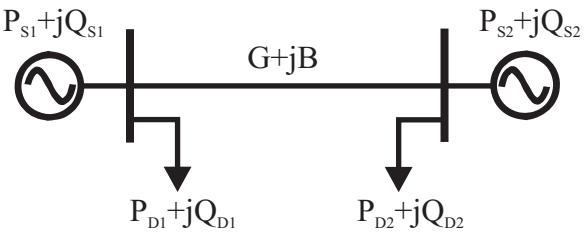

Figure 5.19: 2-bus system

matrix containing the coefficients C_D and C_S of the objective function; A is a matrix containing all the constraints coefficients; and X is a matrix containing all the variables. For example, the objective function in (2.49) for $x = [e_{r_1}\ f_{r_1}\ e_{r_2}\ f_{r_2}\ P_{S_1}\ P_{D_1}\ 1]^T$ yields:

$$X = xx^T = \begin{bmatrix} e_{r_1}^2 & e_{r_1}f_{r_1} & e_{r_1}e_{r_2} & e_{r_1}f_{r_2} & e_{r_1}P_{S_1} & e_{r_1}P_{D_1} & e_{r_1} \\ e_{r_1}f_{r_1} & f_{r_1}^2 & e_{r_2}f_{r_1} & f_{r_1}f_{r_2} & f_{r_1}P_{S_1} & f_{r_1}P_{D_1} & f_{r_1} \\ e_{r_1}e_{r_2} & e_{r_2}f_{r_1} & e_{r_2}^2 & e_{r_2}f_{r_2} & e_{r_2}P_{S_1} & e_{r_2}P_{D_1} & e_{r_2} \\ e_{r_1}f_{r_2} & f_{r_1}f_{r_2} & e_{r_2}f_{r_2} & f_{r_2}^2 & f_{r_2}P_{S_1} & f_{r_2}P_{D_1} & f_{r_2} \\ e_{r_1}P_{S_1} & f_{r_1}P_{S_1} & e_{r_2}P_{S_1} & f_{r_2}P_{S_1} & P_{S_1}^2 & P_{S_1}P_{D_1} & P_{S_1} \\ e_{r_1}P_{D_1} & f_{r_1}P_{D_1} & e_{r_2}P_{D_1} & f_{r_2}P_{D_1} & P_{D_1}P_{S_1} & P_{D_1}^2 & P_{D_1} \\ e_{r_1} & f_{r_1} & e_{r_2} & f_{r_2} & P_{S_1} & P_{D_1} & 1 \end{bmatrix} \tag{5.4}$$

or

$$X = \begin{bmatrix} \bar{e}_{r_1} & e_{r_1}f_{r_1} & e_{r_1}e_{r_2} & e_{r_1}f_{r_2} & e_{r_1}P_{S_1} & e_{r_1}P_{D_1} & e_{r_1} \\ e_{r_1}f_{r_1} & \bar{f}_{r_1} & e_{r_2}f_{r_1} & f_{r_1}f_{r_2} & f_{r_1}P_{S_1} & f_{r_1}P_{D_1} & f_{r_1} \\ e_{r_1}e_{r_2} & e_{r_2}f_{r_1} & \bar{e}_{r_2} & e_{r_2}f_{r_2} & e_{r_2}P_{S_1} & e_{r_2}P_{D_1} & e_{r_2} \\ e_{r_1}f_{r_2} & f_{r_1}f_{r_2} & e_{r_2}f_{r_2} & \bar{f}_{r_2} & f_{r_2}P_{S_1} & f_{r_2}P_{D_1} & f_{r_2} \\ e_{r_1}P_{S_1} & f_{r_1}P_{S_1} & e_{r_2}P_{S_1} & f_{r_2}P_{S_1} & \bar{P}_{S_1} & P_{S_1}P_{D_1} & P_{S_1} \\ e_{r_1}P_{D_1} & f_{r_1}P_{D_1} & e_{r_2}P_{D_1} & f_{r_2}P_{D_1} & P_{D_1}P_{S_1} & \bar{P}_{D_1} & P_{D_1} \\ e_{r_1} & f_{r_1} & e_{r_2} & f_{r_2} & P_{S_1} & P_{D_1} & 1 \end{bmatrix} \tag{5.5}$$

where $\bar{e}_{r_1} = (e_{r_1})^2$; $\bar{f}_{r_1} = (f_{r_1})^2$; $\bar{e}_{r_2} = (e_{r_2})^2$; $\bar{f}_{r_2} = (f_{r_2})^2$; $\bar{P}_{S_1} = (P_{S_1})^2$, and $\bar{P}_{D_1} = (P_{D_1})^2$ are considered variables in the SDP solution process, and the coefficient

matrix can be stated as follows:

$$C = \begin{bmatrix} 0 & \cdots & 0 & 0 & 0 \\ \vdots & \ddots & \vdots & \vdots & \vdots \\ 0 & \cdots & 0 & 0 & -\frac{C_{S_1}}{2} \\ 0 & \cdots & 0 & 0 & \frac{C_{D_1}}{2} \\ 0 & \cdots & -\frac{C_{S_1}}{2} & \frac{C_{D_1}}{2} & 0 \end{bmatrix} \tag{5.6}$$

On the other hand, the coefficients of matrix A_1 corresponding to the active power flow equation (3.10) can be stated as follows:

$$A_1 = \begin{bmatrix} G_{11} & 0 & \frac{G_{12}}{2} & -\frac{B_{12}}{2} & 0 & 0 & 0 \\ 0 & G_{11} & \frac{B_{12}}{2} & \frac{G_{12}}{2} & 0 & 0 & 0 \\ \frac{G_{12}}{2} & \frac{B_{12}}{2} & 0 & 0 & 0 & 0 & 0 \\ -\frac{B_{12}}{2} & \frac{G_{12}}{2} & 0 & 0 & 0 & 0 & 0 \\ 0 & 0 & 0 & 0 & 0 & 0 & -\frac{P_{S_1}}{2} \\ 0 & 0 & 0 & 0 & 0 & 0 & \frac{P_{D_1}}{2} \\ 0 & 0 & 0 & 0 & -\frac{P_{S_1}}{2} & \frac{P_{D_1}}{2} & 0 \end{bmatrix} \tag{5.7}$$

Notice that A_1 is symmetrized, and is composed by elements of the bus admittance matrix and power bids, so that $A_1 \cdot X = b_1$ represents (3.10) with $b_1 = 0$. Similarly, there is a matrix A_2 to represent the reactive power equation (3.11).

Therefore, the objective function and the power flow equations can be represented by means of symmetric matrices and inner products.

Observe that, as defined, X contains quadratic and linear elements, and as per (2.49c) it should be positive semidefinite. This leads to the following problem: Notice that (5.5), in its simplest form has the following structure:

$$\begin{bmatrix} \bar{e}_{r_1} & e_{r_1} \\ e_{r_1} & 1 \end{bmatrix} \succeq 0 \tag{5.8}$$

which implies that $\bar{e}_{r_1} \geq (e_{r_1})^2$. Since $X - xx^T \succeq 0$, and not $X - xx^T = 0$, there is no guarantee that $\bar{e}_{r_1} = e_{r_1} e_{r_1}$ will hold during the SDP solution process. Thus, the

variable matrix (5.5) does not accurately represent the variables of the problem. In conclusion, the nonlinear OPF cannot really be cast as an SDP problem.

It should be mentioned that SDP has been successfully applied to 0/1 problems such as power dispatch [10] and hydrothermal coordination [9], where nonconvex integer-value constraints are replaced by convex quadratic constraints.

5.4 Summary

Two alternative methods to solving the MSV-based VSC-OPF model are studied in this chapter. In the first method, a CP technique is used to handle the VS constraint at every iteration of the primal-dual IPM method. The handling of the VS constraint consist of modifying the upper limit of the demand block bids (adding a cut) when the MSV at a particular iteration is less than a predetermined value. By doing this, the load power dispatch is reduced until the MSV constraint holds, since it is well known that the MSV of the power flow Jacobian decreases when the load increases.

The results obtained for two test systems show that the proposed algorithm successfully solves the VSC-OPF, and that is somewhat comparable with respect to the proposed method in Chapter 4. However, its dependency on both the solution method and on the starting point, as well as the need for an elastic demand, limit the practical application of the algorithm.

The possible use of SDP is also studied, since the inherent constraint on the positivity of the matrix variable in SDP could be related to the required nonsingularity of the power flow Jacobian in the MSV-based VSC-OPF. It is shown that the OPF in rectangular form with social welfare as the objective function can be represented with the inner product of two matrices, as needed in SDP. However, it is also demonstrated that this OPF cannot really be casted as a SDP relaxation problem.

Chapter 6

Conclusions

6.1 Summary

This thesis concentrates on the analysis of an optimization-based method for VS studies, and on the development of solution techniques for VSC-OPF-based auction models. A detailed theoretical study of an optimization method to determine the maximum point of loadability at which a power system experiences a voltage collapse is presented. A novel and practical method to solve a VSC-OPF model which represents VS through the use of the MSV of the power flow Jacobian is proposed. Furthermore, a modified primal-dual IPM to solve a VSC-OPF model using CP is proposed, and SDP is also investigated as a possible solution method.

The following summarizes the main content and conclusions of this thesis:

- Chapter 3 studies in detail the OPF-DM. It is analytically shown that the optimal point of this model corresponds to a SNB or LISB point. This is accomplished by demonstrating that the KKT optimality conditions at the solution of this model yield the same transversality conditions that characterize these bifurcations in nonlinear theory. Numerical examples are also presented to show the numerical equivalence between the OPF-DM and the

CPF technique. The results show that the optimization model is a very flexible tool to study these bifurcations, as current mathematical programming languages and solvers allow one to efficiently solve this problem. Furthermore, this model has been extended to optimize other system parameters so that the loadability of the system is maximized.

- In Chapter 4, a novel and practical method to solve a VSC-OPF which incorporates a VS constraint through the use of the SVD of the power flow Jacobian is proposed. The method consists of iterating to update the SVD of the power flow Jacobian at an optimal power flow solution, until a predetermined MSV is satisfied. A comparison between the proposed VSC-OPF and a typical SC-OPF is presented to highlight the advantages of the VSC-OPF model. The proposed VSC-OPF model is applied to small and large test systems of up to 1211 buses to study its performance and to demonstrate its robustness and practical application in realistic systems. The results from this research yield the following conclusions:

  - The main problem in the formulation of a MSV-based VS constraint is to find an explicit function constraint that can be readily written in terms of the VSC-OPF optimization variables, since the MSV constraint in the originally proposed model is an implicit function.
  - In the proposed VSC-OPF model, the VS constraint ($u_n^T J_{PF} w_n \geq \sigma_c$) becomes explicit. This constraint and corresponding solution technique are shown to computationally outperform the previously proposed MSV-based VSC-OPF model.
  - The main advantages of the proposed model and solution technique are that it is easy to implement using mathematical programming languages, and that there is no need for approximations of the MSV constraint during the solution process. These advantages result in a more robust and practical model.

  - The proposed VSC-OPF model is shown to better represent power system security, resulting in better system and market conditions with respect to SC-OPF models.
  - The main disadvantage of the proposed method is that it requires an iterative solution process, where appropriate parameters (u_n, w_n) are calculated at each iteration. However, experience with different test systems show that the method converges in less than three iterations regardless of the system size.

- In Chapter 5, two alternative techniques to solve the VSC-OPF are proposed. A CP technique to handle the MSV constraint at every iteration of the primal-dual IPM is first proposed to solve the MSV-based VSC-OPF. The developed CP/IPM algorithm is based on a basic concept used in mixed-integer linear optimization, i.e., adding linear constraints (cuts) until the solution holds. In the proposed CP/IPM algorithm the MSV of the power flow Jacobian is monitored at every iteration using a SVD. Then, a cut is added at this iteration if the MSV is less than a predetermined value. The second method tries to formulate the VSC-OPF as an SDP relaxation, so that the positiveness of the eigenvalues of the matrix variable can be related to the MSV constraint. The following conclusions are derived from this investigation:

  - Different optimal solutions are obtained depending upon the initial point and solution method for the Newton direction.
  - The algorithm achieves the desired objective by having to tradeoff between a Newton or predictor-corrector method and flat start or a power flow start. These trade-offs make it less practical than previously proposed methods.
  - It is concluded that the algorithm, in general, has a good performance using a Newton method with a power flow start.
  - The VSC-OPF model cannot be cast as an SDP problem, because the

relaxation of the matrix variables cannot be used to properly formulate the quadratic terms of the power flow equations in rectangular form.

6.2 Contributions

The main contributions of this thesis to the field of power engineering are:

1. A complete theoretical background that supports the use of the OPF-DM to determine the maximum point of loadability of a power system has been developed. This is accomplished by formally demonstrating that the KKT optimality conditions at the solution of the OPF-DM yield the transversality conditions for SNBs and LIBs in bifurcation theory.

2. Two methods to solve a MSV-based VSC-OPF model are proposed.

   - The first method is a novel and practical VSC-OPF model, where the implicit function used in a previously proposed model to represent VS is replaced with an explicit constraint easier to solve and implement, resulting in a more robust and practical model.
   - The second method is a modified primal-dual IPM which makes use of a CP technique to handle the MSV constraint of the VSC-OPF. The CP/IPM is different from traditional IPM schemes, and is specially developed to solve this particular VSC-OPF model.

3. It is analytically shown that the VSC-OPF cannot be cast as an SDP relaxation problem.

The main contents of this thesis has been accepted for publication or is under review for publication in IEEE journals [101,102], and a conference paper has been already accepted for presentation and publication [103].

6.3 Future Work

Further research may be carried out to address the following issues:

- The use of other VSIs in the VSC-OPF should be studied.
- Other optimization methods to solve the proposed VSC-OPF model should be studied, e.g., sequential linear programming.
- Multiperiod OPF models are widely used in power system planning and generation scheduling, among other applications. However, these models are based on linear OPFs which do not include voltage or reactive power variables; therefore, these models do not include voltage security constraints. Hence, developing a linear VSC-OPF would be of great interest.
- The main disadvantage of the proposed CP/IPM algorithm is the dependence on the initial point and solution method for the Newton direction. Therefore, a sensitivity-based approach to calculate the cuts could alleviate this problem.

Appendix A

Test Systems

A.1 6-bus Test System

Figure A.1 shows the 6-bus test system, which has been used by many authors to carry out different studies (e.g., [32,36]) and is also used in this thesis. This system consists of 6 buses, 3 generators, and 11 transmission lines.

Table A.1 show the supply and demand bids for generators and load demands respectively, whereas Table A.2 shows the transmission line parameters. Transmission line limits were computed off-line using a CPF technique, using the generation and load bids as power directions. Bus voltage minimum and maximum limits are considered to be 0.9 p.u. and 1.1 p.u. respectively. The data was obtained from [74].

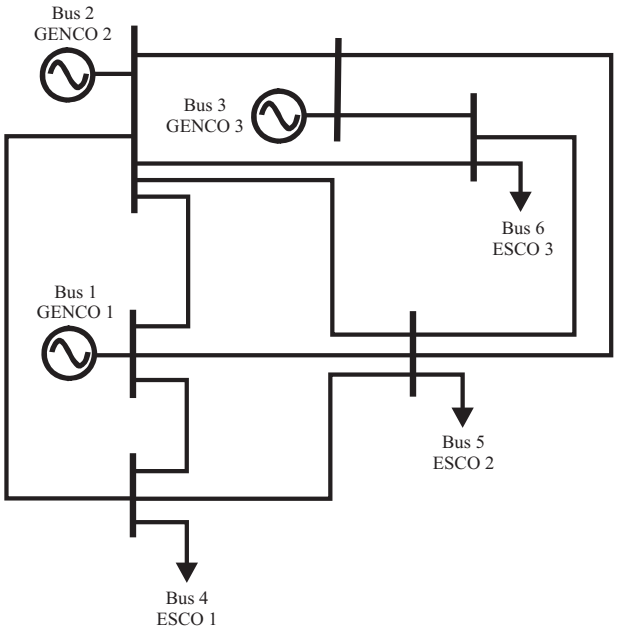

Figure A.1: 6-bus test system.

Table A.1: GENCOs and ESCOs bidding data for the 6-bus test system

Participant	C_S/C_D ($/MWh)	$P_{S_{max}}$ (MW)	$P_{D_{max}}$ (MW)	P_{L_o} (MW)	Q_{L_o} (Mvar)	P_{G_o} (MW)	$Q_{G_{min/max}}$ (MVar)
GENCO 1	9.7	20	0	0	0	90	± 150
GENCO 2	8.8	25	0	0	0	140	± 150
GENCO 3	7.0	20	0	0	0	60	± 150
ESCO 1	12.0	0	25	90	60	0	0
ESCO 2	10.5	0	10	100	70	0	0
ESCO 3	9.5	0	20	90	60	0	0

Table A.2: Line data for the 6-bus test system

From Bus i	To Bus j	R_{ij} [p.u.]	X_{ij} [p.u.]	$B_i/2$ [p.u.]	$P_{max_{ij}}$ [MW]	$I_{max_{ij}}$ [A]
1	2	0.1	0.2	0.02	17.08	37
1	4	0.05	0.2	0.02	59.89	133
1	5	0.08	0.3	0.03	48.89	122
2	3	0.05	0.25	0.03	14.38	46
2	4	0.05	0.1	0.01	92.22	200
2	5	0.1	0.3	0.02	37.68	103
2	6	0.07	0.2	0.025	57.33	132
3	5	0.12	0.26	0.025	33.51	95
3	6	0.02	0.1	0.01	76.65	200
4	5	0.2	0.4	0.04	5.33	26
5	6	0.1	0.3	0.03	0.167	29

A.2 CIGRE-32 Test System

The single-line diagram of the CIGRE-32 test system is depicted in Figure A.2. This system consist of 41 buses, 20 generators, and 52 transmission lines.

Table A.3 show the supply and demand bids for generators and load demands respectively, whereas Table A.4 shows the transmission line parameters. Bus voltage minimum and maximum limits are considered to be 0.9 p.u. and 1.1 p.u., respectively.

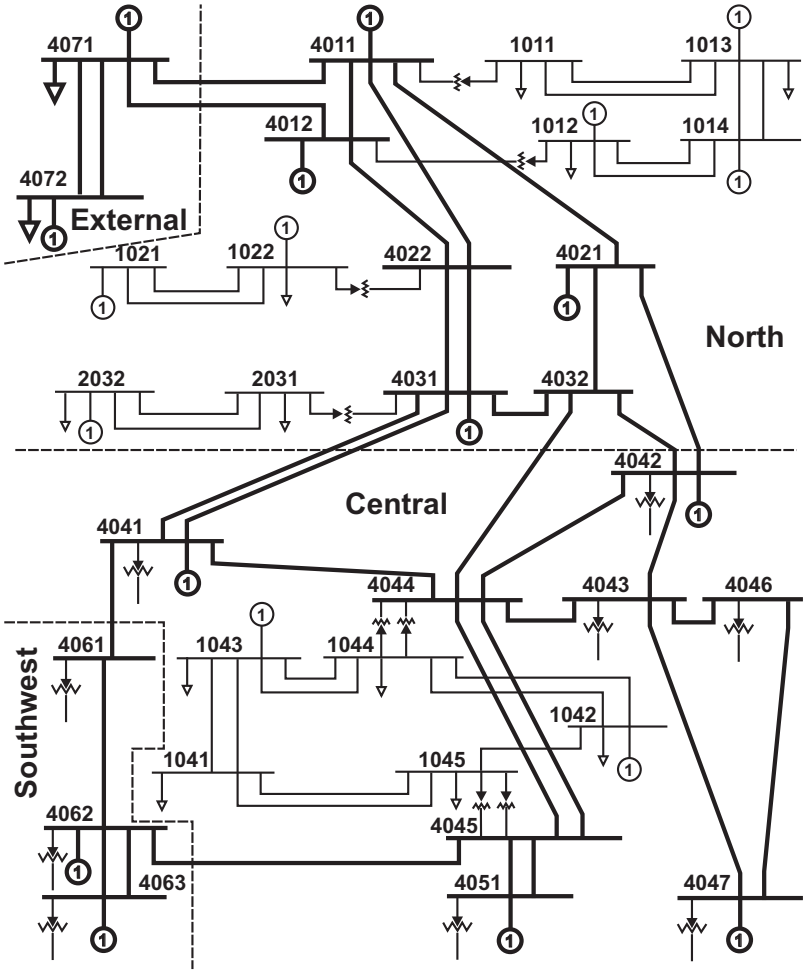

Figure A.2: CIGRE-32 test system.

Table A.3: Bid data for the CIGRE-32 test system.

Bus	C_D [$/MWh]	$P_{D_{max}}$ [MW]	C_S [$/MWh]	$P_{S_{max}}$ [MW]	P_{L_o} [MW]	Q_{L_o} [Mvar]	P_{G_o} [MW]	$Q_{G_{max}}$ [MVar]	$Q_{G_{min}}$ [MVar]
4072	10	20	10	13.33	2000	500	1332.97	1000	-300
4071	9.5	3	9.5	4.70	300	100	469.98	250	-50
4011	0	0	9.0	4.37	0	0	437.39	500	-100
4012	0	0	8.5	6.00	0	0	600.58	400	-160
4021	0	0	8.0	2.82	0	0	281.99	150	-30
4031	0	0	7.5	3.29	0	0	328.99	175	-40
4042	0	0	7.0	6.58	0	0	657.98	350	0
4041	0	0	6.5	2.82	0	0	281.99	300	-200
4062	0	0	6.0	5.64	0	0	563.98	300	0
4063	0	0	5.5	11.2	0	0	1127.97	600	0
4051	0	0	5.0	6.58	0	0	657.98	350	0
4047	0	0	4.5	7.69	0	0	769.58	600	0
2032	8.5	2	4.0	7.99	200	50	798.98	425	-80
1013	9.0	1	7.5	5.43	100	40	543.18	300	-50
1012	9.7	3	9.3	7.52	300	100	751.98	400	-80
1014	0	0	9.5	4.21	0	0	421.09	350	-100
1022	11	2.8	10.1	2.35	280	95	234.99	125	-25
1021	0	0	15.2	5.64	0	0	563.98	300	-160
1043	10.5	2.3	10.3	1.88	230	100	187.99	100	-20
1042	5	3	9.6	3.76	300	80	375.99	200	-40

Continued on next page

Table A.3 – continued from previous page

Bus	C_D [$/MWh]	$P_{D_{max}}$ [MW]	C_S [$/MWh]	$P_{S_{max}}$ [MW]	P_{L_o} [MW]	Q_{L_o} [Mvar]	P_{G_o} [MW]	$Q_{G_{max}}$ [MVar]	$Q_{G_{min}}$ [MVar]
4022	0	0	0	0	0	0	0	0	0
4032	0	0	0	0	0	0	0	0	0
4043	0	0	0	0	0	0	0	0	0
4044	0	0	0	0	0	0	0	0	0
4045	0	0	0	0	0	0	0	0	0
4046	0	0	0	0	0	0	0	0	0
4061	0	0	0	0	0	0	0	0	0
2031	9.0	1	0	0	100	30	0	0	0
1011	9.5	2	0	0	200	80	0	0	0
1041	8.5	6	0	0	600	200	0	0	0
1044	7.6	8	0	0	800	300	0	0	0
1045	11	7	0	0	700	250	0	0	0
42	8.7	4	0	0	400	125.7	0	0	0
41	9.0	5.4	0	0	540	128.8	0	0	0
62	8.5	3	0	0	300	80.02	0	0	0
63	9.2	5.9	0	0	590	256.2	0	0	0
51	8.1	8	0	0	800	253.2	0	0	0
47	15	1	0	0	100	45.19	0	0	0
43	10	9	0	0	900	238.8	0	0	0
46	9.5	7	0	0	700	193.7	0	0	0
61	8.5	5	0	0	500	112.3	0	0	0

Table A.4: Line data for the CIGRE-32 test system.

From Bus i	To Bus j	R_{ij} [p.u.]	X_{ij} [p.u.]	B_i [p.u.]
4011	4012	.001	.008	.4
4011	4021	.006	.060	3.58
4011	4022	.004	.040	2.39
4011	4071	.005	.045	2.79
4012	4022	.004	.035	2.09
4012	4071	.005	.050	2.98
4021	4032	.004	.040	2.39
4021	4042	.010	.060	5.97
4031	4022	.002	.020	1.20
4031	4032	.001	.010	.6
4031	4041	.003	.020	2.39
4042	4032	.010	.040	3.98
4032	4044	.006	.050	4.77
4041	4044	.003	.030	1.79
4041	4061	.006	.045	2.59
4042	4043	.002	.015	.990
4042	4044	.002	.020	1.19
4043	4044	.001	.010	.600
4043	4046	.001	.010	.600
4043	4047	.002	.020	1.19
4044	4045	.001	.010	.6
4045	4051	.002	.020	1.20
4045	4062	.011	.080	4.77
4046	4047	.001	.015	.990

Continued on next page

Table A.4 – continued from previous page

From Bus i	To Bus j	R_{ij} [p.u.]	X_{ij} [p.u.]	B_i [p.u.]
4061	4062	.0015	.015	.900
4062	4063	.0015	.015	.900
4071	4072	.0015	.015	3.00
2031	2032	.00599	.045	.050
1011	1013	.00503	.03491	.130
1012	1014	.00710	.04497	.170
1013	1014	.00349	.02503	.100
1021	1022	.01503	.100	.290
1041	1043	.00503	.030	.120
1041	1045	.00751	.060	.240
1042	1044	.01899	.140	.570
1042	1045	.05000	.300	1.13
1043	1044	.00503	.040	.150
1011	4011	0	.008	0
1012	4012	0	.008	0
1022	4022	0	.012	0
1044	4044	0	.005	0
1045	4045	0	.005	0
2031	4031	0	.012	0
4042	42	0	.013	0
4041	41	0	.010	0
4047	47	0	.040	0
4043	43	0	.007	0
4046	46	0	.010	0
4051	51	0	.007	0
4061	61	0	.013	0

Continued on next page

Table A.4 – continued from previous page

From Bus i	To Bus j	R_{ij} [p.u.]	X_{ij} [p.u.]	B_i [p.u.]
4062	62	0	.020	0
4063	63	0	.010	0

A.3 1211-bus Test System

A more realistic test system which represents an actual European electric power system is also used in this thesis to test a proposed model and solution technique. This test system consists of 1211 buses, 190 generators, and 1567 transmission lines. The data of this system is not provided because it is confidential.

Bibliography

[1] F. Milano, C. A. Cañizares, and M. Invernizzi, "Multi-objective optimization for pricing system security in electricity markets," *IEEE Transactions on Power Systems*, vol. 18, no. 2, pp. 596–604, May 2003.

[2] "Interim report: Causes of the august 14th blackout in the united states and canada," Tech. Rep. [Online]. Available: http://www.nrcan-rncan.gc.ca/media/docs/814BlackoutReport.pdf

[3] "Report on the events of september 28th, 2003 culminating in the separation of the italian power system from the other ucte networks," Tech. Rep., April 2004. [Online]. Available: http://www.autorita.energia.it/docs/04/061-04all.pdf

[4] "The black-out in southern sweden and eastern denmark, 23 september, 2003," Tech. Rep., October 2003. [Online]. Available: http://www.svk.se/upload/3195/DisturbanceSwedenDenmarkSept23.pdf

[5] M. E. Karystianos, N. G. Maratos, and C. D. Vournas, "Maximizing power-system loadability in the presence of multiple binding complementarity constraints," *IEEE Transactions on Circuits and Systems*, vol. 54, no. 8, pp. 1775–1787, August 2007.

[6] W. Rosehart, C. Roman, and A. Schellenberg, "Optimal power flow with complementarity constraints," *IEEE Transactions on Power Systems*, vol. 20, no. 2, pp. 813–822, May 2005.

[7] G. L. Torres and V. H. Quintana, "Power system optimization via successive linear programming with interior point methods," University of Waterloo, Waterloo, ON, Canada, Tech. Rep. UW ECE 93-02, January 1996.

[8] G. D. Irisarri, W. Wang, J. Tong, and S. Mokhtari, "Maximum loadability of power systems using interior point non-linear optimization method," *IEEE Transactions on Power Systems*, vol. 12, no. 1, pp. 162–169, February 1997.

[9] R. Fuentes-Loyola and V. H. Quintana, "Medium-term hydrothermal coordination by semidefinite programming," *IEEE Transactions on Power Systems*, vol. 18, no. 4, pp. 1515–1522, November 2003.

[10] M. Madrigal and V. H. Quintana, "Semidefinite programming relaxations for (0,1)-power dispatch problems," *Power Engineeting Society (PES), summer meeting*, vol. 2, pp. 18–22, 1999.

[11] B. Stott, O. Alsac, and A. J. Monticelli, "Security analysis and optimization," in *Proceedings of the IEEE*, vol. 75, no. 12, December 1987, pp. 1623–1644.

[12] J. Momoh, R. Koessler, M. Bond, and B. Stott, "Challenges to optimal power flow," *IEEE Transactions on Power Systems*, vol. 12, no. 1, pp. 444–447, February 1997.

[13] "Voltage stability assesment: Concepts, practices and tools," IEEE/PES Power System Stability Subcomitte, Tech. Rep., August 2002.

[14] W. D. Rosehart, "Optimal power flows incorporating network stability," in *Proc. IEEE Power Engineering Society, Winter Meeting*, vol. 2, January 2002, pp. 1100–1104.

[15] G. Irisarri, X. Wang, J. Tong, and S. Mokhtari, "Maximum loadability of power systems using interior point non-linear optimization method," *IEEE Transactions on Power Systems*, vol. 12, no. 1, pp. 162–172, February 1997, Siemens Empros Power System Control.

[16] J. Kabouris, C. Vournas, S. Efstathiou, G. Manos, and G. Contaxis, "Voltage security considerations in an open power market," in *Proc. Electric Utility Deregulation and Restructuring and Power Technologies*, April 2000, pp. 278–283.

[17] C. A. Cañizares, N. Mithulananthan, F. Milano, and J. Reeve, "Linear performance indices to predict oscillatory stability problems in power systems," *IEEE Transactions on Power Systems*, vol. 19, no. 2, pp. 1104–1114, May 2004.

[18] W. Marszalek and Z. W. Trzaska, "Singularity-induced bifurcations in electrical power systems," *IEEE Transactions on Power Systems*, vol. 20, no. 1, pp. 312–320, February 2005.

[19] R. Riaza, S. L. Campbell, and W. Marszalek, "On singular equilibria of index-1 DAEs," *Circuits Systems Signal Process*, vol. 19, no. 2, pp. 131–157, 2000.

[20] V. Ajjarapu and C. Christy, "The continuation power flow: A tool for steady state voltage stability analysis," *IEEE Transactions on Power Systems*, vol. 1, no. 1, pp. 416–423, February 1992.

[21] C. A. Cañizares and F. L. Alvarado, "Point of collapse and continuation methods for large ac/dc systems," *IEEE Transactions on Power Systems*, vol. 8, no. 1, pp. 1–8, February 1993.

[22] C. A. Cañizares, "Calculating optimal system parameters to maximize the distance to saddle-node bifurcations," *IEEE Transactions on Circuits and Systems—Part I: Fundamental Theory and Applications*, vol. 3, no. 45, pp. 225–237, March 1998.

[23] T. V. Cutsem, "A method to compute reactive power margins with respect to voltage collapse," *IEEE Transactions on Power Systems*, vol. 6, no. 1, pp. 145–155, February 1991.

[24] E. Vaahedi, Y. Mansour, C. Fuchs, S. Granville, M. D. L. Latore, and H. Hamadanizadeh, "Dynamic security constrained optimal power flow/var planning," *IEEE Transactions on Power Systems*, vol. 16, no. 1, pp. 38–43, February 2001.

[25] W. D. Rosehart, "Optimization of power systems with voltage security constraints," Ph.D. dissertation, University of Waterloo, Waterloo, ON. Canada, 2000.

[26] W. D. Rosehart, C. A. Cañizares, and V. H. Quintana, "Multiobjective optimal power flows to evaluate voltage security cost in power networks," *IEEE Transactions on Power Systems*, vol. 18, no. 2, pp. 578–587, May 2003.

[27] G. L. Torres and V. H. Quintana, "An interior point method for nonlinear optimal power flow using voltage rectangular coordinates," *IEEE Transactions on Power Systems*, vol. 13, no. 4, pp. 1211–1218, November 1998.

[28] O. Alsac, J. Bright, M. Paris, and B. Stott, "Further developments in LP-Based optimal power flow," *IEEE Transactions on Power Systems*, vol. 5, no. 3, pp. 697–711, August 1990, Power Computer Applications Corporation.

[29] M. Huneault and F. Galiana, "A survey of the optimal power flow literature," *IEEE Transactions on Power Systems*, vol. 6, no. 2, pp. 762–770, May 1991.

[30] J. Kubokawa, H. Sasaki, S. Ahmed, and G. Strbac, "Application of optimal power flow for voltage stability problem," in *Proc. International Conference on Electric Power Engineering*, Budapest, May 1999, pp. 134–141.

[31] W. Rosehart, C. Cañizares, and V. Quintana, "Optimal power flow incorporating voltage collapse constraints," in *Proc. IEEE Power Engineering Society, Summer Meeting*, vol. 2, July 1999, pp. 820–825.

[32] F. Milano, C. A. Cañizares, and A. J. Conejo, "Sensitivity-based security-constrained OPF market clearing model," *IEEE Transactions on Power Systems*, vol. 20, no. 4, pp. 2051–2059, November 2005.

[33] A. Berizzi, C. Bovo, M. Innorta, and P. Marannino, "Multiobjective optimization techniques applied to modern power systems," in *Power Engineering Society Winter Meeting*, vol. 3, Columbus, OH, USA, February 2001, pp. 1503–1508.

[34] S. K. M. Kodsi and C. A. Cañizares, "Application of a stability-constrained optimal power flow to tuning of oscillation controls in competitive electricity markets," *IEEE Transactions on Power Systems*, accepted for Publication March 2007.

[35] H. Harsan, N. Hadjsaid, and P. Pruvot, "Cyclic security analysis for security constrained optimal power flow," *IEEE Transactions on Power Systems*, vol. 12, no. 2, pp. 948–953, May 1997, Electricité de France.

[36] A. J. Wood and B. R. Wollenberg, *Power Generation, Operation, and Control*, 2nd ed. John Wiley and Sons, 1996.

[37] A. I. Cohen, V. Brandwajn, and S. K. Chang, "Security constrained unit commitment for open markets," in *Proc. IEEE International Conference PICA'99*, P. I. C. Applications, Ed., May 1999, pp. 39–44, ABB Systems Control.

[38] J. J. Shaw, "A direct method for security-constrained unit commitment," *IEEE Transactions on Power Systems*, vol. 10, no. 3, pp. 1329–1342, August 1995, ALPHATECH.

[39] D. Hur, J.-K. Park, B. H. Kim, and K.-M. Son, "Security constrained optimal power flow for the evaluation of transmission capability on Korea electric power system," in *Proc. IEEE Power Engineering Society, Summer Meeting*, vol. 2, July 2001, pp. 1133–1138.

[40] P. Yang and A. Sekar, "A new approach to security-constrained optimal power flow analysis," in *Proc. IEEE Power Engineering Society, Summer Meeting*, vol. 3, July 2001, pp. 1462–1467.

[41] C. A. Cañizares, H. Chen, and W. Rosehart, "Pricing system security in electricity markets," *Proc. Bulk Power Systems Dynamics and Control-V.*, August 2001.

[42] W. Rosehart, C. Cañizares, and V. Quintana, "Costs of voltage security in electricity markets," in *Proc. IEEE Power Engineering Society, Summer Meeting*, vol. 4, Seattle, WA, July 2000, pp. 2115–2120.

[43] F. Milano, C. A. Cañizares, and M. Invernizzi, "Voltage stability constrained OPF market models considering N-1 contingency criteria," *Electric Power System Research*, vol. 74, no. 1, pp. 27–36, March 2005.

[44] P. Löf, T. Smed, G. Andersson, and D. Hill, "Fast calculation of a voltage stability index," *IEEE Transactions on Power Systems*, vol. 7, no. 1, pp. 54–64, February 1992.

[45] A. Tiranuchit and R. Thomas, "A posturing strategy againts voltage instabilities in electric power systems," *IEEE Transactions on Power Systems*, vol. 3, no. 1, pp. 87–93, February 1988.

[46] G. Huang and T. Zhu, "A new method to find the voltage collapse point," in *Proc. IEEE Power Engineering Society, Summer Meeting*, vol. 2, July 1999, pp. 1324–1329.

[47] A. C. Z. de Souza, "New techniques to efficiently determine proximity to static voltage collapse," Ph.D. dissertation, University of Waterloo, Waterloo, ON. Canada, 1996.

[48] N. Mithulananthan, "Hopf bifurcation control and indices for power system with interacting generator and facts controllers," Ph.D. dissertation, University of Waterloo, Waterloo, ON. Canada, 2002.

[49] A. Berizzi, P. Finazzi, D. Dosi, P. Marannino, and S. Corsi, "First and second order methods for voltage collapse assessment and security enhancement," *IEEE Transactions on Power Systems*, vol. 13, no. 2, pp. 543–551, May 1998.

[50] A. Berizzi, P. Bresesti, P. Marannino, G. Granelli, and M. Montagna, "System-area operating margin assessment and security enhancement againts voltage collapse," *IEEE Transactions on Power Systems*, vol. 11, no. 3, pp. 1451–1461, August 1996.

[51] M. Haque, "Determination of steady-state voltage stability limt using P-Q curve," *IEEE Power Engineering Review*, pp. 71–72, April 2002.

[52] J. Kubokawa, R. Inoue, and H. Sasaki, "A solution of optimal power flow with voltage stability constraints," in *Proc. International Conference on Power System Technology*, December 2000, pp. 625–630.

[53] C. Cañizares, W. Rosehart, A. Berizzi, and C. Bovo, "Comparison of voltage security constrained optimal power flow techniques," in *Proc. IEEE Power Engineering Society, Summer Meeting*, vol. 4, no. 2, Vancouver, BC., July 2001, pp. 2115–2120.

[54] P. Kundur, J. Paserba, V. Ajjarapu, G. Anderson, A. Bose, C. Canizares, *et al.*, "Definition and clasification of power system stability," *IEEE Transactions on Power Systems*, vol. 19, no. 2, pp. 1387–1401, May 2004.

[55] P. Kundur, *Power System Stability and Control*, ser. Power System Engineering. McGraw-Hill, 1994.

[56] J. Machowski, J. W. Bialek, and J. R. Bumby, *Power System Dynamics and Stability*. John Wiley and Sons, 1997.

[57] D. J. Hill and I. M. Y. Mareels, "Stability theory for differential/algebraic systems with application to power systems," *IEEE Transactions on Circuits and Systems*, vol. 37, no. 11, pp. 1416–1423, November 1990.

[58] V. Venkatasubramanian, H. Schättler, and J. Zaborszky, "A taxonomy theory of the dynamics of large power systems with emphasis on its voltage stability," in *Bulk Power System Voltage Phenomena II-Voltage Stability and Security*, L. H. Fink, Ed., August 1991, pp. 9–52.

[59] R. Seydel, *Practical Bifurcation and Stability Analysis: from equilibrium to chaos*, 2nd ed. Springer-Verlag, 1994.

[60] I. Dobson and H. D. Chiang, "Towards a theory of voltage collapse in electric power systems," *Systems & Control Letters*, vol. 13, pp. 253–262, 1989.

[61] C. A. Cañizares, "Conditions for saddle-node bifurcations in ac/dc power systems," *International Journal of Electrical Power and Energy Systems*, vol. 17, no. 1, pp. 61–68, January 1995.

[62] I. Dobson and L. Lu, "Voltage collapse precipitated by the immediate change in stability when generator reactive power limits are encountered," *IEEE Transactions on Circuits and Systems—Part I: Fundamental Theory and Applications*, vol. 39, no. 9, pp. 762–766, September 1992.

[63] V. Venkatasubramanian, H. Schättler, and J. Zaborszky, "Dynamics of large constrained nonlinear systems-a taxonomy theory," in *Proceedings of the IEEE*, vol. 83, no. 11, November 1995, pp. 1530–1560.

[64] N. Balu, T. Bertram, A. Bose, V. Brandwajn, G. Cauley, D. Curtice, A. Fouad, L. Fink, M. G. Lauby, B. F. Wollember, and J. N. Wrubel, "On-Line power system security analysis," in *Proceedings of the IEEE*, vol. 80, no. 2, February 1992, pp. 262–280.

[65] M. Shahidehpour, W. F. Tinney, and Y. Fu, "Impact of security on power systems operation," in *Proceedings of the IEEE*, vol. 93, no. 11, November 2005, pp. 2013–2025.

[66] North American Electric Reliability Council, "Available transfer capability definitions and determination," June 1996. [Online]. Available: http://www.westgov.org/wieb/wind/06-96NERCatc.pdf

[67] E. W. King, C. A. Cañizares, and H. Chen, "A probabilistic approach to evaluate security costs and levels in competitive electricity markets," in *Bulk*

Power Systems Dynamics and Control, vol. 6, Cortina d'Ampezzo, Italy, 2004, pp. 16–23.

[68] I. Dobson, S. Greene, R. Rajaraman, C. L. DeMarco, F. L. Alvarado, M. Glavic, J. Zhang, and R. Zimmerman, "Electric power transfer capability: Concepts, applications, sensitivity and uncertainty," *Power Systems Engineering Research Center PSerc*, vol. 1, no. 34, November 2001. [Online]. Available: http://www.pserc.cornell.edu/tcc/

[69] A. R. Bergen and V. Vittal, *Power Systems Analysis*, 2nd ed. Prentice Hall, 2000.

[70] G. Ejebe, J. Tong, J. Waight, J. Frame, X. Wang, and W. Tinney, "Available transfer capability calculations," *IEEE Transactions on Power Systems*, vol. 13, no. 4, pp. 1521–1527, November 1998.

[71] C. A. Cañizares, "Applications of optimization to voltage collapse analysis," in *IEEE/PES Summer Meeting*, San Diego, CA., July 1998, pp. 1–8, panel Session: "Optimization Techniques in Voltage Collapse Analysis".

[72] ——, "UWPFLOW." [Online]. Available: http://thunderbox.uwaterloo.ca/~claudio/software/pflow.html

[73] H. Y. Benson, D. F. Shanno, and R. J. Vanderbei, "Interior-point methods for nonconvex nonlinear programming: Complementarity constraints," *Operations Research and Financial Engineering*, pp. 1–20, September 2002.

[74] F. Milano, "Pricing system security in electricity markets models with inclusion of voltage stability constraints," Ph.D. dissertation, University of Genova, Genova, Italy, April 2003.

[75] S. Hunt, *Making competition work in electricity*, J. Wiley, Ed. Wiley Finance, 2002.

[76] [Online]. Available: http://www.econ100.com/eu5e/open/glossary.html

[77] G. B. Alderete, "Alternative models to analyze market power and financial transmission rights in electricity markets," Ph.D. dissertation, University of Waterloo, Waterloo, ON. Canada, 2005.

[78] S. Stoft, *Power System Economics*, J. Wiley, Ed. IEEE press, 2002.

[79] K. Xie, Y. H. Song, J. Stonham, E. Yu, and G. Liu, "Decomposition model and interior point methods for optimal spot pricing of electricity in deregulation environments," *IEEE Transactions on Power Systems*, vol. 15, no. 1, pp. 39–50, February 2000.

[80] V. H. Quintana and G. L. Torres, *Introduction to Interior-Point Methods*, University of Waterloo, Waterloo, On. Canada.

[81] G. L. Torres and V. H. Quintana, "Rectangular and polar optimal power flow by a primal-dual interior-point method for nonliner programming," University of Waterloo, Canada, Technical Report UW ECE 97-13, November 1997.

[82] H. Wolkowicz, R. Saigal, and L. Vandenberghe, Eds., *Handbook of Semidefinite Programming*. Springer, 2000, vol. 27.

[83] L. Vandenberghe and S. Boyd, "Semidefinite programming," *SIAM review*, vol. 38, no. 1, pp. 49–95, March 1996.

[84] M. F. Anjos, "Towards and SDP-based algorithm for the satisfiability problem," Operational Research Group, School of Mathematics. University of Southampton. U.K.

[85] C. D. Vournas, M. Karystianos, and N. G. Maratos, "Bifurcation points and loadability limits as solutions of constrained optimization problems," in *Proc. IEEE-PES, Summer Meeting*, vol. 3, July 2000, pp. 1883–1888.

[86] N. G. Maratos and C. D. Vournas, "Relationships between static bifurcations and constrained optima," in *ISCAS 2000*, vol. 2, Geneva, Switzerland, May 2000, pp. 477–480.

[87] I. Dobson, "Observations on the geometry of saddle node bifurcations and voltage collapse in electrical power systems," *IEEE Transactions on Circuits and Systems—Part I: Fundamental Theory and Applications*, vol. 39, no. 3, pp. 240–243, March 1992.

[88] J. Nocedal and S. J. Wright, *Numerical Optimization*. Springer, 1999.

[89] C. A. Cañizares, F. L. Alvarado, C. L. DeMarco, I. Dobson, and W. F. Long, "Point of collapse methods applied to ac/dc power systems," *IEEE Transactions on Power Systems*, vol. 2, no. 7, pp. 673–683, May 1992.

[90] C. D. Vournas, B. M. Nomikos, D. N. Makridou, M. E. Karystianos, and G. A. Manos, "Bifurcation analysis of electrical power systems," January 2000, presented in the 1st Interdisciplinary Symposium of Nonlinear Problems, NTUA, Athens.

[91] F. Zhang, *The Schur Complement and Its Applications*. Springer, 2005.

[92] E. Castillo, A. J. Conejo, C. Castillo, R. Mínguez, and D. Ortigosa, "Perturbation approach to sensitivity analysis in mathematical programming," *J. Optimization Theory and Applications*, vol. 128, no. 1, p. 49–74, January 2006.

[93] R. Fourer, D. M. Gay, and B. W. Kernighan, *AMPL A Modeling Language for Mathematical Programming*, 2nd ed. Thomson, 2003.

[94] M. C. Ferris, R. Fourer, and D. M. Gay, "Expressing complementarity problems in an algebraic modeling languange and communicating them to solvers." [Online]. Available: www.ampl.com

[95] "KNITRO." [Online]. Available: http://www.ziena.com

[96] R. A. Horn and C. R. Johnson, *Matrix Analysis*. Cambridge University Press, 1985.

[97] J. Arrillaga and C. Arnold, *Computer Analysis of Power Systems*. John Wiley and Sons, 1990.

[98] *Ipopt (Interior Point Optimizer)*. [Online]. Available: http://homes.esat.kuleuven.be/~optec/software/ipopt/index.html

[99] *Matlab*. [Online]. Available: http://www.mathworks.com/

[100] X. Yan and V. H. Quintana, "Improving an interior-point-based OPF by dynamic adjustments of step sizes and tolerances," *IEEE Transactions on Power Systems*, vol. 14, no. 2, pp. 709–717, May 1999.

[101] R. J. Avalos, C. A. Cañizares, F. Milano, and A. J. Conejo, "Equivalency of continuation and optimization methods to determine saddle-node and limit-induced bifurcations in power systems," *IEEE Transactions on Circuits and Systems—Part I: Fundamental Theory and Applications*, May 2008. [Online]. Available: http://thunderbox.uwaterloo.ca/~claudio/papers/Rafael1.pdf

[102] R. J. Avalos, C. A. Cañizares, and M. F. Anjos, "Practical solution of voltage-stability-constrained optimal power flows," *IEEE Transactions on Power Systems*, 2007, 12 pages, manuscript submitted for review on November 21, 2007.

[103] ——, "A practical voltage-stability-constrained optimal power flow," in *IEEE PES General Meeting*, Pittsburgh, USA, July 2008, invited paper. [Online]. Available: http://thunderbox.uwaterloo.ca/~claudio/papers/RafaelGM.pdf